MECHANICAL ANALYSIS OF POLYCARBONATE/POLYSILOXANE BLOCK COPOLYMERS AND BLENDS

A Thesis
Submitted to the Graduate Faculty
of the
North Dakota State University
Of Agriculture and Applied Science

By

Tingting Zhou

In Partial Fulfillment
for the Degree of
MASTER OF SCIENCE

Major Department:
Mechanical Engineering

September 2013

Fargo, North Dakota

North Dakota State University
Graduate School

Title

Mechanical Analysis of Polycarbonate/Polysiloxane Block Copolymers and Blends

By

Tingting Zhou

The Supervisory Committee certifies that this ***disquisition*** complies with North Dakota State University's regulations and meets the accepted standards for the degree of

MASTER OF SCIENCE

SUPERVISORY COMMITTEE:

Dr. Chad Ulven
Chair

Dr. Long Jiang

Dr. Xinnan Wang

Dr. Bret Chisholm

Dr. Dean Webster

Approved:

11/7/2013
Date

Dr. Alan R. Kallmeyer
Department Chair

ABSTRACT

Polydimethylsiloxane (PDMS) can be used to react with polycarbonate (PC) to generate PC-PDMS multiblock copolymers and PC/PC-PDMS-PC triblock blends to overcome the notch sensitivity of PC while maintaining its transparency. It was found in this study that PDMS can act as a rubber particle to absorb energy and promote multicrazing. As a result, the incorporation of PDMS can increase PC's toughness. Meanwhile, high optical clarity can be observed even at 62 wt% PDMS in the multiblock copolymers with uniform morphology. However, PC/PC-PDMS-PC triblock blends damage PC's transparency and become opaque due to the phase separation. Furthermore, compared to compression molding, injection molding introduces shear due to the decrease of the area at the nozzle, which leads to the orientation of polymer chains and, subsequently, better properties of specimens.

ACKNOWLEDGEMENTS

During the three-year life in NDSU, I appreciate all the people I know here. They make my life so wonderful.

First of all, I would like to thank my advisor, Dr. Chad Ulven. He encouraged me every time when I came over difficulties in experiments. In addition, he guided me in solving problems in analysis of experimental data. Furthermore, I really appreciate Dr. Ulven to set up such an excellent research group to help me be comfortable in research and daily life.

Additionally, I sincerely thank Dr. Bret Chisholm, Dr. Andrey Chernykh and other people in this group. Dr. Bret Chisholm supplied a lot of help in comprehension of synthesis mechanisms and data analysis of this project. Dr. Andrey Chernykh synthesized the raw materials for this study, provided information of these materials, and helped me to run GPC and NMR tests.

I would like to thank other committee members, Dr. Dean Webster, Dr. Long Jiang, and Dr. Xinnan Wang, for their efforts for reading and advising my thesis. Their suggestion helped a lot in success of this thesis.

I sincerely thank Dr. Mike A. Fuqua, Dr. Shanshan Huo, Dr. Venkata Chevali, and Jessica Lattimer, who helped me a lot in experiments and thesis. Also, I would like to thank other members in our research group for their help in training and guidance in research work.

At last, I would like to thank my family and friends. They supported me in my daily life and gave me a lot of happiness.

TABLE OF CONTENTS

LIST OF TABLES

LIST OF FIGURES

CHAPTER 1. INTRODUCTION

Thermoplastics are commonly used in industry due to their composition stability and remolding ability after heating. Among all kinds of thermoplastics, polycarbonate (PC) stands out in commercial and industrial applications because of its high impact toughness, transparency, thermal stability, and electrical resistance. A method to synthesize bisphenol A PC (BPA-PC) was found in 1956 [1]. Since then, this method has been studied thoroughly, and a well-developed industry of PC has been established. In addition, PC is increasingly known worldwide for a variety of purposes, ranging from bulletproof windows to transparent computer cases, and from compact disks (CDs) to automobile headlights.

Since D. W. Fox [1] and H. Schnell [2] discovered BPA-PC and studied its properties, PC has been more widely known for its commercial applications as an engineering thermoplastic. Based on the production process, BPA-PC is the major product used in the field of PCs. Its structure contributes to the extraordinary physical and chemical properties of PC, such as its high toughness due to the oxygen in the carbonate group [2]. Although PC's properties make it an ideal engineering plastic, it still has weaknesses. For example, both environmental stress cracking and photodegradation can lead to premature failure of PC. The former causes physical damage and the latter causes chemical changes in the polymer [3, 4]. Because of these weaknesses, researchers have modified PC in an attempt to prevent premature failure and make it more versatile in commercial applications.

This chapter will introduce the general properties, history and developments, and applications of PC. Also, the current importance of PC in industry will be shown.

1.1. General Properties of Polycarbonate

Polymer structures determine their properties. The main attributes of PC, such as high impact toughness and transparency, are a result of PC's specific structures. For example, large aromatic content in PC leads to high backbone stiffness, and the moderately large pendent groups and hydrogen bonds formed between the polar carbonates on adjacent molecules increase the resistance to intermolecular movement [5]. The carbonate groups contribute to the solubility of PC in organic solvents, while the oxygen in carbonate groups plays a key role in PC chain's flexibility and, subsequently, its toughness [6]. Moreover, as an amorphous polymer, PC shows high transparency because the size of amorphous regions is too small to scatter the visible light [7]. These structural features of PC cause high impact toughness, mechanical strength, glass transition temperature (T_g), and transparency. However, after annealing, lamellar structure can be generated to form a crystalline region in PC, but the process takes a long time due to its slow crystallization rate [8, 9].

Table 1 [10] provides a general set of PC properties. PC's moisture absorption at humidity equilibrium is quite low (0.120-0.200 %). Its Izod impact strength is 0.481-9.61 J/cm, which is relatively high among plastics. Due to the high T_g (145-150 °C), PC retains its properties over a temperature range from -137 °C to 135 °C [11]. In addition, PC possesses high electrical resistance because of the relatively high values of dielectric constant (2.90-3.17) and dielectric strength (15.7-34.0 kV/mm). Furthermore, PC shows its extraordinary transparency by the 86-92% transmission to visible light. Finally, PC is quite easy to be molded and thermoformed at relatively low processing temperature (270-343 °C) and molding temperature (60-120 °C), which can reduce the cost of PC manufacturing and, consequently, enlarge the production and application fields. Although PC has these important properties, it has weaknesses,

too. Its radiation resistance and ultraviolet resistance are only fair, which lead to aging issues and photo-degradation issues [12-14]. Also, stress crazing, stress cracking [15, 16], solvent resistance, and incompatibility with other materials limit the application of PC.

Table 1. General properties of PC [10].

Properties	Metric
Moisture Absorption at Equilibrium, %	0.120-0.200
Izod Impact, Notched, J/cm	0.481-9.61
Modulus of Elasticity, GPa	1.79-3.24
Glass Transition Temperature, °C	145-150
Ignition Temperature, °F	1070
Dielectric Constant	2.90-3.17
Dielectric Strength, kV/mm	15.7-34.0
Transmission, Visible, %	86.0-92.0
Processing Temperature, °C	270-343
Mold Temperature, °C	60-120

1.1.1. Impact Properties of Polycarbonate

Although amorphous thermoplastics usually show brittle failure when impacted, PC exhibits ductile behavior at high temperature [17]. Many factors have been investigated to explain this phenomenon. For example, thermal pretreatment of PC is found to contribute to the greater degree of order within the amorphous regions, which enhances its strength [18]. Molecular weight is another factor to be correlated with the ductile behavior of PC; the higher the molecular weight, the higher the probability that PC performs a ductile failure [19].

LeGrand and Locoti [20, 21] proposed that low temperature transition below T_g caused the change of fracture failure from ductile to brittle of annealed PC in a notched Izod impact test. Ductile-brittle transition temperature (DBTT) is the critical temperature of fracture failure change for polymers. Below DBTT, polymers usually perform brittle fracture; above DBTT, ductile manner is the major behavior of polymer fracture. However, this hypothesis was doubted

for two reasons: (a) other aromatic polymers also showed the same ductile-brittle LeGrand transition at low temperature, but did not perform in a ductile manner in the notched Izod impact test; and (b) the thermal annealing was found to greatly affect the impact strength without changing the low-temperature ductile-brittle transition, which is contradictory to the low-temperature transition hypothesis [17]. Other research [22, 23] proposed that strain rate, molecular weight, and temperature are the major factors affecting the ductile-brittle transition of PC. These factors influence the morphology of PC, which determines its impact property.

1.1.2. Optical Property of Polycarbonate

PC is usually applied as a lens and refractor due to its transparency and low weight. In general, optical properties include refraction, reflection, absorption, diffusion, and diffraction, where the first three are based on the inherent properties of materials, and the remaining two on the manufacturing [24]. Figure 1 illustrates these five optical properties.

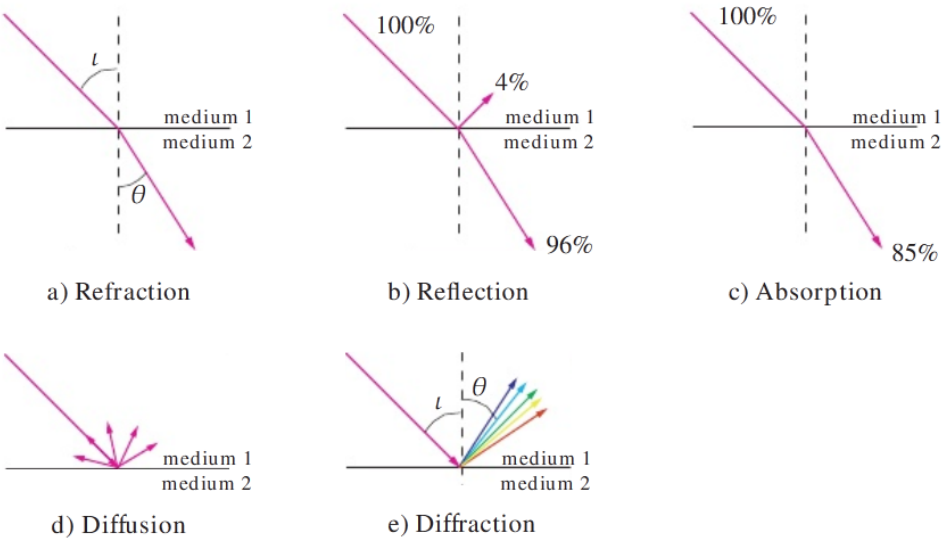

Figure 1. Five optical properties: a) refraction; b) reflection; c) absorption; d) diffusion; e) diffraction [24].

The refraction property is quantified as refractive index (RI), which is defined as the ratio of light velocity in a vacuum to that in a medium. PC's RI is determined by the molecular structures that include the phenyl rings and the large angular correlation between neighboring chains [17]. Also, it depends on temperature [25] as well as molecular weight and moisture [26]. PC's RI (1.585) is a little higher than that of glass (1.54) and is the average among all polymers. High RI indicates a strong capability of the refracting the incident light, which leads to reduced thickness of lenses and thus lowers the manufacturing cost.

Light absorption happens when materials absorb the energy of the incident light and then transfer it to other forms of energy like heat. For instance, sunglasses are made of PC because of its absorption of wavelengths that are harmful to human eyes. Also, the light absorption of PC can be used to identify it in unknown materials. For example, in infrared absorption characterization, characteristic peaks in the infrared spectrum are the main evidence of the presence of PC: C=O vibration causes the strong infrared absorption at 1235 and 1770 cm, C-O group at 1220 cm, and –OH group at 1383 cm [17].

1.1.3. Rheological Properties of Polycarbonate

The rheological behavior of materials describes their flow status when they melt and is influenced by their microstructural features such as molecular weight, polydispersity, and interaction between molecules. Additionally, a material's rheological performance has a strong relationship with processing. For instance, the shear rate and temperature dependence of viscosity give a general knowledge of the procedural conditions of injection processing, such as melting temperature and applied force. Similarly, the rheological properties of materials play a

key role in extrusion processing mechanisms, for example, the mixing dynamics, pressure at the die, and degree of extruder swell [27].

Storage modulus (G'), loss modulus (G"), and complex viscosity $|\eta^*|$ are usually present in rheological figures to show a material's rheological properties. G' stands for the relative elasticity of materials, while G" describes their viscous behavior and the slope of G" represents the dissipated energy during structural deformation. The $|\eta^*|$ is a frequency-dependent viscosity function when shear stress is applied. It represents the angle between the viscous stress and the shear stress and is in accordance with the amount of dissipated energy in structural change. As frequency increases, shear strain increases, which leads to reorientations of PC molecules, including the rearrangements of these molecules. As a result, the rheological properties of PC change [28].

A typical rheological figure of PC at 275 °C, including G', G", and $|\eta^*|$, is shown in Figure 2. At low frequency, G' and G" of PC increase linearly with a slope of two and one, respectively, which is in accordance with typical rheological properties of linear polymers. At high frequency, a plateau shows up in G', and the value of G' at the plateau is governed by the density of molecular entanglement. The intersection of G' and G" curves is the equilibrium point between PC's viscosity and elasticity. When the frequency is lower than the intersection, PC represents elasticity with higher G'. On the other hand, when G" is higher than G', PC exhibits viscous behavior. The $|\eta^*|$, at low frequency, stays at a value equal to the zero shear rate viscosity measured from steady-state shear viscosity tests. This steady value contributes to the flexible backbones of PC. As frequency rises, some of the rearrangements of PC molecules fail due to the rapid change of shear rate. Subsequently, less energy is dissipated at high frequency

compared to that at low frequency. Consequently, $|\eta^*|$ decreases with frequency as shown in Figure 2.

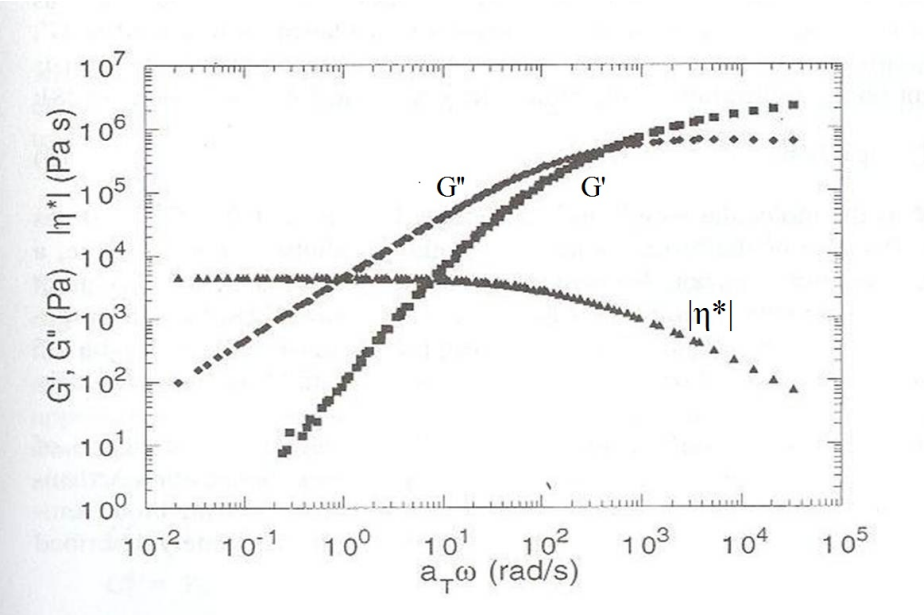

Figure 2. Typical rheological figure of PC at 275 °C [27].

To summarize, the unique structures of PC determine its distinctive properties and lead PC into a high performance commercial plastic. As a result, PC can replace some metals or glasses without compromising the required properties, such as the cockpit canopy of the F-22 Raptor jet and glazing of greenhouses. These examples indicate that PC has become a more and more important part of a person's life.

1.2. History and Development of Bisphenol A Polycarbonate

It took a long time to figure out the manufacturing procedure of PC although it is quite simple now. Over time, many types of PCs have been synthesized to satisfy various industrial requirements. The first synthesized PCs were hydroquinone and resorcinol PC, reported by Einhorn [29] in 1898, and the reaction schemes are shown in Figure 3. Hydroquinone and

resorcinol were reacted with phosgene under the catalyst of pyridine, and they successfully produced hydroquinone and resorcinol PCs, respectively. Despite having a low molecular weight, these two PCs showed advantages over other materials at that time. Hydroquinone PC contained crystal structure that made it infusible and insoluble, while resorcinol PC was amorphous and could melt at about 200 °C. Several years later, Bischoff and Hedenstrom [30] developed the ester exchange reaction to synthesize these two PCs.

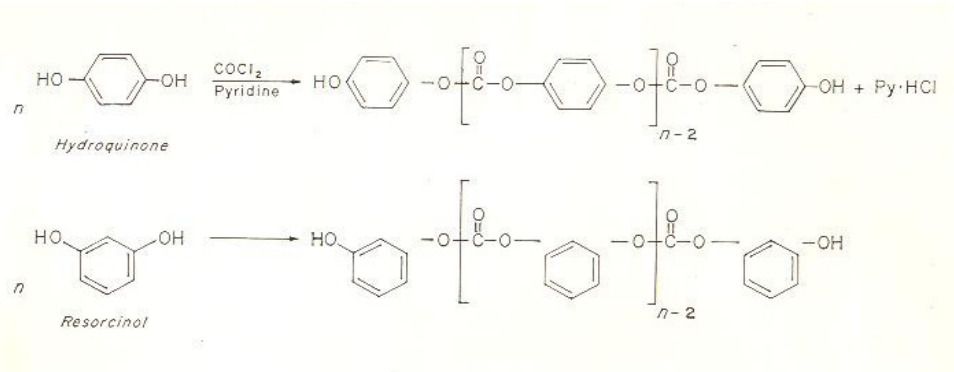

Figure 3. Reaction scheme of hydroquinone and resorcinol PC [1].

PC was not considered a valuable polymer in industry until H. Schnell [2] used bisphenol A to react with phosegene in pyridine and obtained an unexpectedly high melting temperature and toughness polymer. This method has become a major approach to produce BPA-PC nowadays, and the reaction scheme is shown in Figure 4. After H. Schnell, other researchers [31, 32] focused on the best conditions under which BPA-PC reacts and investigated its properties. After years of study, BPA-PC showed great advantages in the balance of all properties such as high impact strength, controllable molecular weight, and thermal stability; as a result, it is ideal for commercial applications. Currently, PC usually refers to BPA-PC, and in the remaining chapters of this thesis, PC refers to BPA-PC.

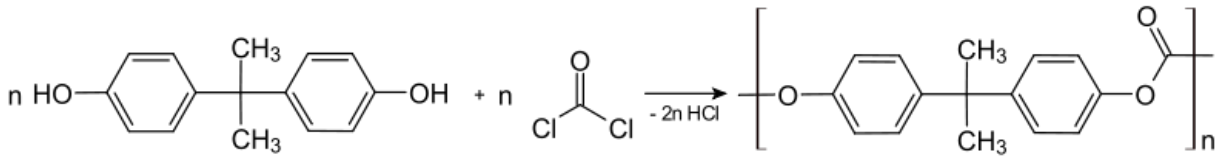

Figure 4. Reaction scheme of bisphenol A polycarbonate [2].

To date, PC has been used in industrial production on a large scale as an engineering plastic. Engineering plastics stand for those plastics used in engineering structures due to their high mechanical properties, heat resistance, and dimension stability. There are five engineering plastics used most widely: PC, polyamide, polyoxymethylene, polybutylene terephthalate, and polyphenylene oxide. PC is the only transparent product in these five engineering plastics and its industrial yield has increased by about 12% every year from 2000 to 2005. In 2009, the global yield of PC was 4.072 million tons, and it is predicted to be about 5.4 million tons in 2015 [33]. So far, the largest consumer markets of PC are electrical and electronic fields, and the second are data storage and films. Clearly, PC plays a more and more vital role in commercial and industrial applications.

1.3. Industrial Applications of Bisphenol A Polycarbonate

PC shares large market volumes due to its combination of strength, high impact toughness, transparency, dimensional stability, high heat resistance, and light weight. PC products can be found in a wide variety of fields. For example, bulletproof windows in banks and some cars make use of the high impact strength and light weight of PC; eyeglasses take advantage of PC's transparency, durability, and high refractive index; compact discs and DVDs benefit from the high impact toughness and electrical resistance of PC. In addition, PC's high heat resistance makes it ideal for tableware and food storage containers in both refrigerator and microwave. Switches in the houses and in industry are commonly made of PC due to its high

electrical resistance. Furthermore, PC has been widely used in medical products, such as blood bowls, dialysis tube holders, and valves, due to its clarity, dimensional stability, chemical resistance to ethylene oxide sterilization, and heat resistance to steam sterilization.

Besides the individual applications, PC is also usually blended with other polymers or fillers to meet specific industry needs. For instance, PC/polybutylene terephthalate (PC/PBT) blends are used to make gearboxes and bumpers; PC provides high toughness and dimensional stability while PBT provides chemical resistance, heat resistance, and lubricity [34]. In addition, PC is blended with acrylonitrile butadiene styrene (ABS) to make PC/ABS copolymer. The flexibility of ABS makes the copolymer superior in automotive, electronic, and telecommunication applications added to the high strength and heat resistance of PC [35]. Furthermore, polydimethylsiloxane (PDMS) is added into PC to improve its impact strength [36]. Similarly, core-shell latex particles can be added as additives to enhance the impact strength of PC [37].

In summary, based on an optimum balance on mechanical, thermal, optical, and electric properties, PC can be applied at high temperatures and under strong impact while transparency is required in commercial and industrial applications. As the industrial demands are inclined to be more specific and strict, modification of PC will attract more and more attention, especially on the modification of PC's impact toughness while maintaining its transparency.

CHAPTER 2. BACKGROUND

Polycarbonate (PC) possesses a unique combination of properties that contributes to its various applications in industries. Among these good properties, impact strength and transparency are the most studied. Although it has high impact toughness, PC, like other polymers, tends to suffer from a change from ductile failure to brittle failure in notched impact tests [38]. This change is caused by the change from plane stress to plane strain at the notch, and subsequently transformation from shearing to crazing in failure mechanism. According to many studies, rubber toughening is an effective way to overcome this fracture failure change.

This chapter addresses several mechanisms and approaches that modify PC by enhancing its impact strength. Specifically, this chapter investigates how different polymers increase PC's toughness as components or additives in copolymers and blends.

2.1. Mechanisms of Polycarbonate Impact Modification

When a load is suddenly applied to a polymer, it tends to resist the impact until it breaks. This impact resistance, also known as toughness, of polymers is significant in their service life. In general, there is two fracture types for polymers: brittle fracture and ductile fracture. The former is featured as a linear relationship between impact stress and strain, while the latter is characterized by plastic yielding, where impact stress is not linearly correlated with strain. In brittle fractures, local crazing usually occurs when defects exist in polymers, and relatively low fracture energy is required to make it happen. On the other hand, ductile fractures require sufficient energy to generate multiple crazing or shear yielding.

To date, there are two approaches to improve polymers' impact strength [39]. The first effective way is rubber toughening through blending or copolymerization. Not only can rubber

particles stretch to absorb plenty of impact stress, but they also promote multiple crazing or form cavitations to relieve hydrostatic strain energy and increase shear yield, which requires more energy to break polymers. Second, impact reinforcements can be added into polymers to form high-toughness composites. The reinforcements can dissipate impact stress to improve polymer toughness. This study will focus on the rubber toughening mechanism to increase PC's toughness.

This study also focuses on the notch sensitivity of PC. After PC is notched, stress concentration occurs at the notch, which makes the stress higher than the average stress that is applied to the whole material and leads to a state of sufficient large hydrostatic tension. As a result, a brittle fracture with crazing occurs in notched PCs instead of a ductile fracture with shear yielding as initially expected. Therefore, the impact strength of notched PCs is lower than that of unnotched PCs. In this study, polydimethylsiloxane (PDMS) was chosen to overcome PC's notch sensitivity by copolymerization and blending via rubber toughening mechanism. PDMS possesses low glass transition temperature (T_g, -125 °C), which makes PDMS stay rubber-like at room temperature [40]. As is known, above T_g, polymer chains are more flexible and, subsequently, absorb more energy. As a result, PDMS can improve PC's impact strength. However, the morphology needs to be carefully manipulated such that the PDMS does not destroy PC's transparency.

2.2. Polycarbonate Blends

To date, there has been much research focus on improving the impact strength of PC. For example, epoxidized ethylene propylene dienes (eEPDMs), as rubber-reinforcements in PC matrix, increased the impact strength of neat PC by a factor of 25 times due to their homogeneous dispersion. This consistent dispersion leads to the good adhesion between these

two phases [41]. Another example was poly(methyl methacrylate-co-methylphenyl siloxane-co-styrene) and poly(methyl methacrylate-co-styrene) studied by Shuangyue Sun et al. [42]. They were used as core-shell structure latexes to form cavitations to enhance impact strength of PC. These cavitations helped relieve triaxial stress and lead to the massive shear yielding, resulting in the ductile tearing under plane stress condition in the notched Izod impact testing. Similarly, the poly(styrene-co-maleic anhydride) and poly(acrylonitrile-butadiene-styrene) [43, 44] also increased the impact toughness of PC by introducing the cavitations of these latex particles.

The modification of core-shell structured latexes outweighs other rubber reinforcements because of the controllable particle size of latexes. The particle size of latexes depends on the mixing process and the adhesion between the latexes and PC. In addition, the predetermined particle size improves the dispersion of latexes in the PC matrix. Moreover, not only do latexes with core-shell structure enhance the impact strength of PC, but they also allow PC to remain its other ideal mechanical properties.

Cheng et al. [38] demonstrated the advantages of latexes with core-shell structure to enhance PC's impact strength by comparing the toughening effect on PC of three butadiene-based modifiers, a linear polybutadiene (PB), a styrene-butadiene-styrene block copolymer (SBS), and a structured latex particle with a PB core and methyl methacrylate/styrene shell (MBS). The comparison showed that the MBS improved PC's impact strength more significantly than the other two. The toughening mechanisms of core-shell structured modifiers were addressed by Parker et al. [45], who concluded that rubber particle cavitations occurred first, therefore the matrix went though massive shear yielding.

Later, Kilwon Cho et al. [37] investigated the influence of rubber additive content and particle size of the core-shell structured latexes on the toughening of PC. The latexes used in this study were the ones with poly(butyl acrylate) as the core and poly(methyl methacrylate) as the shell. Their study showed that the maximum impact strength was exhibited by a 4 wt% rubber phase content with a 0.25-μm-diameter core. When the rubber phase content was below 4 wt% or the core diameter was below 0.25 μm, the impact strength of the PC blend increased with increasing core diameter and rubber phase content. This increase can be attribute to the suppression of internal crazing and the introduction of shear deformation. Conversely, the blend impact strength decreased when the core diameter and rubber phase content increased above the critical value. This decrease occurred because when rubber content was above 4 wt%, these rubbers were intended to interact with each other, which leads to the growth of voids. As a result, the voids got large enough to be defects, causing a decrease in capacity of load carrying and, subsequently, in the impact strength of PC.

Xu et al. [46] also investigated this particle-size effect of core-shell latex particles on the toughening of PC. They found the maximum impact strength was obtained by the addition of acrylic core-shell latex modifiers with particle sizes ranging from 115.7 nm to 231.4 nm. They also proposed equations for the spatial dispersion of modifiers; these equations showed the relationship between the interparticle distance (T), particle size (d), and modifier volume fraction (φ) in two possible morphologies, $T = d[\frac{0.91}{(\varphi)^{1/3}} - 1]$ in cubic center crystal distribution and, $T = d[\frac{0.88}{(\varphi)^{1/3}} - 1]$ in hexagonal crystal distribution. All these equations showed that particle size of modifiers and their content in PC blends should be optimal in order to obtain the maximum impact strength.

Besides the modifier size and content, Kayano et al. [47] found that the process methods (i.e. single and twin screw extruder processing) played a role in the toughening effect of core-shell-structured rubber on PC. The twin-screw extruder provided a better compounding that indicated a better dispersion of rubber additives in PC matrix, which led to higher impact strength of PC blend.

Recently, in contrast to various core-shell structured impact modifiers, nanomodifiers have attracted more attention. Nanoparticles are materials that range in the size from 1 to 100 nanometers and exhibit close relationships between particle sizes and material properties, which is not shown in bulk materials. Due to their small size, nanomodifiers can disperse better in a PC matrix, which indicates a better interaction between the modifiers and PC and, subsequently, increases the impact toughness of the PC matrix. Goitisolo et al. [48] added amorphous polyamide-based nanocomposites into a PC matrix and found that these nanocomposites formed compatibilization due to their small size and homogenous dispersion; as a result, they enhanced the toughness of the PC matrix.

A PC/ABS blend is one of the most widely used PC impact modification blends. It retains the major mechanical properties of PC and also costs less than PC; thus, it can meet the economic market demands. As more PC/ABS blends are developed, various compatibilizers are incorporated to achieve strong interfacial adhesion, such as poly(methyl methcrylate) [49] and ABS-grafted-maleic anhydride [50]. Furthermore, H. A. Stretz et al. [43] tried to replace ABS with styrene-maleic anhydride (SMA) in a PC matrix. SMA showed an advantage because it did not damage the transparency of PC, although it could not increase the impact toughness as ABS did due to the weaker interfacial force between SMA and PC.

Another remarkable example of PC toughness modification is PC/low density polyethylene (PC/LDPE) [51]. The interfacial bonding strength of this blend can reach 30 MPa, which is extraordinarily strong compared to other PC blends. In addition, the cavitation toughening mechanism is similar to that of core-shell structure latex. The debonding at the interface between PC and LDPE generates internal cavitations, which relieves the plane strain constraint and then introduces shear yielding at the matrix.

Equally important to the improvement of impact resistance, PC modifiers also focus on maintaining PC's transparency. Domain size of modifiers is important to modified PC's transparency. It was found that transparent materials were achieved with the 20 nm size of siloxane domain, while opaque ones contain 30 nm or larger size [52]. Moreover, a different refractive index (RI) between PC and modifiers can lead to light scatter and reduce PC's transparency. For example, SMA (RI=1.577) can intensify PC (RI=1.585)'s clarity better than ABS (RI=1.53-1.55) due to the small mismatch in their RI [43].

In summary, PC modifications have shown their advantages in enhancing PC's impact strength. In this well-developed mechanism, modifiers improve PC's toughness and modified PCs play an increasing significant part in PC applications. Furthermore, an increasing number of materials are considered as modifiers to increase the impact strength of PC to make it economically worthwhile.

2.3. Polysiloxane

In addition to the impact modifiers mentioned above, polysiloxane is also considered as an effective toughening modifier due to its intrinsic properties. With the structure $[SiRR'\text{-}O\text{-}]_x$, polysiloxanes have been used as high-performance materials in applications due to their

excellent chemical and physical properties. For example, the low level of interactions between molecules in polyethoxysiloxane contributes to the effective sol-gel process to form silica fibers at a considerably low temperature [53]. In addition, the flexible end groups in polymethylsilsesquioxane interact both chemically with organic materials and physically with the substrates, which makes it useful in chemical coating [54]. Furthermore, polysilsesquioxanes are able to form thin films to overcome the limitation in electronic device preparation at high temperature (400-450 °C) for organic materials with low dielectrics [55]. Moreover, polydimethylsiloxane (PDMS) shows many advantages in biomedical applications because of its physiological inertness, blood compatibility, thermal stability, and low toxicity [56].

Silicone and its derivatives have been used as flame-retardants for thermoplastics due to their high heat resistance and nontoxicity. For example, phenyl silicone contains phenyl groups that can be soluble in aromatic thermoplastics (e.g. PC), and it can be well dispersed in PC; once combusted, silicone is inclined to migrate to the material's surface to form flame-resist char barrier [57]. Indeed, not only can the silicone and its derivatives be flame-retardants, but they also do not affect other properties of PC. Furthermore, PC with silicone and its derivatives shows higher impact strength than PC with a bromine compound as a flame retardant.

In addition to those physical and chemical properties, polysiloxane can also be applied to improve impact resistance of PC, either by being incorporated as an additive in blends or as a component in a copolymer.

2.4. Polycarbonate/Polydimethylsiloxane Blends and Copolymers

Polydimethylsiloxane (PDMS) has been used in many applications such as contact lenses, medical devices, lubricating oils, and modifications for other polymers. Due to its low glass transition temperature (T_g, -125 °C), PDMS is widely used to improve PC's properties, including

impact strength, surface and wear properties, and flame retardancy. In addition, the low viscosity of PDMS makes PDMS blends and copolymers easier to process.

2.4.1. PC-PDMS Block Copolymers

PC-PDMS block copolymers consist of soft siloxane blocks and hard PC blocks and are widely applied as elastomers with high toughness at low temperatures. PC-PDMS block copolymer was first prepared by H. A. Vaughn et al. [58]. Its structure is shown in Figure 5 as follows: x, y, and z are integers ranging from 1 to 200, 5 to 200, and 1 to 1000, respectively.

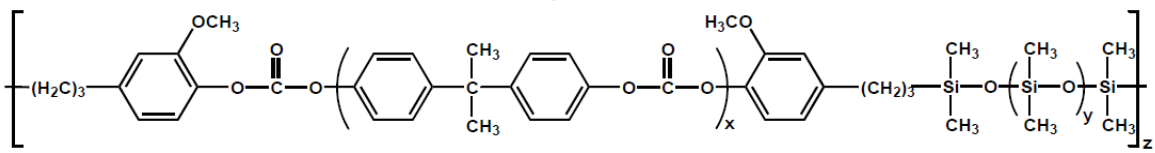

Figure 5. The structure of PC-PDMS block copolymer.

PC-PDMS block copolymers are widely used in industry because they can be either flexible thermoplastic elastomers with high PDMS content (40-70 wt %) and low degree of polymerization (DP, 10-20) or rigid thermoplastics with low PDMS content (1-20 wt %) and high DP (20-100). When a rigid thermoplastic, PC-PDMS block copolymer possesses relatively high T_g (140-150 ˚C) and different grades of transparency (from opaque to clear). This change in transparency is attributed to the DP of PC and PDMS block and the size of PDMS domain and its dispersion in copolymer. In general, opaque copolymers contain the larger size of PDMS domain such as 30 nm to 100+ nm, while clear ones include the smaller PDMS domain around 20 nm. Moreover, the refractive index (RI) of PC (1.585) is higher than that of PDMS (1.400); this mismatch in RI causes the increase in light scatter and, subsequently, leads to the opaque of the copolymer [52].

Ham Van Aert et al. [36] found that the microphase separation of PC-PDMS block copolymers was strongly influenced by block lengths that were based on the block molecular weight. Their study is in accordance with that of Ma et al. [59] who used aminopropyl PDMS to synthesize PC-PDMS block copolymers. In Ma's work with the same PC block, both T_g and intrinsic viscosity of the block copolymers decreased as PDMS content increased, which may be caused by the phase separation of these two immiscible components. In addition, their melt flow index increased linearly with increasing PDMS block content when PDMS contents were below 10 wt%.

2.4.2. PC/PDMS Blends

Besides copolymerization, physical blending PC with PDMS is another effective way to improve PC's toughness and it costs less than chemical copolymerization. However, PDMS is insoluble in PC, which introduces a phase separation in the blends. In order to solve the immiscibility, PC-PDMS copolymers are blended into PC in order to strengthen the interphase interaction between PC and PDMS.

Wenjun Zhou et al. [60] found hydroxyl terminated PDMS can react with PC to form reactive PC-PDMS copolymers in PC/PDMS blends and found that this reaction made these PC/PDMS blends perform as high impact strength as PC-PDMS copolymers at a low temperature (-40 °F). The reactive PC/PDMS blends showed similar mechanism for increasing PC's impact strength to PC-PDMS copolymer. In reactive PC/PDMS blends, the low T_g and wide spread of PDMS contributed to a decrease of PC's ductile-brittle transition temperature (DBTT), which led to higher impact strength at a low temperature. While in PC-PDMS copolymers, the DBTT of PC was lowed by adding PDMS into PC backbones. On the other hand,

Wenjun Zhou found that reactive PC/PDMS blends had a stronger influence than PC/PDMS copolymers on PC's rheological properties. Compared to PC, the former performed stronger shear thinning behavior while the latter represented a similar shear viscosity change with PC. This strong shear thinning behavior was due to free PDMS domains in reactive PC/PDMS blends. These free PDMS domains possessed low viscosity that lubricated PC chains and could migrate to the capillary wall during rheological testing.

Pesetskii et al [61] studied non-reactive PDMS/PC blends, that is, the polysulphone-PDMS (PSN-PDMS) block copolymers/PC blends. They found that 5-7 wt% PSN-PDMS can enhance the impact strength of PC by 20 times and attributed this enhancement to the homogenous dispersion of PSN-PDMS and high interphase adhesion. Pesetskii et al [62] also found that, similar to PSN-PDMS additives, PC-PDMS block copolymers have a significant influence on PC's impact toughness when blending into PC. These PC-PDMS copolymers introduced multi-crazing to absorb impact energy during fracture. However, the immiscibility of PC and PDMS led to a weak interphase interaction that reduced the compatibility of PC-PDMS modifier and PC matrix. As a result, the content of PC-PDMS modifier in PC matrix should be carefully controlled. Indeed, 7-10 wt % was found to be the optimized content of PC-PDMS modifier to obtain both high impact toughness and superior compatibility in PC.

In summary, PC/PDMS blends and block copolymers show superior mechanical properties like impact strength at low temperatures. In addition, PC-PDMS block copolymers can achieve relatively high transparency compared to PC/PDMS blends because the phase separation occurs in PC/PDMS blends due to the immiscibility of PC and PDMS.

CHAPTER 3. OBJECTIVES

As discussed above, polycarbonate (PC) can overcome its notch sensitivity to improve impact toughness by incorporating rubber particles. Based on early research [36, 59, 63], polydimethylsiloxane (PDMS) has been chosen to be the toughening rubber to enhance PC's impact strength via copolymerization and blending in this project.

In traditional copolymerization of PC and PDMS, a group of randomly alternating PC-PDMS block copolymer are prepared by in *situ* polymerization of siloxane oligomer and bisphenol A and phosgene [64]. As a consequence, the geometry of PC and PDMS chains cannot be controlled, and the visible light PDMS scatters have a negative influence on the transparency of PC. To obtain the best balance between the improvement of impact toughness and the avoidance of scattering visible light, a novel synthesized method inspired by Kim et al. [65] was applied to produce a PC-PDMS multiblock copolymer to precisely control the geometry, length, and distribution of the block. To obtain this balance, a series of PC-PDMS multiblock copolymers with different block molecular weight and ratios of PC and PDMS were produced by North Dakota State University's Center for Nanoscale Science and Engineering.

When blending, the compatibility of PC and PDMS should be considered because PDMS cannot be soluble in PC. Therefore, a PC-PDMS-PC triblock copolymer was used to blend with PC to form the PC/PC-PDMS-PC mixture. Three batches of PC-PDMS-PC triblock copolymers were synthesized with different PC block molecular weight, PDMS block molecular weight, and PDMS content. Then these triblock copolymers were blended with PC through extrusion to target a 3 wt% PDMS mixture.

After PC-PDMS multiblock copolymers and PC/PC-PDMS-PC blends were made, many tests were done to determine the phase morphology, optical properties, impact properties, and rheological properties of these copolymers. These tests were dynamic mechanical analysis (DMA), transmission electron microscopy (TEM) characterization, atomic force microscopy (AFM) characterization, scanning electron microscopy (SEM), notched impact tests, and rheological tests.

Meanwhile, processing methods were found to affect the properties of copolymers to a certain extent. As is known, materials exhibit different flow modes in different processing machines. Two processing methods, compression and injection molding, were used to study the effect of processing method on copolymer properties. In compression molding, materials are set in the mold compactly and as a result, there is little space for materials to flow and mix with each other to make consistent properties. In contrast, materials are mixed under shear stress in the injection machine promoted a uniform mixture and subsequently a series of better properties.

Therefore, the objectives of this project are that, by the end of this study: 1) the addition of PDMS should increase the impact toughness of PC, and the higher PDMS content increases PC's toughness more; 2) the higher molecular weights of PC and PDMS blocks suggest a higher toughness in the PC/PDMS materials; 3) the higher PDMS percentage and higher block molecular weight can damage the clarity of PC; 4) injection molding will show advantages over compression molding in polymer chain orientation and provide better properties of specimens.

CHAPTER 4. MATERIALS, PROCESSING AND CHARACTERIZATION METHODS

This chapter describes three main experimental aspects of this study in detail. First, materials used in this study are divided into three groups, pure polycarbonate (PC), traditional PC-polydimethylsiloxane (PDMS) block copolymer, and experimental PC-PDMS copolymers/blends. Second, compression molding and injection molding are illustrated, including molding machines, procedures, processing conditions and so on. Finally, there are introductions for characterization methods, such as notched impact test, rheological test, dynamic mechanical analysis (DMA), transmission electron microscopy (TEM), atomic force microscopy (AFM), scanning electron microscopy (SEM), tensile test and flexural test.

4.1. Materials

There are four kinds of PC copolymers applied in this study, pure PCs, commercial PC-PDMS block copolymers, experimental PC-PDMS copolymers and experimental blends. The former two are commercially available, and the latter two were synthesized by Dr. Bret Chisholm's group in the Center for Nanoscale Science and Engineering, North Dakota State University.

4.1.1. Pure Polycarbonate

Pure PC was provided by Dow Chemical Company and marked as Dow caliber 303-15. Table 2 shows the critical properties of these transparent Dow PC pellets. Dow PC possesses properties in the range of the properties of general PC that are shown in Table 1. For instance, Dow PC obtains 850 J/m during the notched Izod impact test, which is in the range of 48.1-961

J/m for general PC. Its tensile modulus, 2.34 GPa, is between the lowest 1.79 GPa and highest 3.24 GPa of general PC. In addition, Dow PC's light transmission is 89%, which is quite average in general PC (86-92 %). The molecular weight of Dow PC was measure by gel permeation chromatography (GPC), and the number average molecular weight (Mn) was 21900, the weight average molecular weight (Mw) was 39400 with the polydispersity index (PDI) 1.8.

Table 2. Properties of Dow PC caliber 303-15 [66].

Properties	Metric
Water Absorption, %	
@ 23 °C, 24 hrs	0.15
@ 23 °C, 50% Rh @Equilibrium	0.32
Notched Izod Impact, J/m, @ 23 °C	850
Tensile Modulus, GPa	2.34
Deflection Temperature Under Load, °C	
Annealed @ 0.45 MPa	143
Annealed @ 1.8 MPa	140
Unannealed @ 1.8 MPa	127
Flammability Rating	
@ 1.6 mm	HB
@3.2 mm	HB
Dielectric Constant	
@ 60 Hz	3.0
@ 1MHz	3.0
Dielectric Strength, kV/mm	17
Refractive Index, n_D	1.586
Light Transimission, %	89
Melt Flow Rate, g/10 min, 300 °C/1.2 kg	15

4.1.2. Commercial Block Polycarbonate

PC-PDMS was also investigated as block copolymers. This material was a SABIC Lexan® 9030 grade and was received as a fine white powder before being manufactured into final sheet applications. SABIC PC/PDMS consists of 95% of PC and 5% PDMS. According to GPC results, the Mn of SABIC PC/PDMS was 27600, and the Mw was 39400 with the PDI 1.43. Table 3 shows the properties of commercial SABIC PC/PDMS. Compared to the Dow PC,

SABIC PC/PDMS shows little difference except the notched Izod impact strength. Due to the different methods to report impact strength, SABIC PC/PDMS cannot be directly compared with Dow PC.

Table 3. Properties of SABIC Lexan® 9030 PC/PDMS [67].

Properties	Metric
Water Absorption, @ 23 °C, Saturation, %	0.35
Notched Izod Impact, kJ/m^2	
@ 23 °C	65
@ -30 °C	10
Tensile Modulus, 1mm/min, GPa	2.35
Vicat B/120, °C	145
Thermal Conductivity, W/m. °C	0.2
Dissipation Factor @ 50 Hz	3.0
Light Transimission, 3mm, %	89

4.1.3. Experimental PC-PDMS Multi-Copolymers

A series of experimental PC-PDMS copolymers were provided with different block Mns and ratios. Table 4 lists the Mn and percentage of PC and PDMS blocks as well as the Mn of PC-PDMS block copolymers.

Table 4. Molecular weight and percentages of experimental PC-PDMS copolymers.

Sample code	PC		PDMS		PC-PDMS
	Mn (g/mol)	wt%	Mn (g/mol)	wt%	Mn (g/mol)
1	3009	81.5	765	18.5	16493
2	3009	73.3	1210	26.7	19093
3	3009	38.1	5285	61.9	25706
4	3009	20.8	20200	79.2	15243
5	4760	86.8	765	13.2	14342
6	4760	80.5	1210	19.5	18327
7	4760	48.0	5285	52.0	19548
8	4760	28.3	20200	71.7	28348
9	7600	91.2	765	8.8	17558
10	7600	86.7	1210	13.3	28102
11	7600	59.3	5285	40.7	26633
12	7600	38.3	20200	61.7	29113

These experimental PC-PDMS block copolymers were synthesized by a novel two-step method that is shown in Figure 6. In the first step (a), bisphenol A was used with the end-capping monomer (eugenol) and the carbonate source (triphosgene) to synthesize allyl-PCs by interfacial polymerization. The next step (b) involved the hydrosilylation reaction of allyl-PC and hydride-terminated PDMS oligomers with the catalyst platinum (Pt).

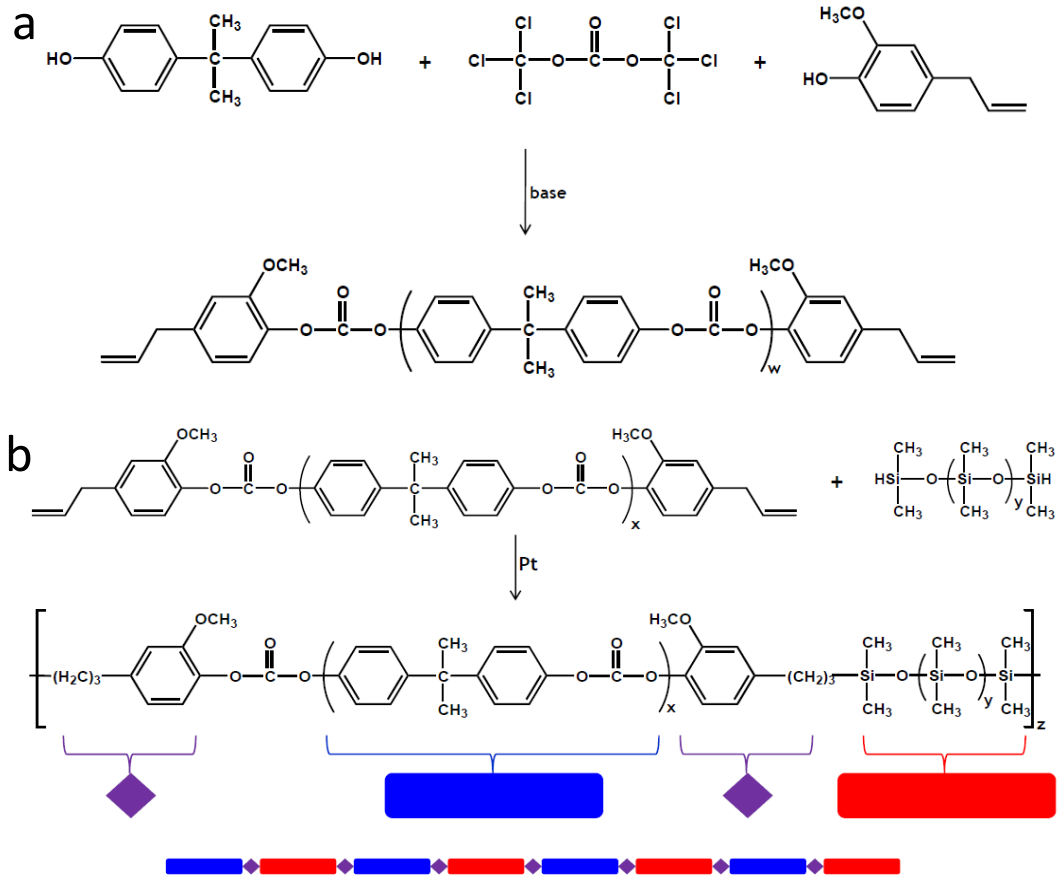

Figure 6. Synthesis scheme for allyl-PC and PC-PDMS, a) first step to synthesize allyl-PC; b) second step to generate PC-PDMS block copolymer, the order of monomers listed as the colored bars.

A typical procedure for generating allyl-PC was as follows. A 1 L flask was equipped with a high-speed overhead stirrer, nitrogen inlet, inlet tube, outlet tube, and a thermometer, where the inlet tube was for adding triphosgene and the outlet tube for connecting to a solium

hydroxide (NaOH) scrubbing solution. 4.79 g of BPA, 0.69 g of eugenol, and 5.04 g of NaOH were dissolved in 200 mL of H_2O in the l L flask and cooled below 5 °C in an ice bath. Meanwhile, 2.49 g of triphosgene was prepared in a 500 mL one-neck and round-bottom flask dissolving in 200 mL of anhydrous methylene chloride (CH_2Cl_2) inside a glove box. Before adding triphosgene, a proprietary catalyst was added to the aqueous phase in the 1 L flask. The addition of triphosgene was under high speed stirring (900 rpm) by a syringe pump and 5 °C reaction temperature. After completion of the triphosgene addition, high-speed stirring continued for 90 minutes at a higher temperature (15 °C). Afterwards, the CH_2Cl_2 phase was separated and washed with water until the pH of the solution was 7.0. By using methanol, allyl-PC was precipitated from CH_2Cl_2 solution and then dried at 80 °C under vacuum.

A representative process of producing the PC-PDMS block copolymer was listed as follows. 0.25 g of allyl-PC was dissolved in 20 mL of anhydrous tetrahydrofuran (THF) in a 50 mL round-bottom flask equipped with nitrogen inlet and condensation. Then 20 μL of Pt catalyst dissolved in 5 mL of THF was added as drop by drop. Afterwards, 62 μL of hydride-terminated PDMS was added to start the reaction at 60 °C under nitrogen flow for 16 hours. After the reaction, the PC-PDMS products were filtered and precipitated by methanol. The final precipitate was dried overnight at 80 °C under vacuum.

This novel PC-PDMS multiblock copolymer possesses advantages over traditional ones (Figure 7) in controllable block length and architecture of PC and PDMS. This control is achieved by controlling the ratio of bisphenol A to eugenol in the first step. In addition, the terminating allyl groups are obtained in the second step to take hydrosilation reaction between PC and PDMS that results in block copolymer. Comparing the colorful bars which stand for PC and PDMS blocks in novel (Figure 6) and traditional (Figure 7) copolymers, it is observed that

traditional PC-PDMS multiblock copolymer is a random block copolymer and the lengths of PC and PDMS blocks are not under control; while the lengths of the blocks are controlled in the novel multiblock copolymers.

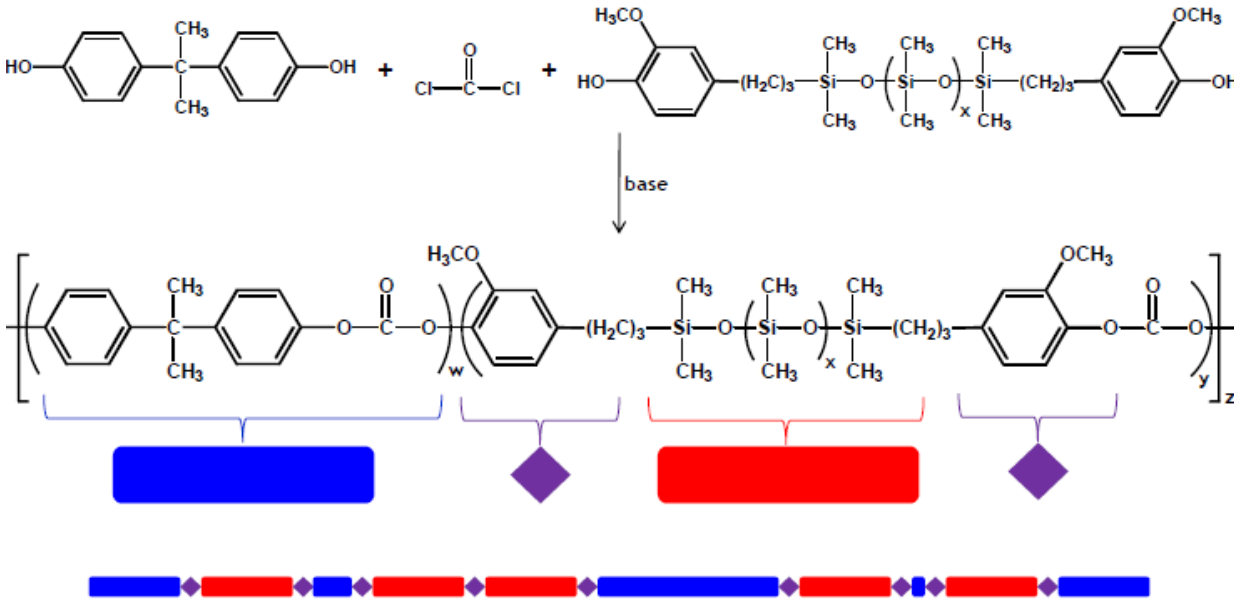

Figure 7. The synthesis of traditional PC-PDMS multiblock copolymers.

4.1.4. PC/ PC-PDMS-PC Blends

Before blending, PC-PDMS-PC triblock copolymers were synthesized, and their synthesis scheme is shown in Figure 8. A typical synthesis of these triblock copolymers was as follows: 6.3 g of eugenol terminated PC and 13.78 g of hydride terminated PDMS-H25 were dissolved in 120 mL of chloroform in a round bottom flask equipped with condenser and magnetic stirrer. 250 µL of Karstedt catalyst (2 wt% in toluene) was then added, and the reaction was refluxed under nitrogen atmosphere for 4 hours. The copolymer was precipitated in fourfold excess of methanol, filtrated, and dried at 65 °C for 4 days. The results are listed in Table 5.

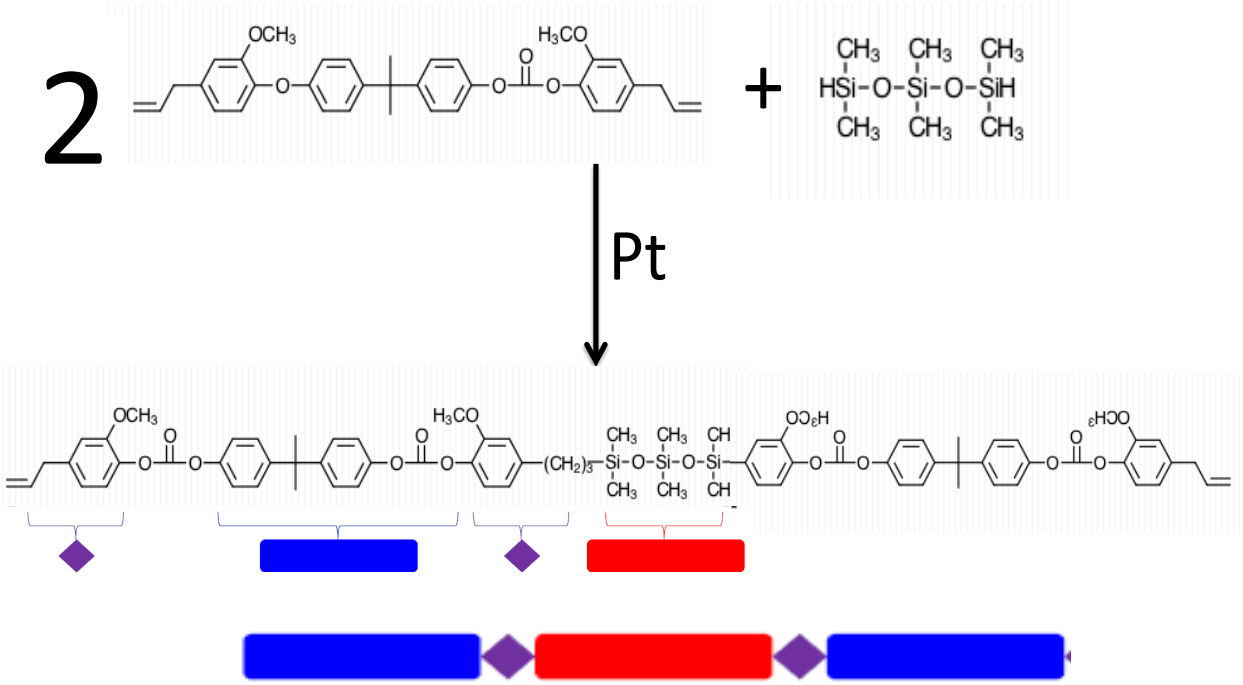

Figure 8. The synthesis of PC-PDMS-PC triblock copolymers.

Table 5. Molecular weight and percentages of triblock PC-PDMS-PC copolymers.

Sample code	PC		PDMS		PC-PDMS Mw (g/mol)
	Mw (g/mol)	wt%	Mw (g/mol)	wt%	
T1	2700	28	12400	72	20080
T2	4600	43	12400	57	20950
T3	4600	28	23200	72	20070

In order to obtain 3 wt% PDMS in the final blends, a certain ratio of PC-PDMS-PC triblock copolymers and Dow PC were weighted and put into the oven to dry at 80 ˚C for 24 hours. After drying, the triblock copolymers were compounded with Dow PC in a co-rotating twin-screw extruder (Leistritz Micro-18/GL-40D). The screw rotation rate was 250 rpm, and the temperatures from the hopper to die were as follows: 260 ˚C, 288 ˚C, 282 ˚C, 282 ˚C, 277 ˚C, 271 ˚C, 266 ˚C, and 266 ˚C. In addition, the dwell time was set at 75 seconds. After extruded from the die, the material was quenched in water and chopped into pellets.

Twin-screw extrusion enables continuous processing to produce homogenous compounds for various applications. Unlike the single screw extruder, the twin-screw extruder consists of two identical screws that are stacked one beside another on a splined shaft and can co-rotate and intermesh. With this advanced design, twin-screw extruders can perform transporting, conveying, mixing, compressing, kneading, and shearing of raw materials. These features make twin screw extrusion flexible to process, which is preferred in manufacturing.

4.2. Processing

To compare the influence of processing methods on materials' properties, two processing approaches are performed in this study, compression and injection molding. Details in processing are illustrated as follows.

4.2.1. Compression Molding

Compression molding is originally used to produce composites to replace metals [68] and mainly applied to thermosetting plastics to date. With heat and pressure, materials are pressed to an open and preheated mold until they fully fill the mold and get cured. Compression molding has been widely used due to its simple procedure, low cost, and low waste of raw materials. However, compression molding cannot guarantee product consistency, control flashing, or provide complicated products.

A Carver Heated-Platen compression machine was used with hydraulic press in this study. A square mold and a rectangular mold were applied to make square and rectangular samples; the square samples were prepared for DMA tests and rheological tests, and the rectangular ones for

notched Izod impact tests. Figure 9 shows the Carver Heated-Platen compression machine, the square mold, square mold in press, and the final compression specimen.

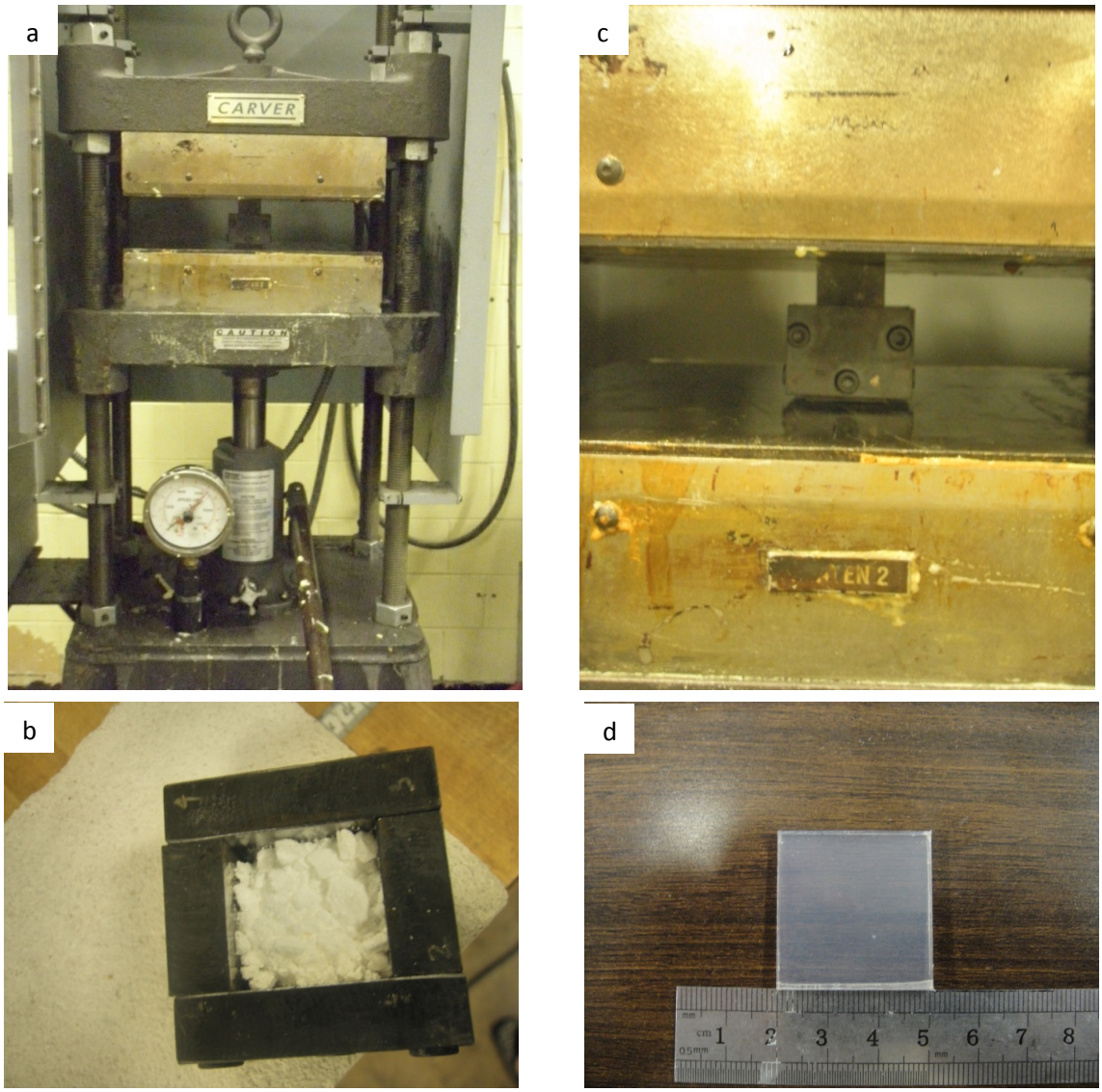

Figure 9. Carver heated-platen compression machine (a), the square mold (b), square mold in press (c), and final compression specimen (d).

The compression molding process is described as follows. Before molding, the mold was cleaned by acetone and preheated at 270 °C for 2 hours in an oven. Then 4 g of molding material was added to the square mold cavity with the plug on, and 6.5 g of materials to the rectangular mold cavity. The mold system kept heating for half an hour at 270 °C while preheating the

compression machine to 150 °C. After the half an hour heating, materials melted completely and the mold system was placed into the compression machine and stayed for 5 minutes for cooling. Then 1 metric ton pressure (8.2 MPa for rectangular mold and 10.9 MPa for square mold) was applied to the mold system and remained for an hour at 150 °C and for another hour after turning off the temperature of the compression machine. The final specimen was taken out when the mold cooled down to room temperature and then cut into the required dimension for different tests. The challenge in compression molding was to control flashing, which wasted too much raw materials and reduced the thickness of the specimen.

4.2.2. Injection Molding

The injection machine used in this study was a ram injection machine. The injection molding process is as follows: granular materials are fed from a hopper into a heated barrel, melted in the chamber, and forced by a plunger into a cold mold to form a shape as the contour of the mold cavity. Injection molding is applied in both thermoplastics and thermosetting plastics in industries and shows advantages in high production rate, high repeatability, wide materials suitability, low scrap loss and little need to finish product after molding. Nevertheless, high cost in equipment and running machines limits the development of injection molding.

Mini-Jector model 45-3/4 injection machine was used to manufacture specimens in this study. It is a manual or semi-automatic vertical injection machine with pneumatical operation, plunger-type plasticizing system, and V-mold technology. The vertical clamp can provide 12 tons of clamping force and can produce 9.36-42.52 grams for each shot. 115 V and 10 A services are required during the injection process. Figure 10 shows the Mini-Jector model 45-3/4 injection machine, the V-mold, and the final injection specimen.

Sample preparation was needed for injection molding due to the large size of raw experimental PC-PDMS block copolymers that cannot be forced into the heated barrel. Raw materials were cracked into pellets in a metal mortar and pestle with liquid nitrogen, which made materials brittle to break easily. After cracking, materials were dried at 80 °C under vacuum for 48 hours.

Because of the limited amount of experimental PC-PDMS block copolymers, a paper funnel was used to feed materials into the heated barrel instead of the hopper. Before injection molding, the V mold was sprayed by mold release on its surface and preheated at 80 °C in an oven for 2 hours. The whole injection molding was processed at 300 °C with 98.13 MPa injection pressure at 861 kPa air pressure with a 12-second cycle. After molding, polypropylene was injected to clean the barrel and chamber, and the mold needed to be sprayed again with the mold release to prevent oxidation. The cycle time was the most challenging part during injection molding. Materials could not melt completely if the cycle time was too short while they would oxidize with longer cycle time.

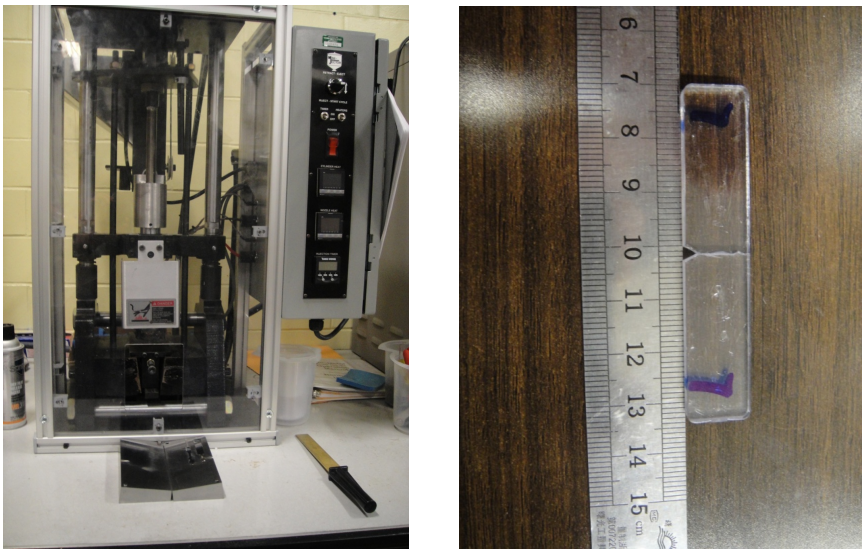

Figure 10. Mini-Jector model 45-3/4 injection machine,
the V-mold, and the final injection specimen.

4.2.3. Comparison Between Compression Molding and Injection Molding

Contrasting to compression molding, injection molding shows plenty of advantages in various aspects. For instance, the preheating temperature of injection mold (80 °C) is much lower than that of compression mold (270 °C), which is preferred in industry. Also, the short molding cycle time (12 seconds) of injection molding greatly increases its production rate and make it effective in manufacturing. In addition, SABIC PC/PDMS was molded in both compression molding and injection molding to compare the optical clarity of the specimens, the one molded from injection machine was more transparent than that from compression machine, which is clearly illustrated in Figure 11.

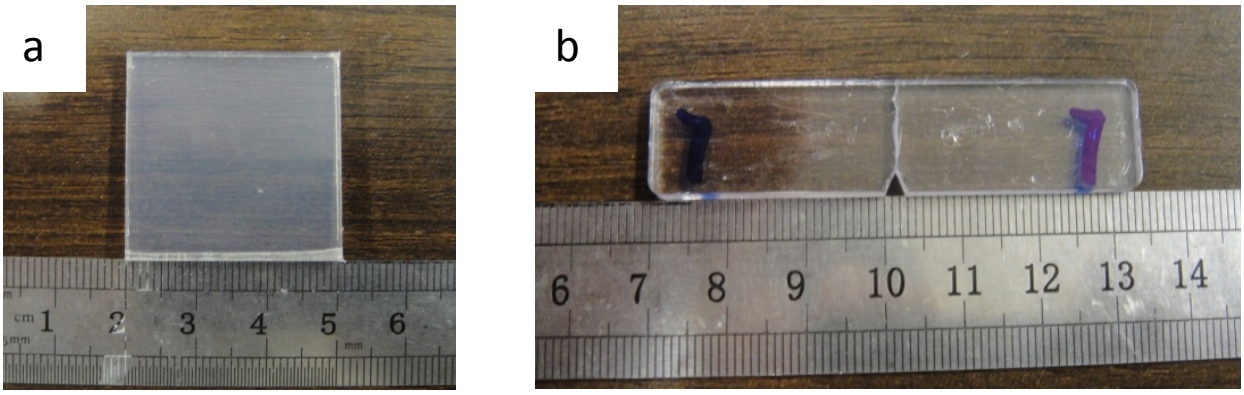

Figure 11. Final molding SABIC PC/PDMSs from a) compression molding and b) injection molding.

On the other hand, injection molding has more requirements than compression molding. For example, mold release is needed before and after molding on the mold surface to protect it from oxidation, which is not required in compression molding. Also, sample preparation is needed for injection molding due to the specific size issue in this study. Moreover, molding temperature in injection molding is a little higher (300 °C) than that of compression molding (270 °C). This may be because of the shorter molding cycle time in injection molding. The

shorter molding cycle time requires a quicker material melting procedure in the barrel and chamber of injection machine, as a consequence, a higher molding temperature is required to make materials quickly melt. Table 6 summarizes the differences between compression molding and injection molding.

Table 6. Comparison between compression molding and injection molding.

		Compression Molding	Injection Molding
Before Molding	**Sample Preparation**	No	Yes
	Mold Preheating Temperature, °C	270	80
	Mold Preheating Time, hour	2	2
	Mold Release	No	Yes
During Molding	**Molding Temperature, °C**	270	300
	Molding Pressure, MPa	8.2/10.9	98.13
	Molding Cycle Time, second	7200	12

4.3. Characterization Methods

In order to compare the influence of block molecular weight and ratio on toughness and transparency of PC-PDMS copolymer and blends, several characterization methods were conducted in this study, such as notched Izod impact test, DMA, rheological test, TEM, SEM, and AFM.

4.3.1. Notched Izod Impact Test

Izod impact strength test followed ASTM D256 standard in this study to determine the impact strength of notched samples with 4.497 N weight and 334.949 mm radius setting. The material's impact strength is correlated to its toughness, which is defined as the ability to absorb energy when plastic deformation happens. Low toughness in materials is caused by the small undertaking amount of plastic deformation. In general, impact strength of materials can be

influenced by temperature and sample size. It tends to decrease when lowering temperature and increasing sample size.

Due to the difficulty in controlling flashing in compression molding and the limited mass of raw materials, the thickness of specimens was lower than that required by ASTM D 256. To compensate, the width of specimens was also reduced to be in accordance with their thickness. The Izod impact test machines made by Tinius Olsen are shown in Figure 12.

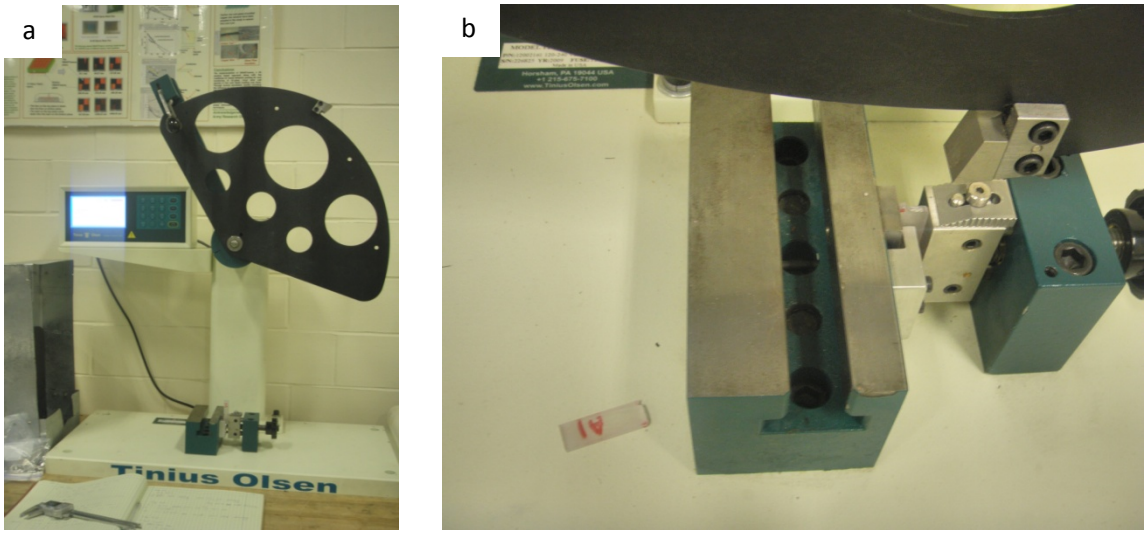

Figure 12. Izod impact test machine overall (a) and part (b).

4.3.2. Dynamic Mechanical Analysis

Dynamic mechanical analysis (DMA) is an efficient method to determine the glass transition temperature of materials to study their chain motion when exhibiting viscoelastic behavior. A sinusoidal stress is applied to materials, resulting in a strain that is the measurement in DMA tests. Storage modulus, loss modulus, and tan delta are collected to represent elastic portion, viscous portion, and phase angle, respectively.

A rectangular specimen was tested in Q800 DMA test machine made by TA Instruments Company, which is shown in Figure 13. DMA multi-frequency-strain module was conducted in a single cantilever clamp under nitrogen atmosphere. A temperature ramp procedure from -130 °C to 180 °C was applied with the 5 °C/min ramp and 10 Hz frequency. Liquid nitrogen was used to lower the temperature.

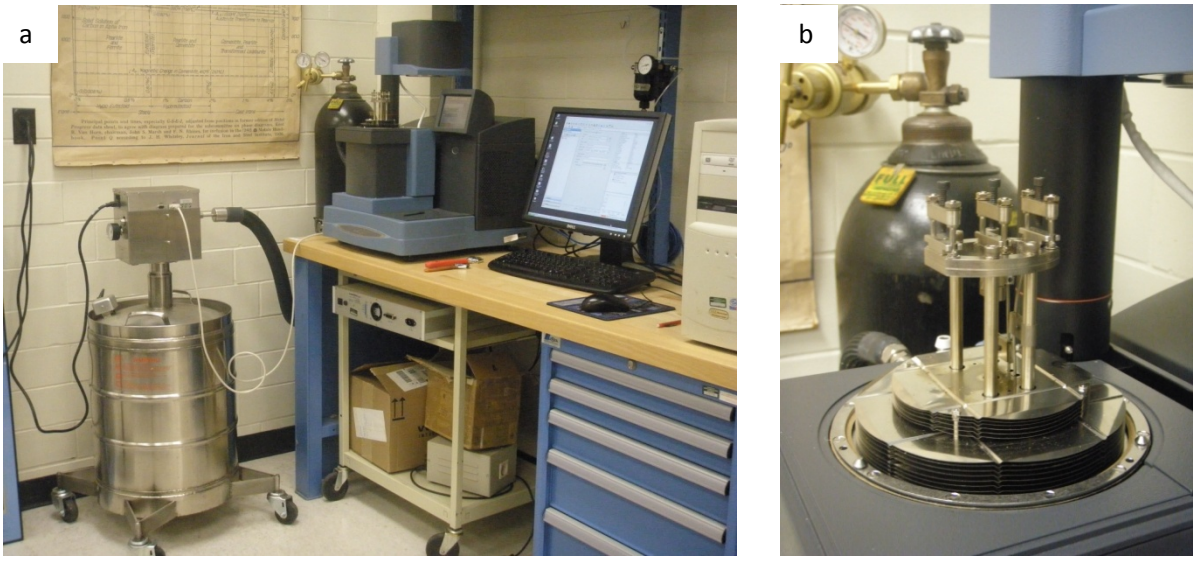

Figure 13. Q800 DMA test machine (a) and its cantilever (b).

4.3.3. Rheological Test

Rheology is the science of flow and deformation of materials. Rheological measurements present the viscoelastic properties of polymers, the subsequent nature, the rates of polymer chain rearrangements, and the nature of the molecular interactions over a range of time. The rheological properties of polymers are important for processing and characterizing the copolymer microstructure. Several significant factors of the rheological behavior include material microstructure, the degree of the phase dispersion, the ratio of the components, and the interaction between polymer chains.

TA AR series Rheometer was used to test materials' rheological properties in this study and is shown in Figure 14. A frequency sweep test was applied with angular frequency ranging from 0.06283 rad/s to 628.3 rad/s at 270 °C and 10 % strain.

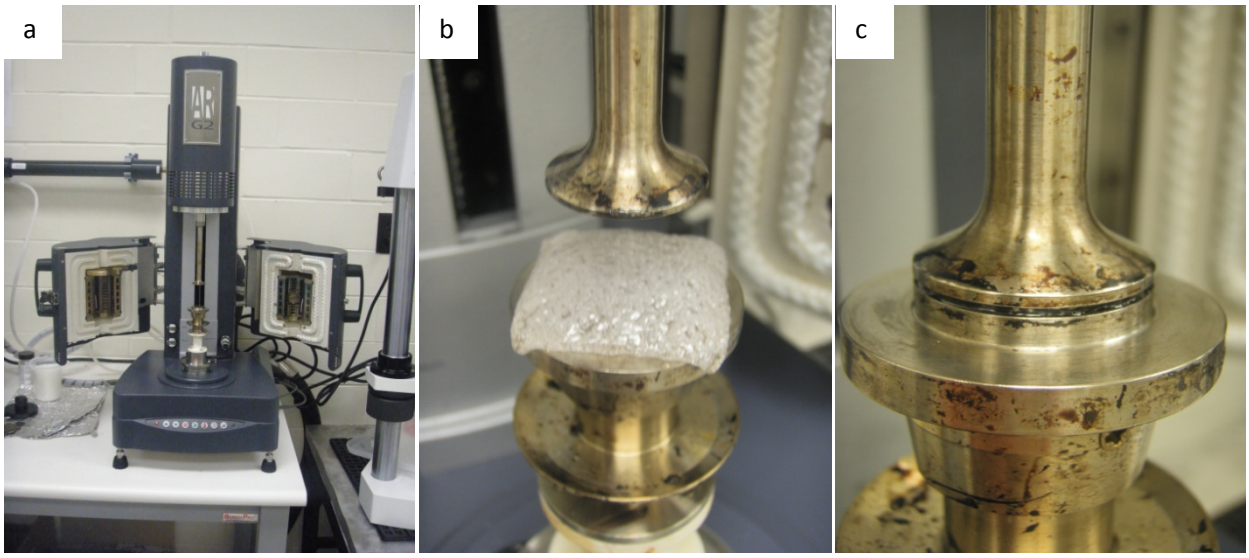

Figure 14. TA AR series Rheometer (a), material melt (b), and test mode (c).

4.3.4. Transmission Electron Microscopy

Transmission electron microscopy (TEM) is a type of electron microscope technique whereby an image is generated when the electron beam interacts with the material when transmitting through it. TEM can achieve a high resolution to represent a profile of materials' structure at the atomic level. This high resolution contributes to the major advantage of TEM compared to other electron microscopy. However, TEM is not widely used in industry for certain reasons. First, the structure of materials may be changed because of the interaction between the electron beam and the material. In addition, it is time consuming or difficult to obtain such thin samples for TEM, usually tens of nanometers thick. Thirdly, both the instrument and the test cost are relatively high compared to other electron microscope techniques.

TEM was done by RJ Lee Company in this study. Samples were prepared by microtoming and placed onto a 3 mm coppor TEM grid, and then they were analyzed at 30 kV in a Hitachi S-5500 FESEM/STEM with energy dispersive X-ray spectroscopy (EDS), or at 200 kV in a Hitachi HD-2300 STEM with EDS.

4.3.5. Atomic Force Microscope

Atomic force microscopy, abbreviated as AFM, is a type of scanning probe microscopy with very high resolution, at least the nanometer level. It describes contour of materials' surface in three dimensions by moving a mechanical probe on the surface. In order to precisely present the morphology of a material's surface, the testing sample surface could not be too steep or have overhangs.

AFM studies were performed in tapping mode using a Dimension 3100® microscope with a Nanoscope IIIa controller from Veeco Incorporated, shown in Figure 15. Topographical images were collected in air, at room temperature, using a single-lever silicon probe from NanosensorsTM. Cantilever length, width, and thickness of the silicon probe were 225 ± 10 µm, 25 ± 7.5 µm, and 3.0 ± 1.0 µm, respectively. The spring constant was 0.5-9.5 N/m with a resonant frequency 75 kHz. The set point ratio was 0.8-0.9.

Figure 15. AFM machine.

4.3.6. Three-Point Bending Flexural Test

The three-point bending flexural test measures flexural strength and flexural modulus of materials. Flexural strength shows the capability of materials to resist deformation when forced by external load while the flexural modulus indicates materials' stiffness.

In this study, ASTM D790 Procedure A was followed to run a three-point bending flexural test in Instron 5567 load frame (Figure 16). Five specimens were run for each batch of materials with rectangular cross section. The load was 2000 N, support span was 52.2 mm, and crosshead rate was around 1.4 mm/min. The flexural strength and elasticity modulus were calculated when flexural strain reaches 0.05 mm/mm by the following equations:

$$\sigma_f = \frac{3PL}{2bd^2} \tag{4-1}$$

$$E_f = \frac{L^3 m}{4bd^3} \tag{4-2}$$

where σ_f stands for the flexural strength, E_f stands for the flexural modulus, P is the load at 0.05 mm/mm flexural strain, L is the support span, b is the width of specimens, d is the thickness of specimens, and m is the slope of the initial straight-line portion of the load defection curve.

Figure 16. Three-point bending flexural machine.

4.3.7. Tensile Test

Tensile test is a common test for materials to obtain their reaction under tension. Elastic modulus and ultimate strength can be measured in the tensile test. Elastic modulus is correlated to materials' stiffness, while ultimate strength indicates the maximum working load.

In this study, only elastic modulus was measured according to ASTM D638 using an Instron 5567 load frame (Figure 17). Three specimens were tested for each batch of sample types at a speed of the crosshead of 1.0 mm/min. The elastic modulus was calculated by the slope of the stress-strain curve in the linear region.

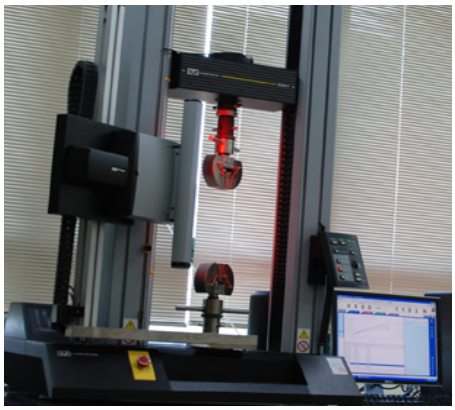

Figure 17. Tensile test machine.

4.3.8. Scanning Electron Microscopy

In scanning electron microscopy (SEM), the image is formed by an electron beam focused on the surface of the specimen. This electron beam is collimated by electromagnetic condenser lenses and is focused by an objective lens and then scanned over the specimen in a series of lines and frames. The raster movement is enabled with small coils of wire carrying the controlling current.

For observation of the fractured surface, the samples in this study were attached to aluminum mounts using colloidal silver paste. A conductive gold-palladium coating was applied with a Balzers SCD 030 sputter coater (BAL-TEC RMC, Tucson AZ). Images were obtained using a JEOL JSM-6490LV scanning electron microscope (JEOL USA, Peabody MA), shown in Figure 18, at an accelerating voltage of 15 keV.

Figure 18. SEM machine.

CHAPTER 5. RESULTS AND DISCUSSION

This chapter discusses the results of PC-PDMS block copolymers, PC/PC-PDMS-PC blends, and the comparison of injection molding and compression molding in three separate sections. A series of tests were conducted to show the material's impact strength, glass transition temperature, rheological properties, morphology, flexural strength, and optical clarity. Based on the data collected from these tests, explanations are provided to describe the relationship between the structure and properties of these copolymers.

5.1. Results and Discussion of PC-PDMS Mulitblock Copolymers

All the PC-PDMS block copolymers synthesized in-house and commercial PC were processed in compression molding. The details of the synthesized copolymers as well as Dow PC and SABIC PC/PDMS are listed in Table 7. Only No.5 (PC5k-PDMS0.7k_13%), No.9 (PC8k-PDMS0.7k_9%), and No.10 (PC8k-PDMS1.2k_13%) were chosen as typical experimental PC-PDMS copolymers because of limited experimental specimen quantities. When discussing the synthesized copolymers, the label after the name includes the molecular weight of each block and the PDMS percentage in the copolymers. For example, No.5 (PC5k-PDMS0.7k_13%) shows that in the No.5 specimen, the block molecular weights of PC and PDMS are around 5000 g/mol and 700 g/mol, respectively, and the PDMS block is in 13% of the whole copolymer.

Table 7. Details of experimental PC-PDMS copolymers, Dow PC, and SABIC PC/PDMS.

Sample		PC		PDMS		PC-PDMS Mn (g/mol)
		Mn (g/mol)	wt%	Mn (g/mol)	wt%	
Experimental PC-PDMS Multiblock Copolymers	**No.5**	4760	86.6	765	13.2	14342
	No.9	7600	91.2	765	8.8	17558
	No.10	7600	86.7	1210	13.3	28102
Dow PC		-	100	-	0	21900
SABIC PC/PDMS		-	95	-	5	27600

5.1.1. Notched Izod Impact Results

Figure 19 shows the Izod impact performance of the three experimental specimens, No.5 (PC5k-PDMS0.7k_13%), No.9 (PC8k-PDMS0.7k_9%), No.10 (PC8k-PDMS1.2k_13%), and Dow PC. Comparing the performance of the experimental specimens, it is observed that No.9 (PC8k-PDMS0.7k_9%), the lower PDMS content specimen, performs at lower impact strength than the higher PDMS content specimens as was initially expected. This comparison shows that PC's toughness can be improved by the addition of PDMS.

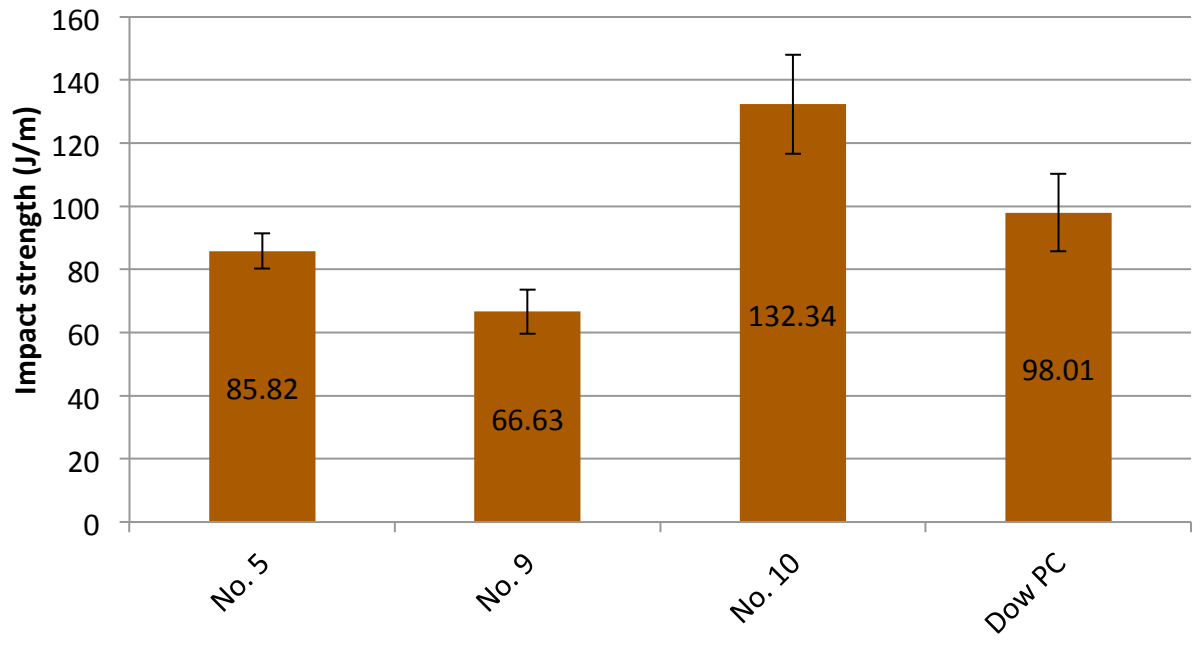

Figure 19. Nothced Izod impact strength of compression-molded synthesized PC and Dow PC.

Examining the two higher PDMS content experimental specimens, it is observed that the Izod impact strength of No.10 (PC8k-PDMS1.2k_13%) is higher than the one of No.5 (PC5k-PDMS0.7k_13%). This can be attributed to the higher block molecular weight of No.10 (PC8k-PDMS1.2k_13%). The higher molecular weight implies longer polymer chains and, subsequently, the energy can be transmitted along the longer chain and shared over more atoms, eventually being dissipated through vibrations, minor translations, and heat, and therefore the impact toughness increases [69].

It is also worth noting that shows No. 10 (PC8k-PDMS1.2k_13%) has higher impact strength than Dow PC. This phenomenon can be caused by two factors: a) the addition of PDMS in improves the impact strength via rubber toughening mechanism; b) the higher molecular weight of No.10 (PC8k-PDMS1.2k_13%) indicates its higher capability in absorbing impact energy.

5.1.2. DMA

Glass transition temperature (T_g) can be obtained by a DMA test and is usually based on either storage modulus or tan delta. The values of T_g in this study were obtained by TA Universal Analysis software at the onset point of the storage modulus curve and the peak point of the tan delta curve. The final outcome is shown in Figure 20.

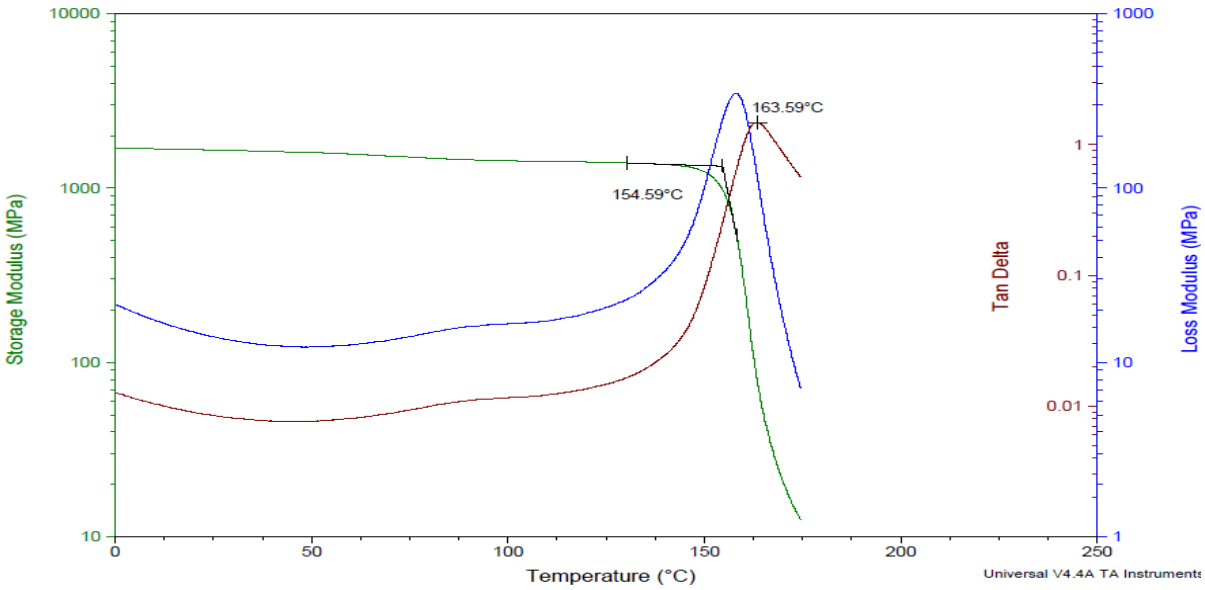

Figure 20. The T_g values marked in storage modulus and tan delta.

Figure 21 shows the storage modulus, loss modulus, and tan delta performances obtained by the DMA tests of the three experimental specimens, No.5 (PC5k-PDMS0.7k_13%), No.9 (PC8k-PDMS0.7k_9%) and No.10 (PC8k-PDMS1.2k_13%), as well as Dow PC and SABIC PC/PDMS. The curves are obtained from the average data of two specimens for each sample. The right figures are the curves in the whole temperature range (-130 °C, 180 °C), and the left ones are the curves in the partial temperature range (-110 °C, -50 °C), where the β transition occurs. Compared to α transition (i.e. glass transition), β transition refers to a smaller range of chain movement and only includes side chains and localized groups of 4-8 backbones atoms.

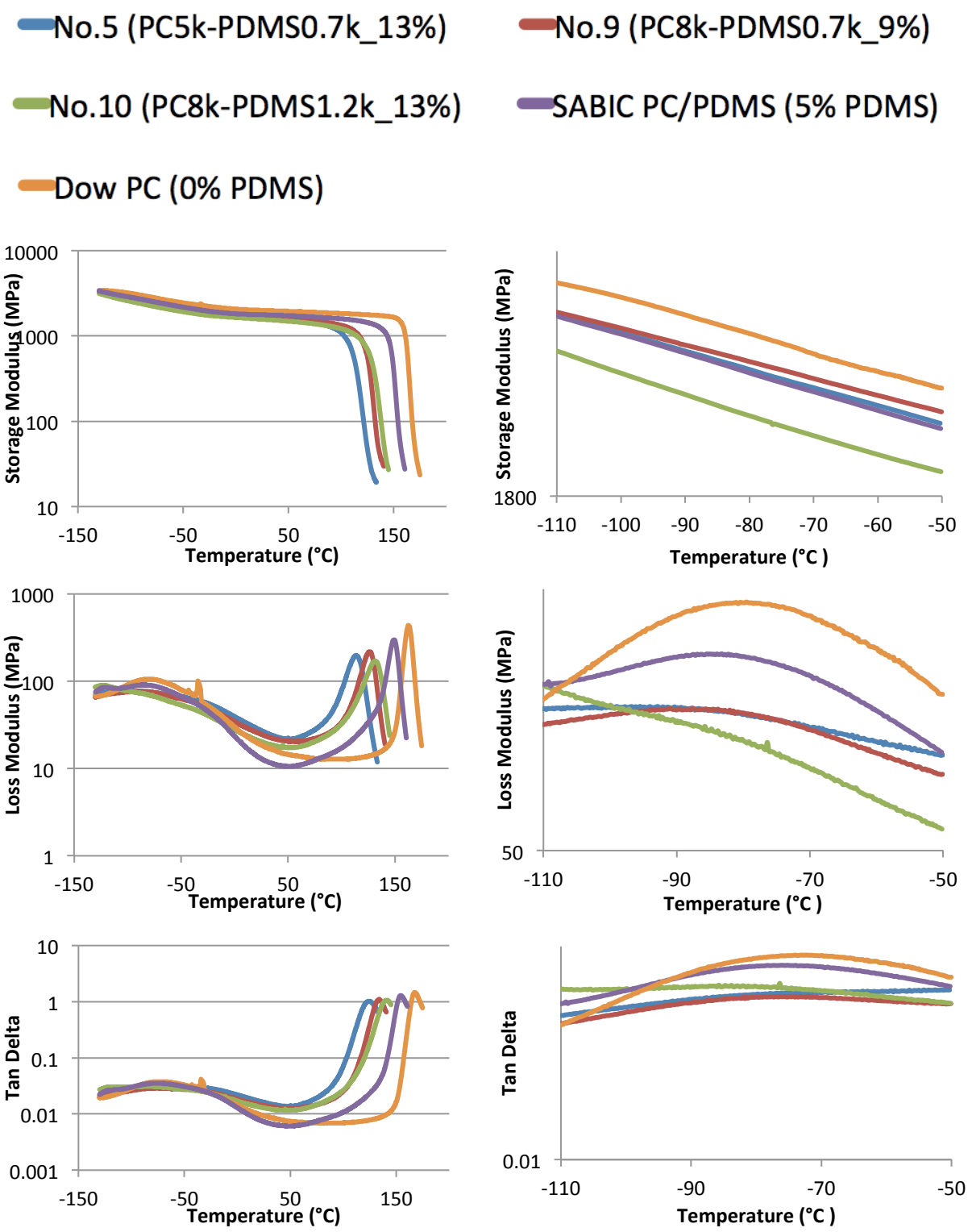

Figure 21. DMA results for compressed specimens. The left figures are in the whole temperature range, and the right ones are in the temperature range from -110 °C to -50 °C

Due to the similar trends in DMA performances, storage modulus behavior is taken as an example to analyze the difference between these materials. The storage modulus retains a high value and decreases drastically until the temperature reaches a certain value, which indicates a distinct α transition from glass state to rubber state. Moreover, before glass transition all the materials maintained similar storage modulus values, indicating that there is not a huge discrepancy within the elastic domain of each. When comparing the values of the storage modulus, it is found that Dow PC shows a higher storage modulus than other PC-PMDS copolymers. This indicates that the incorporation of PDMS lowers the modulus of PC due to the low elastic modulus of PDMS (360-870 kPa) compared to that of PC (1.79-3.24 GPa).

The area under the loss modulus curves in Figure 21 can be used to indicate the chain mobility of the polymer. The area can be calculated by differential calculus in the range of -130 ℃-180 ℃. A decrease in the area indicates restriction of polymer chain movements, which makes it more difficult for polymers to transfer from glass state to rubber state and therefore T_g increases. Based on loss modulus curves in Figure 21, Dow PC has the smallest area and highest T_g, and No.5 (PC5k-PDMS0.7k_13%) has the largest area and lowest T_g, which is in good agreement with the results obtained by storage modulus and tan delta.

Figure 22 compares the average T_gs obtained from the storage modulus and tan delta curves for the various specimens. It is found that all of the experimental PC-PDMS specimens have lower T_g values compared to the Dow PC and SABIC PC/PDMS specimens tested. The addition of PDMS lowers the T_g in the range of 36 ℃-53 ℃ based on the storage modulus curves and in the range of 27 ℃-43 ℃ according to tan delta curves. This decrease indicates that the incorporation of PDMS lowers the T_g of PC-PDMS copolymer because the T_g of PDMS is extremely low (-123 ℃) compared to that of PC (145-150 ℃).

Focusing on the experimental systems, it is observed that No.9 (PC8k-PDMS0.7k_9%) with a median modular weight and lower PDMS content shows a median T_g between No.5 (PC5k-PDMS0.7k_13%) and No.10 (PC8k-PDMS1.2k_13%). Moreover, the lowest molecular weight system No.5 (PC5k-PDMS0.7k_13%) has the lowest T_g, and the highest molecular weight system No.10 (PC8k-PDMS1.2k_13%) has the highest T_g. This trend indicates the T_g of experimental PC-PDMS copolymers are more affected by molecular weight than by PDMS content. It is explained that with higher molecular weight, polymers tend to contain more entanglements between polymer chains, which makes polymers harder to transfer from a hard and relatively brittle state into a molten or rubber-like state [69].

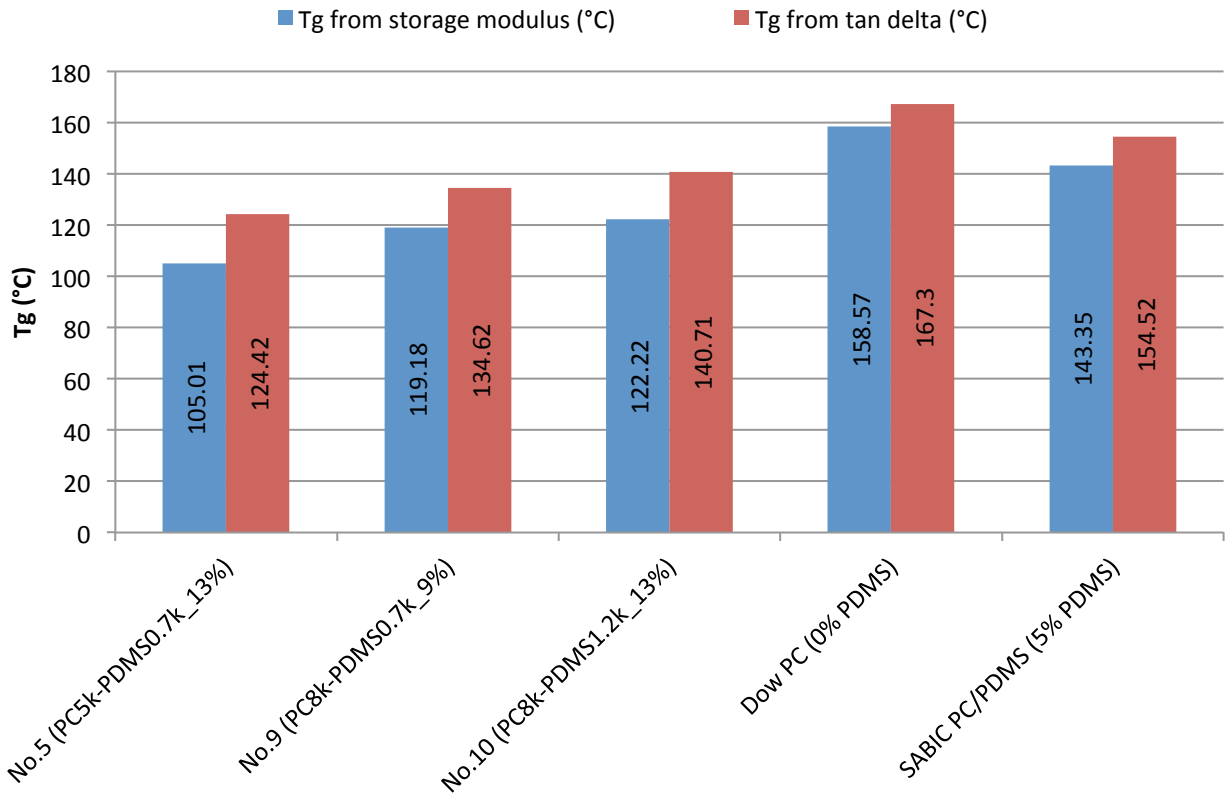

Figure 22. Comparison of T_g from storage modulus and tan delta for compressed specimens.

5.1.3. Rheological Results

The rheological performance of the compression specimens is shown in Figure 23. In the complex viscosity figure, Dow PC performs in a Newtonian plateau at low frequency, while SABIC PC/PDMS and experimental PC-PDMS copolymers perform in a non-Newtonian behavior. As is known, non-Newtonian behavior at low frequency can be caused by the heterogeneity that is due to the immiscibility of components in the copolymer or blend [70]. In this study, SABIC PC/PDMS and PC-PDMS copolymers contain PC and PDMS that are immiscible to each other; as a result, heterogeneity occurs and leads to non-Newtonian behavior. Moreover, the complex viscosities of SABIC PC/PDMS and PC-PDMS copolymers start to yield as the frequency increases. This is because with the increase of frequency, the shear intensity increases, which can remove the chain entanglement and, subsequently, orient the molecular chains along the shear direction [71].

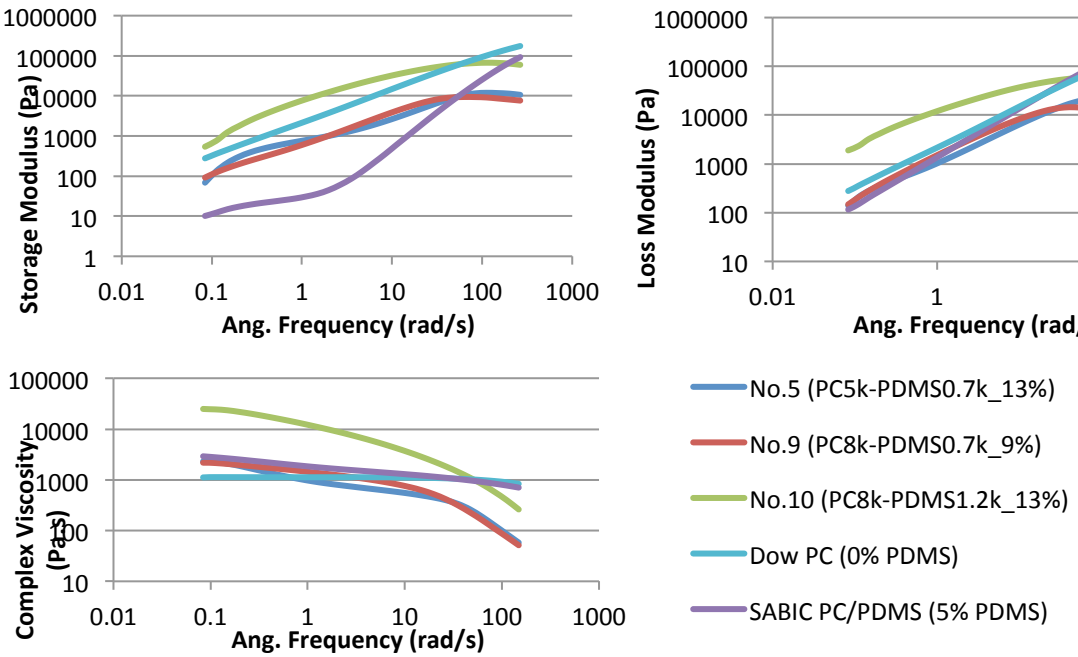

Figure 23. Storage modulus (left top), loss modulus (right top), and complex viscosity (bottom) obtained by rheological tests.

Contrasting the three synthesized PC-PDMS block copolymers' rheological curves, they flow in a similar path while No. 10 (PC8k-PDMS1.2k_13%) possesses higher storage modulus and loss modulus due to its higher molecular weight. With higher molecular weight, the relaxation time for entanglement and disentanglement rises, leading to a higher storage modulus and loss modulus [72].

Synthesized PC-PDMS block copolymers and Dow PC and SABIC PC/PDMS also show different rheological behaviors at high frequency. For example, the storage modulus and loss modulus of Dow PC and SABIC PC/PDMS increase linearly with rising angular frequency. On the other hand, a plateau is observed in storage modulus curves and loss modulus curves of the three synthesized PC-PDMS copolymers at high angular frequency. This may be caused by the effective friction within the polymer chains and at the end of the polymer chains [73].

The model of effective friction can be described in the research of Y. Mastumiya et al. [73]. They assumed the microphase-separated structure played an important role in the rheological properties of block copolymer, and usually when one block A of the triblock copolymer took the bridge/loop conformation, the ends of block A would be anchored on the same/different block B domains. Under shear flow, the conformation was disrupted and changed from bridge type into loop one, and then the elasticity recovery happened. The elasticity of ABA copolymer was fully recovered only when the bridges were re-formed from loops, and this re-formation required the A blocks that were connected to the loop-type B blocks to be thermally pulled out/mixed into B phase. The rate of elasticity recovery was governed by the A/B mixing barrier, which was closely related by the effective friction for the chain motion.

Assuming block B is the minor component in the copolymer and is located at the end of all copolymer chains, the effective friction coefficient of different molecular weight M_B at the end of polymer chains and in the polymer chains ξ_{end} and ξ_{in} can be modeled as follows:

$$\xi_{end} = Kexp(\frac{\Delta G_{M_B}}{k_B T}) \quad (5\text{-}1)$$

$$\xi_{in} = Kexp(\frac{2\Delta G_{M_B}}{k_B T}) \quad (5\text{-}2)$$

Where K is a proportionality constant, $k_B T$ stands for the thermal energy, ΔG_{M_B} represents the free energy increment for mixing the end of block Bs into A phase for certain molecular weight M_B.

Since the multiblock copolymers contains various lengths of polymer chains, the Rouse model [74] for short chains (i.e. triblock chains) and reputation model [75] for longer chains (e.g. heptablock chains) are considered at the same time. Y. Mastumiya et al. [73] summarize relaxation time for short chains and longer chains based on these two models, that is:

$$\tau_{tri} = K'\{2\zeta_{end}\}R^2_{g,tri} \quad (5\text{-}3)$$

$$\tau_{penta} = K'\{2\zeta_{end} + \zeta_{in}\}R^2_{g,penta} = K''\{2\zeta_{end} + \zeta_{in}\}L^2_{penta} \quad (5\text{-}4)$$

$$\tau_{hepta} = K''\{2\zeta_{end} + 2\zeta_{in}\}L^2_{hepta} \quad (5\text{-}5)$$

Here, K' and K'' are the proportionality constants, R_g is the radius of gyration, and L is the equilibrium contour length.

These relaxation times can be applied into the equations of storage modulus G' and loss modulus G'' that are derived by the Rouse model [74]:

$$G'(\omega) = \sum_{p=1}^{N} \frac{G_i(\omega\tau_p)^2}{1 + (\omega\tau_p)^2} \quad (5\text{-}6)$$

$$G''(\omega) = \sum_{p=1}^{N} \frac{G_i \omega \tau_p}{1 + (\omega \tau_p)^2} \tag{5-7}$$

Where N stands for the total number of spring in the polymer chains, p=1, 2, 3, …, N, ω is the frequency, and τ_p stands for the relaxation time of polymer chain of No. p.

Base on the theory of Gramespacher and Meissner [76], the G' and G'' of PC-PDMS copolymer in my study can be calculated as follows:

$$\begin{aligned} G'_{PC-PDMS\ copolymer} &= \phi_{PC} G'_{PC} + \phi_{PDMS} G'_{PDMS} + G'_{effective\ friction} \\ &= \phi_{PC} G'_{PC} + \phi_{PDMS} G'_{PDMS} + \sum_{p=1}^{N} \frac{G_i (\omega \tau_p)^2}{1 + (\omega \tau_p)^2} \end{aligned} \tag{5-8}$$

$$\begin{aligned} G''_{PC-PDMS\ copolymer} &= \phi_{PC} G''_{PC} + \phi_{PDMS} G''_{PDMS} + G''_{effective\ friction} \\ &= \phi_{PC} G''_{PC} + \phi_{PDMS} G''_{PDMS} + \sum_{p=1}^{N} \frac{G_i \omega \tau_p}{1 + (\omega \tau_p)^2} \end{aligned} \tag{5-9}$$

Where ϕ_{PC} and ϕ_{PDMS} are the volume fraction of PC and PDMS, respectively.

When ω tends to infinity, $(\omega \tau_p)^2$ is much larger than 1, and the equation (5-8) and (5-9) can be integrated by:

$$\begin{aligned} G'_{PC-PDMS\ copolymer} &= G'_{PC} + G'_{PDMS} + \sum_{p=1}^{N} \frac{G_i (\omega \tau_p)^2}{(\omega \tau_p)^2} \\ &= G'_{PC} + G'_{PDMS} + N G_i \end{aligned} \tag{5-10}$$

According to (5-10), this model might explain the reason that $G'_{PC-PDMS\ copolymer}$ retains a constant value at higher frequency, which shows a plateau in the storage modulus curve at high frequency. Similarly, a plateau is also shown in loss modulus curve at high frequency. However, more research needs to be done to verify the model.

5.1.4. TEM

Figure 24 shows the dark field TEM (DF TEM) images of SABIC PC/PDMS. In dark field images, the direct beam is blocked by the aperture while diffracted beams are allowed to pass the objective aperture. Since diffracted beams have strongly interacted with the specimen, very useful information is present in DF images, such as planar defects, stacking faults or particle size [77]. In Figure 24, PDMS domains are diffracted to be white and noted in SABIC PC/PDMS. In the left figure, the PDMS domains segregate and appear to be fairly consistent in size, ranging from 5 nm to 20 nm. While in the right figure, slightly larger domains of silicon rich material are shown in the bright domain. These silicon domains range from about 20 nm to 150 nm. The presence of those large domains may be attributed to the random copolymerization of PC and PDMS, which cannot compare with the novel synthesis from this study in controlling the length of PC and PDMS block as well as their architecture.

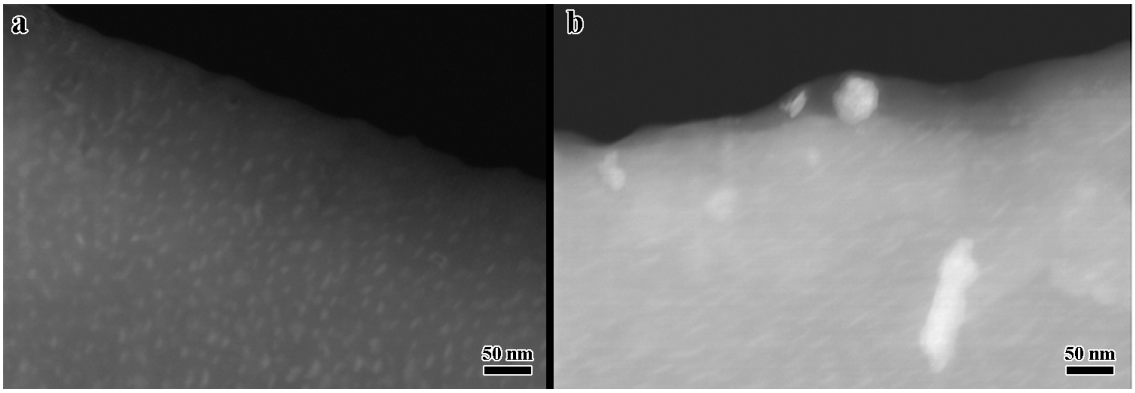

Figure 24. TEM figures for SABIC PC/PDMS.

Figure 25 presents bright field TEM (BF TEM) images of four batches of experimental PC-PDMS block copolymers, No.1 (PC3k-PDMS0.7k_19%), No.5 (PC5k-PDMS0.7k_13%), No.9 (PC8k-PDMS0.7k_9%), and No.10 (PC8k-PDMS1.2k_13%). In the bright field mode, an aperture is placed in the back focal plane of the objective lens that allows only the direct beam to

pass. In this case, the image results from a weakening of the direct beam by its interaction with the sample. Therefore, mass-thickness and diffraction contract contribute to image formation: thick areas, areas in which heavy atoms are enriched, and crystalline areas appear with dark contrast [78]. As a result, the PDMS molecules are weaken to become dark domains.

Comparing image (b) and (c) in Figure 25, it is observed that No.10 (PC8k-PDMS1.2k_13%) shows clear microphase separation, which suggests that a higher block molecular weight leads to a higher probability that microphase separation will occur in a PC-PDMS copolymer. It can be explained that with higher block molecular weight, the PC and PDMS block are more immiscible with each other, leading the PC-PDMS copolymer more likely to form microphase separation. Besides the influence of block molecular weight, PDMS content also has an effect on the microphase separation. No.9 (PC8k-PDMS0.7k_9%) shows only one phase and suggests the miscible state in PC and PDMS. As the PDMS content increases, microphase separation can be easily observed in No.10 (PC8k-PDMS1.2k_13%).

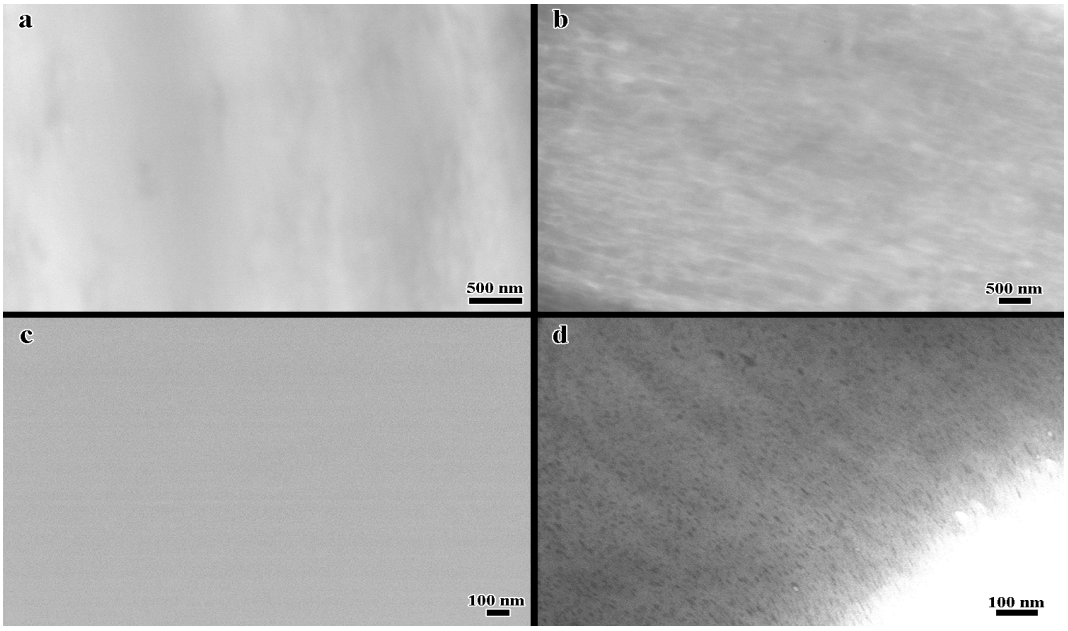

Figure 25. TEM Figures for No.1 (a), No.5 (b), No.9 (c), and No.10 (d) in experimental PC-PDMS copolymers.

5.1.5. AFM

Thin films of Dow PC, SABIC PC/PDMS, and No.5 (PC5k-PDMS0.7k_13%) were spin coated over glass slides from 10 wt% solutions in methylene chloride and also characterized in AFM, as shown in Figure 26. Dow PC is a neat PC, and therefore only one phase is observed in its AFM figure. SABIC PC/PDMS contains 5% PDMS which are present as yellow domains in its figure. The apparent yellow domain stands for the different mechanical properties of components from the matrix. It is noted that the yellow domains disperse randomly, which is in good agreement with the presence of larger domains in the TEM figures (Figure 24). Compared to SABIC PC/PDMS, No.5 (PC5k-PDMS0.7k_13%) includes more PDMS segments and shows more uniform phase dispersion and domain dimension. This can be attributed to the random copolymerization of SABIC PC/PDMS that cannot control the block length or architecture as effectively as block copolymerization applied in this study.

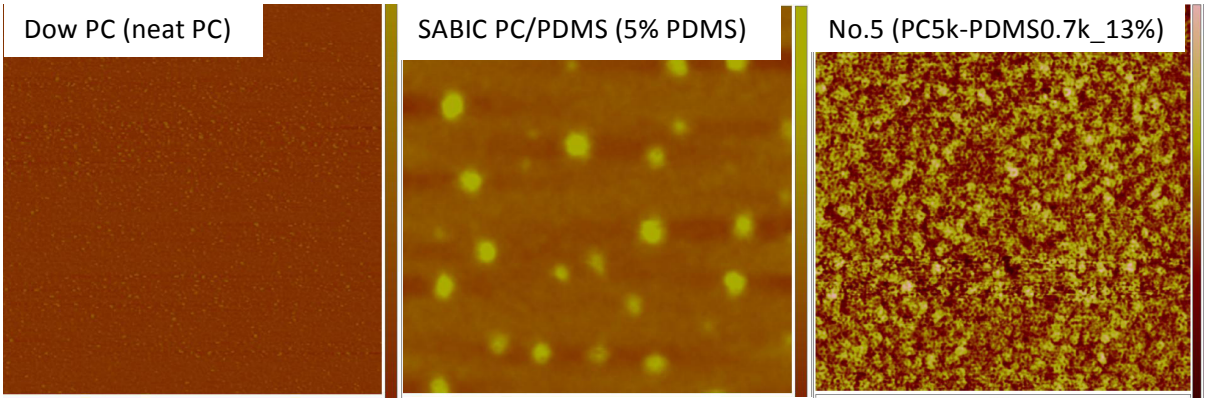

Figure 26. Comparison of AFM figures (1 μm * 1μm) for Dow PC, SABIC PC/PDMS, and No.5 (PC5k-PDMS0.7k_13%).

AFM figures for the entire 12 batches of experimental PC-PDMS block copolymers are shown in Figure 27, and the percentages shown in the figure are the percentages of PDMS in those copolymers. Compared to neat PC, the addition of PDMS leads to the surface

heterogeneity in experimental PC-PDMS copolymers. With the increase of PDMS content, the surface of copolymers concentrates more PDMS blocks, and those PDMS blocks make the surface more heterogeneous. However, when PDMS content increases to a certain value, the surface becomes smooth again. This may be because PDMS blocks have a tendency to migrate to the solid/air interface and cover the whole surface, which leads the surface to be full of one phase. It is reported by Xin Chen et al [79] that 6 wt% of PDMS in the copolymer can lead to 95 wt% of PDMS concentration on its surface when annealed at a certain temperature. Similarly, the molecular weight of PDMS block performs the same tendency. Compared to PDMS, PC has less influence on surface morphology. However, the surface becomes more heterogeneous as the content and molecular weight of PC block increases.

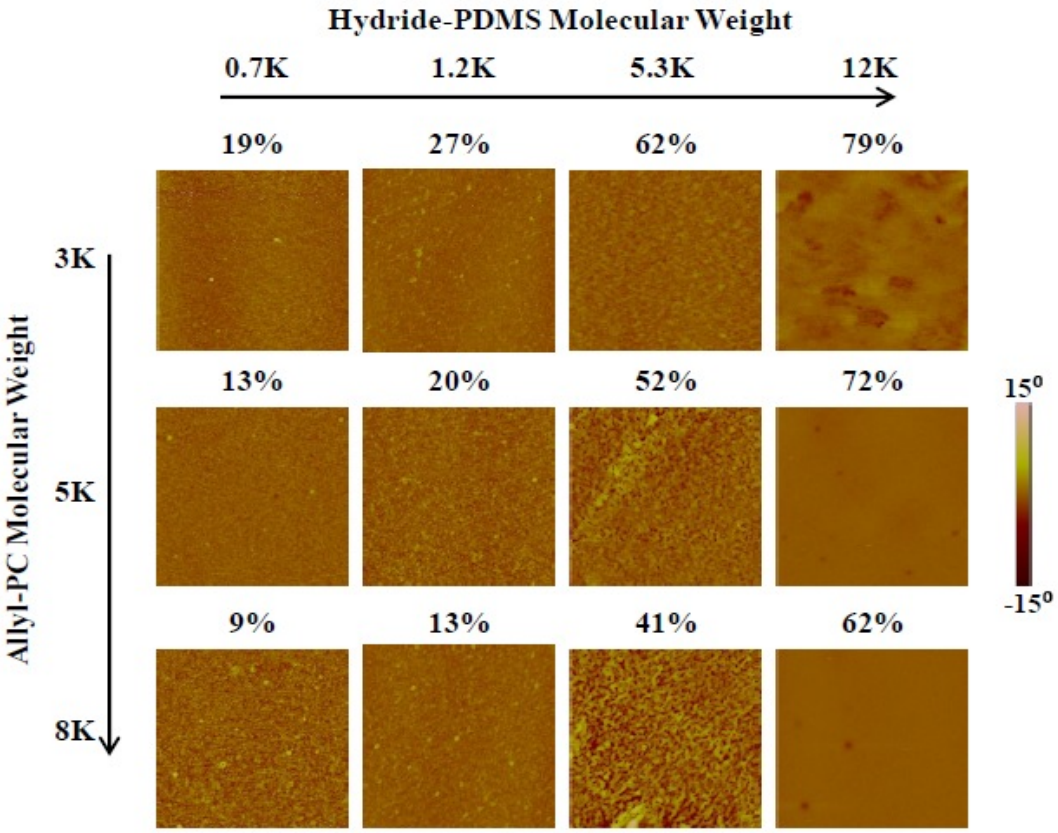

Figure 27. AFM figures (1 μm * 1μm) for experimental PC-PDMS.

5.1.6. Optical Clarity

The 12 batches of experimental PC-PDMS block copolymers were cast from chloroform into films on glass slides at room temperature to compare their optical clarity, and the results are shown in Figure 28. The percentages shown in the figure are the amounts of PDMS in the copolymers. Because of the immiscibility of PC and PDMS, microdomains rich in PC or in PDMS are formed and, consequently, microphase separation occurs. As a result, the specimens become hazy. Highly transparent materials can be observed even at 62% PDMS with relatively low molecular weights of PC and PDMS blocks. As PDMS content and the molecular weights of PC and PDMS block increase, copolymer films become hazier. This haziness is because of mismatch in the refractive indices of PC and PDMS, which are 1.585 and 1.425, respectively [52]. Similar to AFM figures, lower molecular weight PC and PDMS blocks provide higher optical clarity.

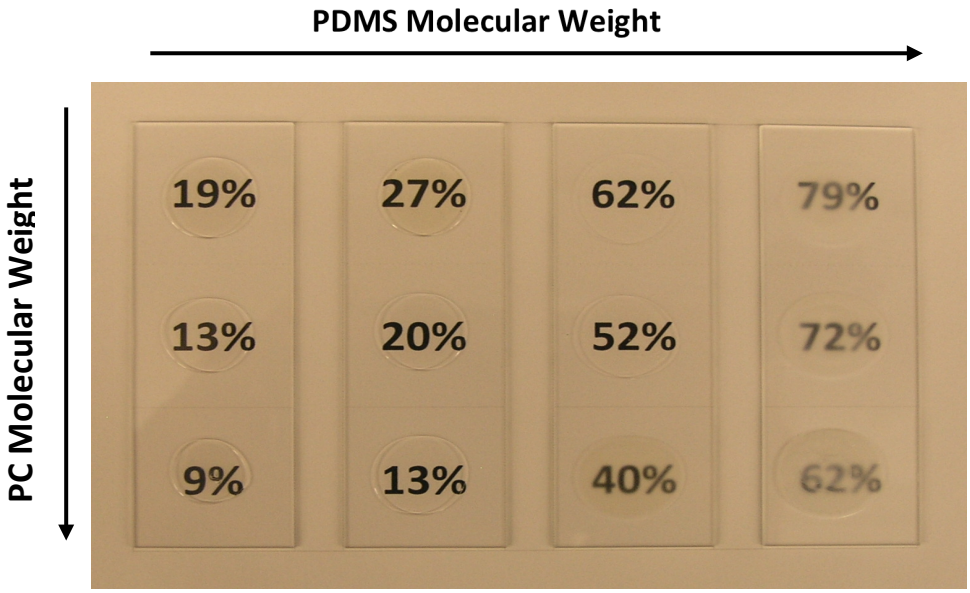

Figure 28. Comparison of optical clarity. The PDMS percentages in copolymers are shown in the figure.

The microphase-separation assumption can be supported by the calculation of the Flory-Huggins interaction parameter between PC and PDMS. The initial Flory-Huggins theory [80] is used to investigate the dissolution of a polymer in a solvent based on the assumptions: a) the freedom of polymers chains to be placed randomly on a lattice; and b) the mixing process of the flexible chains with solvent molecules. Later, Ludwik Leibler [81] applied the Flory-Huggins theory to polystyrene-polyimide (PS-PI) block copolymers and found that the Flory-Huggins interaction parameter χ_{12} and polymerization index N of PS-PI block copolymers can be calculated to determine the critical value for microphase separation transition in PS-PI.

According to the Flory-Huggins theory, the Gibbs' free energy increase of mixing, ΔG_m, for a polymer-polymer system in absence of solvent can be written as follows:

$$\Delta G_m = RT\left[\ln \emptyset_1 + (1 - \frac{m_1}{m_2})\emptyset_2 + \chi_{12} m_1 \emptyset_2^2\right] \quad (5\text{-}11)$$

where $\emptyset_i$ is its volume fraction of the ith component in the mixture, and $\emptyset_i = \frac{m_i n_i}{m_i n_i + m_j n_j}$ ($i, j = 1,2$ and $i \neq j$). χ_{12} refers to the Flory-Huggins interaction parameter between polymer 1 and 2. m_i is essentially the degree of polymerization, relating the molar volumes V_1 and V_2 of the polymers to a fictitious molar volume V_0 of one submolecule of polymer:

$$m_1 = {V_1}/{V_0} \quad (5\text{-}12)$$

$$m_2 = {V_2}/{V_0} \quad (5\text{-}13)$$

$$\frac{m_1}{m_2} = \frac{{\bar{M}_{n,1}}/{\rho_1}}{{\bar{M}_{n,2}}/{\rho_2}} \quad (5\text{-}14)$$

where $\bar{M}_n$ is the number average molecular weight and ρ is the density of polymer. In the original Flory-Huggins theory, the choice of V_0 should be the smallest among the molar volume of the solvent and the molar volumes of the repeating units of the polymer in the mixture [82]. In the PC-PDMS system, the repeating units of PC and PDMS are listed in Table 8 below:

Table 8. Molar volume of PC and PDMS.

	PC	PDMS
Repeating Unit	$-C_6H_4-C(CH_3)_2-C_6H_4-O-CO-O-$	$-Si(CH_3)_2-O-$
Molecular Weight, M (g/mol)	254	74
Density, ρ (g/cm^3)	1.2	0.97
Molar Volume, $V = {}^{M}/_{\rho}$ (cm^3/mol)	211.67	76.29

Based on the values in Table 8, the repeating unit of PDMS is smaller than that of PC; as a result, the molar volume of PDMS is considered as V_0.

In general, a mixture obtains a critical condition that is the co-existing phases of two polymers when the first and second derivatives of ΔG_m are equal to zero. Thus, a critical Flory-Huggins interaction parameter, $(\chi_{12})_{critical}$, can be obtained as

$$(\chi_{12})_{critical} = \frac{1}{2}\left(\frac{1}{\sqrt{m_1}} + \frac{1}{\sqrt{m_2}}\right)^2 \quad (5\text{-}15)$$

In addition, the miscibility between two polymers can be estimated by their solubility parameters δ that are determined by the energy related with cohesive energy density [83]. Once the solubility parameters of polymer components are obtained, the Flory-Huggins interaction parameter χ_{12} can be calculated by the following equation:

$$\chi_{12} = \frac{V_0(\delta_1 - \delta_2)^2}{RT} \quad (5\text{-}16)$$

where δ_1, δ_2 are the solubility parameters of polymer 1 and 2, respectively. R is the universal gas constant, and T is the absolute temperature.

After calculating $(\chi_{12})_{critical}$ and χ_{12}, the miscibility between two polymers can be determined by comparing their values. If the value of χ_{12} is smaller than the critical value, two polymers in the mixture are completely miscible. If χ_{12} is considerably greater than the critical

value, the two polymers are totally immiscible and phase separation occurs, and only one polymer can be in both phases. On the other hand, if χ_{12} is slightly greater than the critical value, the mixture is partially miscible and two polymers can be found in each phase [82].

By applying equations (5-11) to (5-16), $(\chi_{12})_{critical}$ and χ_{12} can be calculated for PC-PDMS multiblock copolymers, No.5 (PC5k-PDMS0.7k_13%), No.9 (PC8k-PDMS0.7k_9%), and No.10 (PC8k-PDMS1.2k_13%), and the results are shown in Table 9.

Table 9. $(\chi_{12})_{critical}$ and χ_{12} for PC-PDMS multiblock copolymers.

	No.5 (PC5k-PDMS0.7k_13%)	
	PC	PDMS
δ (cal$^{1/2}$/cm$^{3/2}$)	9.5	7.5
Mn (g/mol)	4760	765
ρ (g/cm^3)	1.2	0.97
V (cm^3/mol)	3966.67	788.66
m (m=V/V_0)	52.00	10.34
$(\chi_{12})_{critical}$	0.10	
χ_{12}	0.28	

According to Table 9, it is found that χ_{12} (0.28) is slightly greater than the critical value (0.10) for No.5 (PC5k-PDMS0.7k_13%); as a result, PC and PDMS are partially miscible in the copolymer and it is possible that microphase separation can occur. Similarly, No.9 (PC8k-PDMS0.7k_9%) ($\chi_{12} = 0.28$) and No.10 (PC8k-PDMS1.2k_13%) ($\chi_{12} = 0.28$) are also slightly greater than their critical values (0.088 for No.9 and 0.064 for No.10). Therefore PC and PDMS are also partially miscible in the copolymer, and microphase separation occurs. As a consequence, the optical clarity decreases in PC-PDMS block copolymers.

5.2. Results and Discussion of PC/PC-PDMS-PC Blends

Three batches of PC/PC-PDMS-PC blends were compounded in this study using PC-PDMS-PC triblock copolymers T1 (PC3k-PDMS12k_72%), T2 (PC5k-PDMS12k_57%), and T3 (PC5k-PDMS23k_72%). In order to match triblock copolymers to its blends, T1, T2, and T3 in the following discussion stand for the related PC/PC-PDMS-PC blends. These blends were all injected into rectangular bars, so that the notched Izod impact test, DMA, and rheological test could be applied to obtain those blends' various properties. The three-point bending flexural test and tensile test were also applied to measure materials' stiffness and flexural strength. In addition, Dow PC and SABIC PC/PDMS were injected to compare the properties of those blends. The details of material used in this section are listed in Table 10.

Table 10. Details of PC/PC-PDMS-PC Blends, Dow PC, and SABIC PC/PDMS.

Sample		PC in Triblock Copolymers		PDMS in Triblock Copolymers		PC-PDMS-PC Mn (g/mol)	PDMS Content in Blends (%)
		Mn (g/mol)	wt%	Mn (g/mol)	wt%		
PC/PC-PDMS-PC Blends	**T1**	2700	28	12400	72	20080	3.0
	T2	4600	43	12400	57	20950	3.0
	T3	4600	28	23200	72	20070	3.0
Dow PC		-	100	-	0	21900	0
SABIC PC/PDMS		-	95	-	5	27600	5

5.2.1. Notched Izod Impact Results

PC/PC-PDMS-PC blends, Dow PC, and SABIC PC/PDMS were impacted to obtain their impact strength. Five specimens were used for each kind of those materials, and the results are shown in Figure 29. During the impact tests, all specimens did not fail completely; instead, they hinged above 95%. This phenomenon may indicate that these impact tests are near the highest capacity of the test machine. It is noted that Dow PC and SABIC PC/PDMS possess the higher

impact strength than the triblock blends. The reason might be that the three triblock blends are prepared by physical blending, while SABIC PC/PDMS and Dow PC are chemically polymerized. The interaction is weaker in physical blends than chemical polymers.

Comparing the three triblock blends, it is observed that they have overlap in their standard deviations; as a result, there is little difference in impact strengths among the three triblock blends at room temperature. This little difference may be caused by the small portion of PC-PDMS copolymer in the whole blend. 3 wt% of PC-PDMS copolymer could not affect the impact toughness of the whole blend that much.

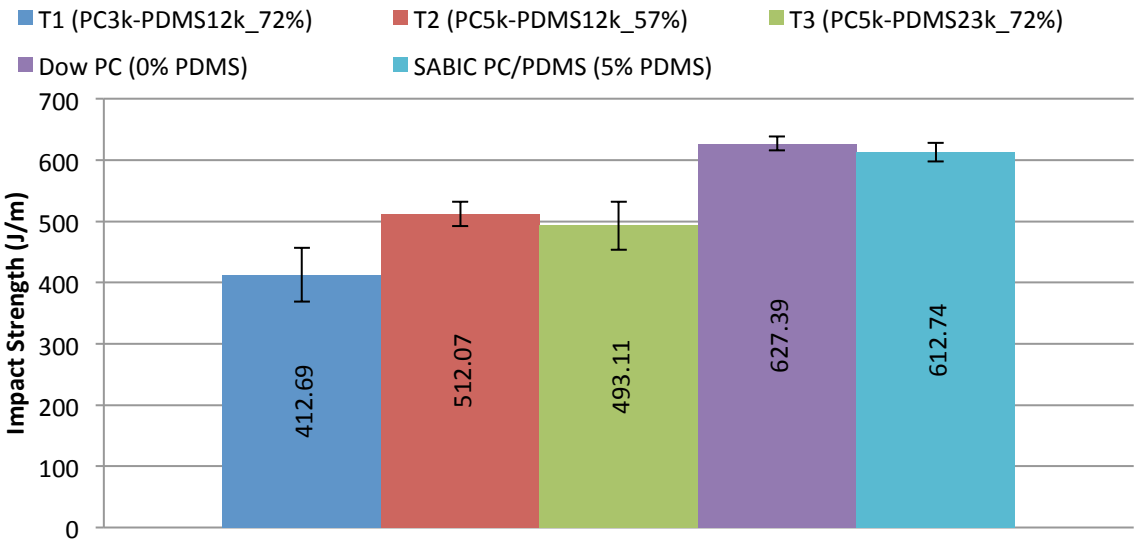

Figure 29. Notched Izod impact strength of PC/PC-PDMS-PC blends, Dow PC, and SABIC PC/PDMS.

5.2.2. Impact Strength-Temperature Relationships

Since the influence of PDMS on PC's impact strength is not as significant as expected, impact strength-temperature relationships are investigated to study the PDMS's effect on PC's ductile-brittle transition temperature (DBTT). The ductile-brittle transition can be observed in

notched Izod impact tests, and it happens because the yield stress is lower than the fracture stress. At low temperature, the yield stress is higher than fracture stress, which leads to a brittle fracture. As temperature increases, yield stress decreases with a faster speed than that of fracture stress; as a result, ductile fracture replaces brittle fracture, and plastic deformation occurs and then is dissipated as heat [84].

Impact strength-temperature curves are shown in Figure 30. It can be observed that three types of impact strength-temperature relationship are present: A) Dow PC and T1 (PC3k-PDMS12k_72%); B) T2 (PC5k-PDMS12k_57%); C) SABIC PC/PDMS and T3 (PC5k-PDMS23k_72%). In type A, the impact strength remains steady before 10 °C and then increases dramatically after it, which indicates the DBTTs of Dow PC and T1 (PC3k-PDMS12k_72%) are in the range of 10 °C to room temperature. It is in accordance with the fact that the DBTT of pure PC is around room temperature. T1 (PC3k-PDMS12k_72%) performs a similar ductile-brittle transition because the molecular weights of PDMS and PC blocks in the copolymer phase are so low that they affect PC matrix little. As the molecular weight of PC block in the copolymer phase increases, the DBTT of T2 (PC5k-PDMS12k_57%) decreases to the range of -10 °C to 0 °C. When the molecular weights of PDMS and PC blocks in the copolymer phase increases at the same time, the DBTT of T3 (PC5k-PDMS23k_72%) decreases even lower, which is in the range of -30 °C to -20 °C and similar to the DBTT of SABIC PC/PDMS. Based on these trends, it can be concluded that the addition of PDMS lowers PC's DBTT, which makes PC blends easier to transfer from brittle failure to ductile failure and, subsequently, improves PC's toughness at relatively low temperature. In addition, block molecular weight in the copolymer phase plays a more important role than PDMS content, and DBTT lowers as the PC

or PDMS block molecular weight increases. It can be attributed to the effect of block molecular weight on the domain size in blends, which will be discussed in part 5.2.3.

In the ductile-fracture region, most of the specimens keep their impact strength in a relative high value except T3 (PC5k-PDMS23k_72%). The impact strength of T3 (PC5k-PDMS23k_72%) decreases at room temperature. One reason is that as temperature increases, the domain of the ductile deformation ahead of the notch actually gets smaller instead of larger; in other words, ductile deformation is more localized around the notch at higher temperature [85].

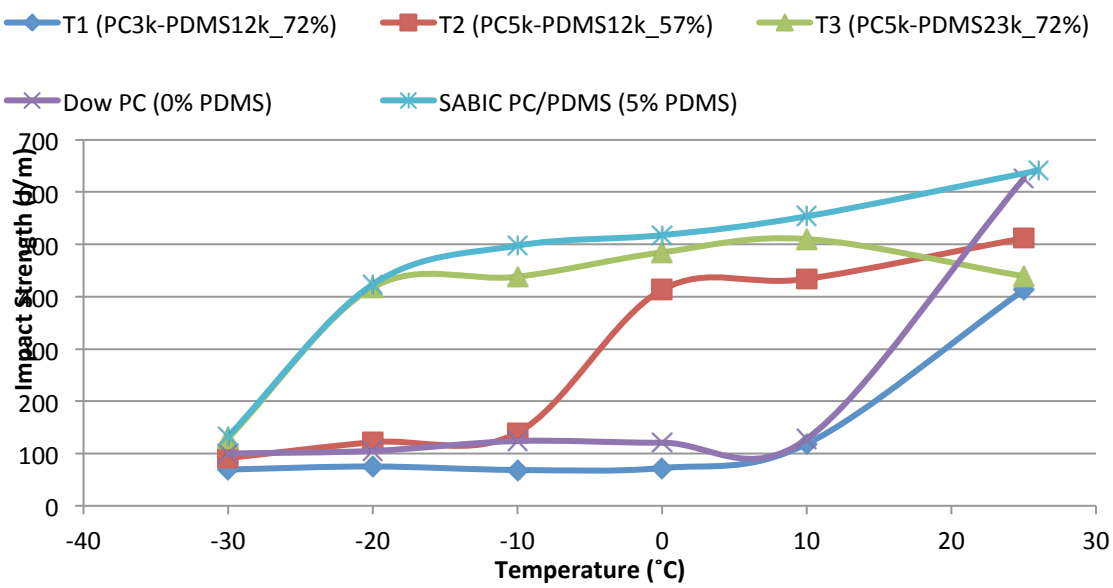

Figure 30. Impact-temperature relationships of triblock blends, Dow PC, and SABIC PC/PDMS.

5.2.3. SEM

In order to explain the decrease of DBTT in triblock blends, the morphology of the fracture surface is characterized by SEM. As is known, brittle fracture and ductile facture are the two typical fractures in materials. Not only can they be quantified by impact energy, but they also can be qualified by the morphology of the fracture surface.

A typical brittle fracture surface includes origin (crack initiation), smooth mirror (slow crack growth), mist (transitional region from slow crack growth to fast crack growth), and hackle (fast crack growth, can be elongated to form "river markings"). During a brittle fracture, the fracture is generally controlled by plane strain, and the crazing is usually observed in the surface as the plastic deformation; while a ductile fracture usually occurs under plain-stress conditions, and it is featured by shear yielding and multiple crazing in the surface as the plastic deformation, leading to a fibril-like surface shown in the SEM image [86].

Crazes are generated by the interpenetrated network of microvoids in materials; as a result, crazing occurs with an increased volume in materials. In addition, crazes can weaken materials' toughness as lower-energy crack paths when pre-existing; conversely, they are formed to dissipate energy during their formation. The shear yielding consists of strain localization with little or no volume change. Moreover, a high degree of strain softening can lead to shear bands, which suppress the formation of crazes. This suppression is because the direction of the uniaxial tensile stress in shear bands is 45° ± 8°, while the orientation of stress in crazes is 90° [87]. In addition, surface flaws and internal defects can be used as stress concentrators to initiate shear bands, which, subsequently, dissipate more energy and increase materials' toughness.

Rubber toughening is a widely used way to improve materials' impact strength and shift ductile-brittle transition point into a lower temperature. Rubber particles can be used as stress concentrators due to their lower modulus compared to the matrix, and they concentrate applied stress around them to generate local nucleations of plastic deformation like shear yielding. When the rubber particles are dispersed separately, the concentrated stress does not affect others, leading to a little improvement in materials' impact strength; conversely, when the particles have a fine dispersion and are close enough to each other, the concentrated stress will interact

effectively to enhance materials' yielding and shift ductile-brittle transition to a lower temperature [87].

Cavitation toughening is one of the rubber toughening mechanisms. The formation of the cavities occurs when the stored volumetric strain energy is greater than the energy required for the creation and expansion of the surface area of the void [88]. Then the relatively weak interaction between rubber particles and polymer matrix is broken and debonding between these two phases occurs, which leaves cavitation in one surface of the polymer matrix and rubber particle on the other surface. Therefore, these cavities suppress the generation of crazing of polymers and develop plastic deformation and thus increase materials' toughness [89].

Figures 31-35 show the SEM figures of T1 (PC3k-PDMS12k_72%), T2 (PC5k-PDMS12k_57%), T3 (PC5k-PDMS23k_72%), Dow PC and SABIC PC/PDMS, respectively. These left figures were taken at the area near the notch on the fracture surface of samples with a low magnification (X150), and the right figures are the high magnifications (X3000) of the left figures. It is observed that all blends show cavitation at high magnification while Dow PC and SABIC PC/PDMS do not. This is because Dow PC is a neat PC and therefore a homogenous single phase. For SABIC PC/PDMS, the domain size of PDMS phase is too small to form cavitation. According to Eldridge M. Mount [90] and Clive B. Bucknall [91], rubber particles with diameters between 0.1 and 10 microns are more likely to generate cavitation in blends. The PDMS domain is ranged from 5 to 150 nm in SABIC PC/PDMS according to Figure 24, and the triblock copolymer domain is ranged from 0.3 to 4 microns in T1, 0.2-2.5 microns in T2, and 0.04-0.8 microns in T3 according to Figure 31 (d), Figure 32 (f), and Figure 33 (d), respectively. As a consequence, cavitations are shown in T1, T2, and T3, not in Dow PC or SABIC PC/PDMS.

According to these images, it can be clearly seen that there is a ductile-brittle transition in fractures. Take T2 (PC5k-PDMS12k_57%) as an example. When comparing Figure 32 a), c) and e), it can be noted that Figure 32 a) shows a jagged and cratered appearance on the surface that suggests a rapid crack propagation; while Figure 32 c) contains fibrils morphology as well as the jagged appearance that implies the presence of large plastic deformation before the rapid crack propagation; Figure 32 e) shows more fibrils and yielding that indicates more plastic deformation and more absorbed impact energy. As a result, the DBTT of T2 (PC5k-PDMS12k_57%) should be in the range of -10 °C to 0 °C. Similarly, the DBTTs of T1 (PC3k-PDMS12k_72%) and Dow PC should be between 10 °C and room temperature, and those of T3 (PC5k-PDMS23k_72%) and SABIC PC/PDMS should be between -30 °C and -20 °C. These DBTT results are in good accordance with the results of Figure 29.

When contrasting high magnification images of triblock blends, it can be observed that all the images contain voids below DBTT. As is known, materials are prone to show brittle fracture belows DBTT; in addition, these voids are smooth-surface spherical without any deformation. As a result, these voids are internal defects generated due to the poor bonding of PC phase and PC-PDMS-PC copolymer phase. As temperature increases, materials go through the ductile-brittle transition, and some cavitation is formed as shown in the SEM images. The cavitation are the voids that are stretched and may have whitening around them.

After differentiating from cavitation and internal defects, it can be clearly noted that T3 (PC5k-PDMS23k_72%) has finer cavitation with smaller size and higher quantity, T2 (PC5k-PDMS12k_57%) is in the second place, and T1 (PC3k-PDMS12k_72%) has the least fine cavitation. As discussed above, cavitation is the mechanism of rubber toughening of these blends; based on these SEM images, it can be concluded that T3 (PC5k-PDMS23k_72%), which has the

finest cavitation, improves toughness at low temperature most effectively, T2 (PC5k-PDMS12k_57%) follows, and T1 (PC3k-PDMS12k_72%) is the least effective one. This result is in good agreement with the DBTTs of these blends, which is T3 (PC5k-PDMS23k_72%) has the lowest DBTT, T2 (PC5k-PDMS12k_57%) has higher DBTT, and T1 (PC3k-PDMS12k_72%) has the highest one. It can be explained that T1 (PC3k-PDMS12k_72%) contains shorter polymer block chains and therefore the blocks in the copolymer phase are more miscible with each other than T3 (PC5k-PDMS23k_72%). When the blends are mixed in the extruder at high temperatures, the miscibility between blocks increases, thus the T1 (PC3k-PDMS12k_72%) blocks are more miscible with each other and the tri-block polymer domains are less interacted with the surrounding PC matrix. Conversely, the T3 (PC5k-PDMS23k_72%) blocks repulse each other and are prone to interact with the surrounding PC matrix. As a result, T3 (PC5k-PDMS23k_72%) has lower interface repulsion between the PC matrix and copolymer phase and, subsequently, smaller and more homogenous domain size and lower DBTT.

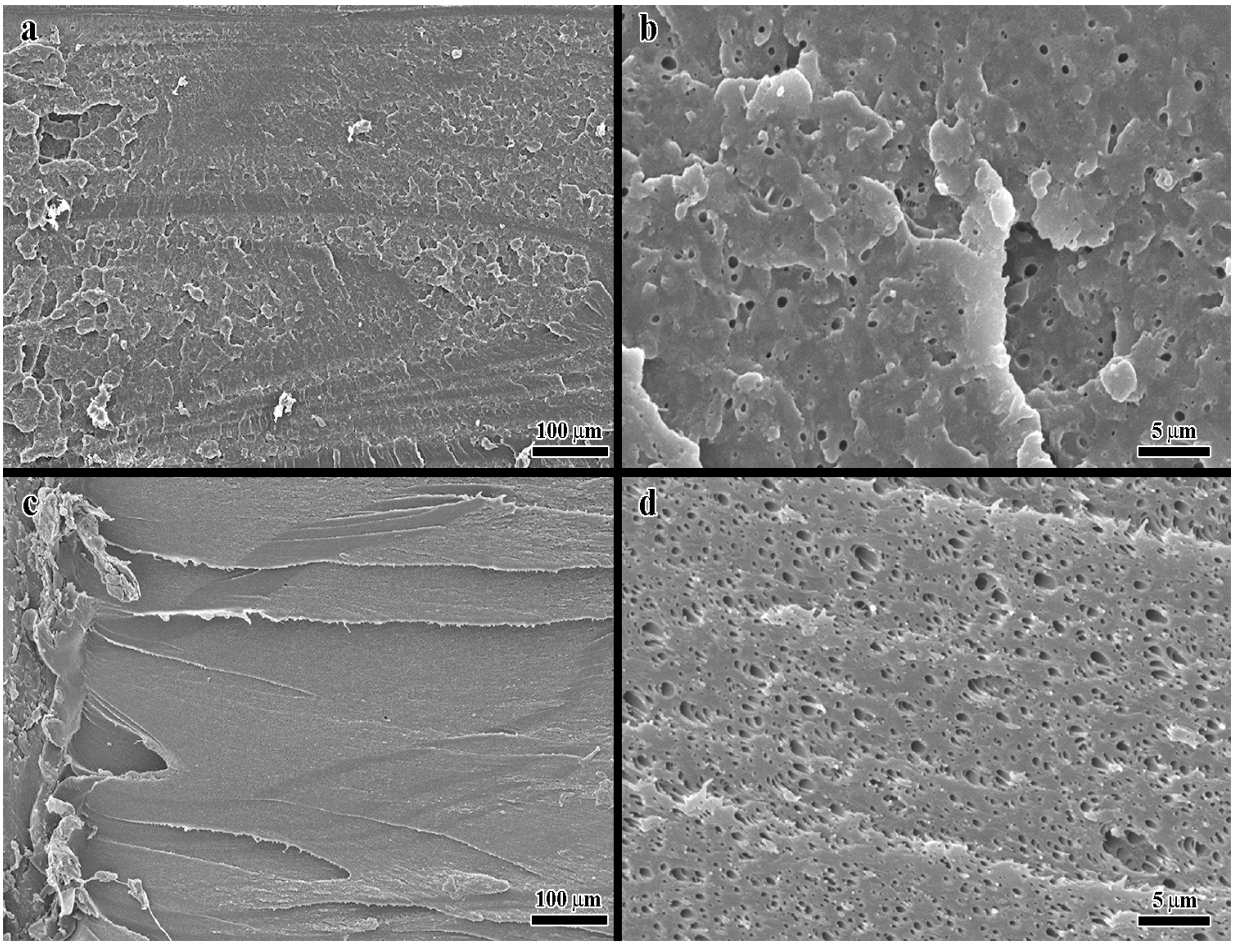

Figure 31. SEM figures of T1 (PC3k-PDMS12k_72%), a) T1 at 10 °C and X150; b) T1 at 10 °C and X3000; c) T1 at room temperature and X150; and d) T1 at room temperature and X3000.

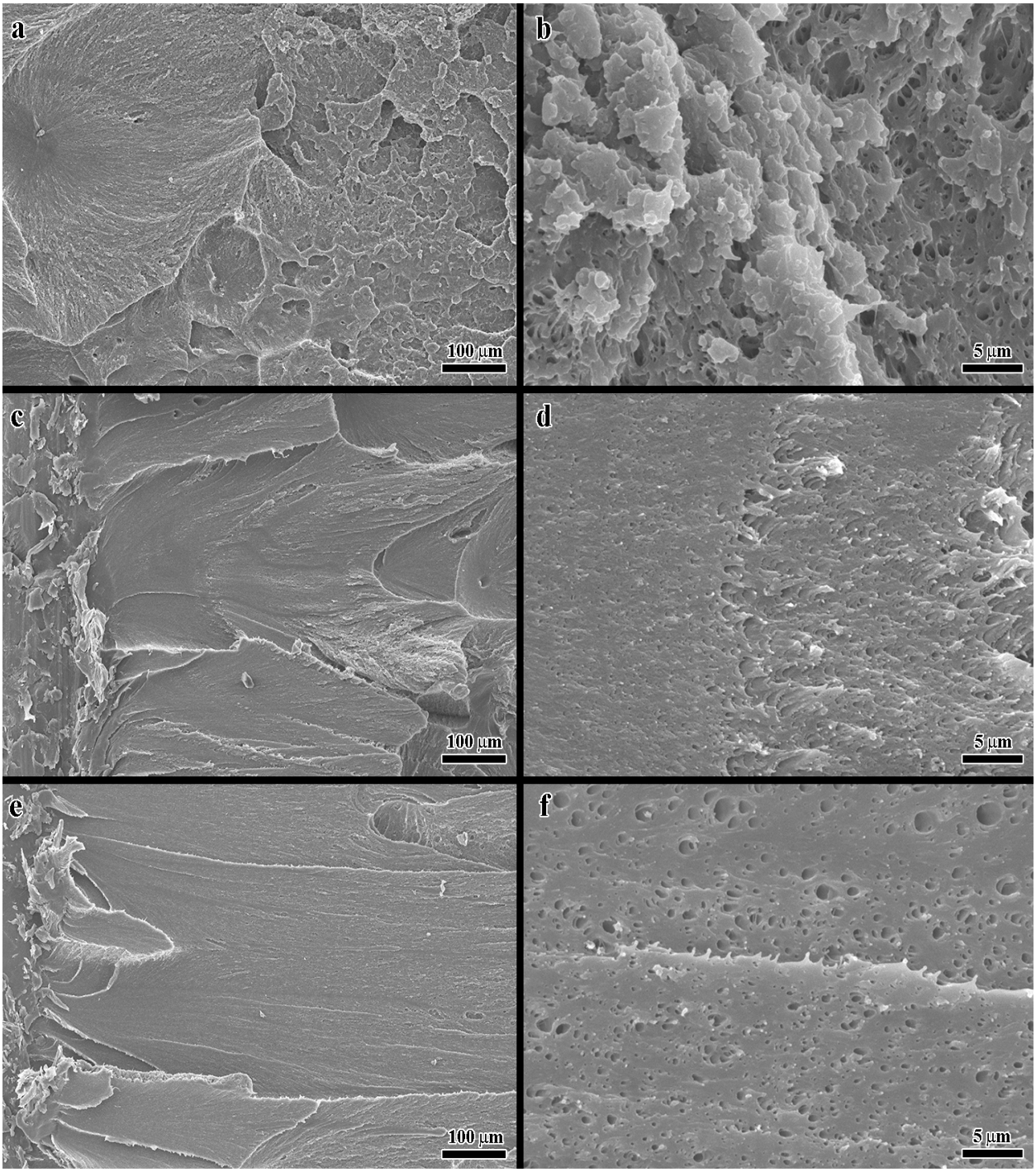

Figure 32. SEM figures of T2 (PC5k-PDMS12k_57%), a) T2 at -10 °C and X150; b) T2 at -10 °C and X3000; c) T2 at 0 °C and X150; d) T2 at 0 °C and X3000; e) T2 at 10 °C and X150; and f) T2 at 10 °C and X3000.

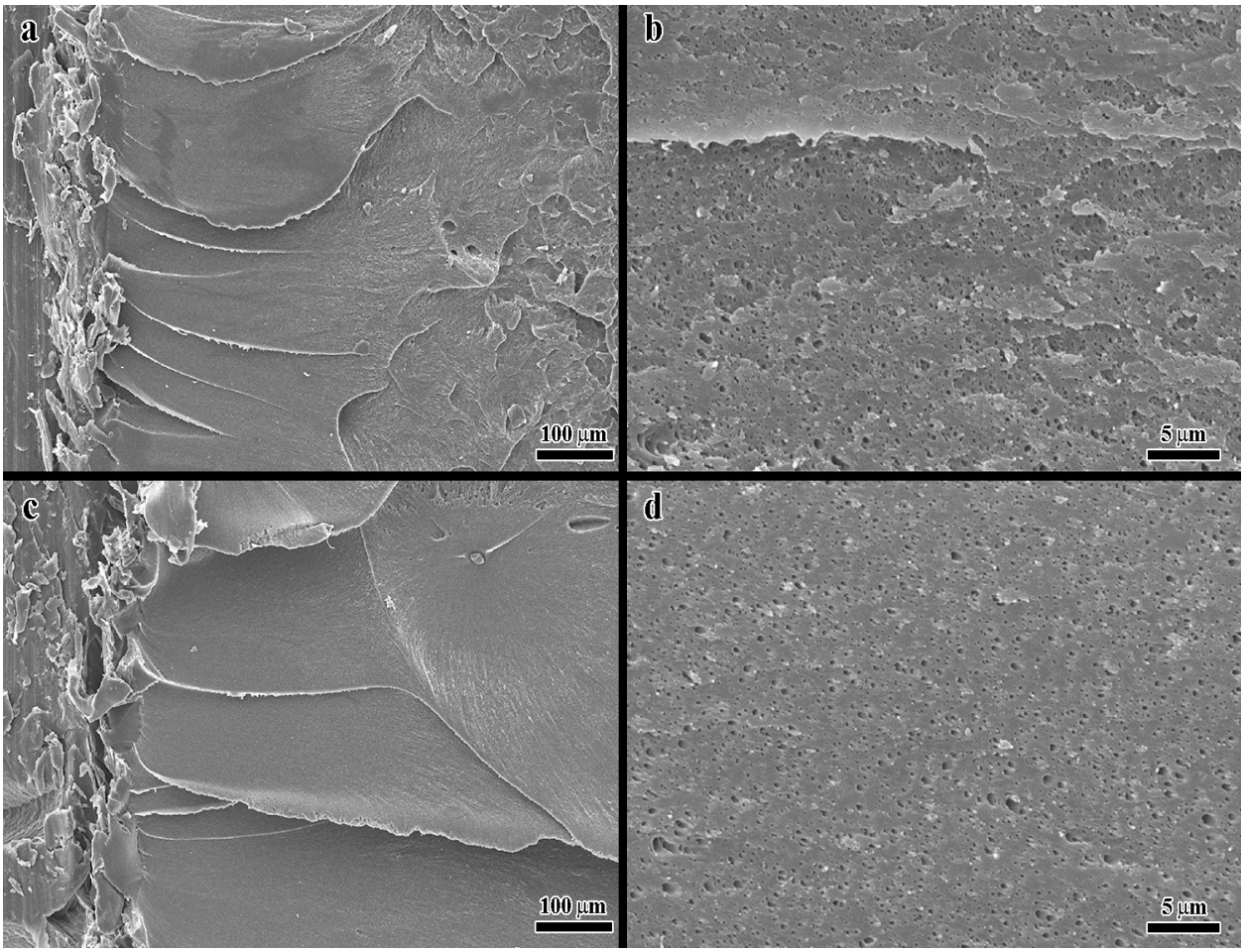

Figure 33. SEM figures of T3 (PC5k-PDMS23k_72%), a) T3 at -30 °C and X150; b) T3 at -30 °C and X3000; c) T3 at -20 °C and X150; d) T3 at -20 °C and X3000.

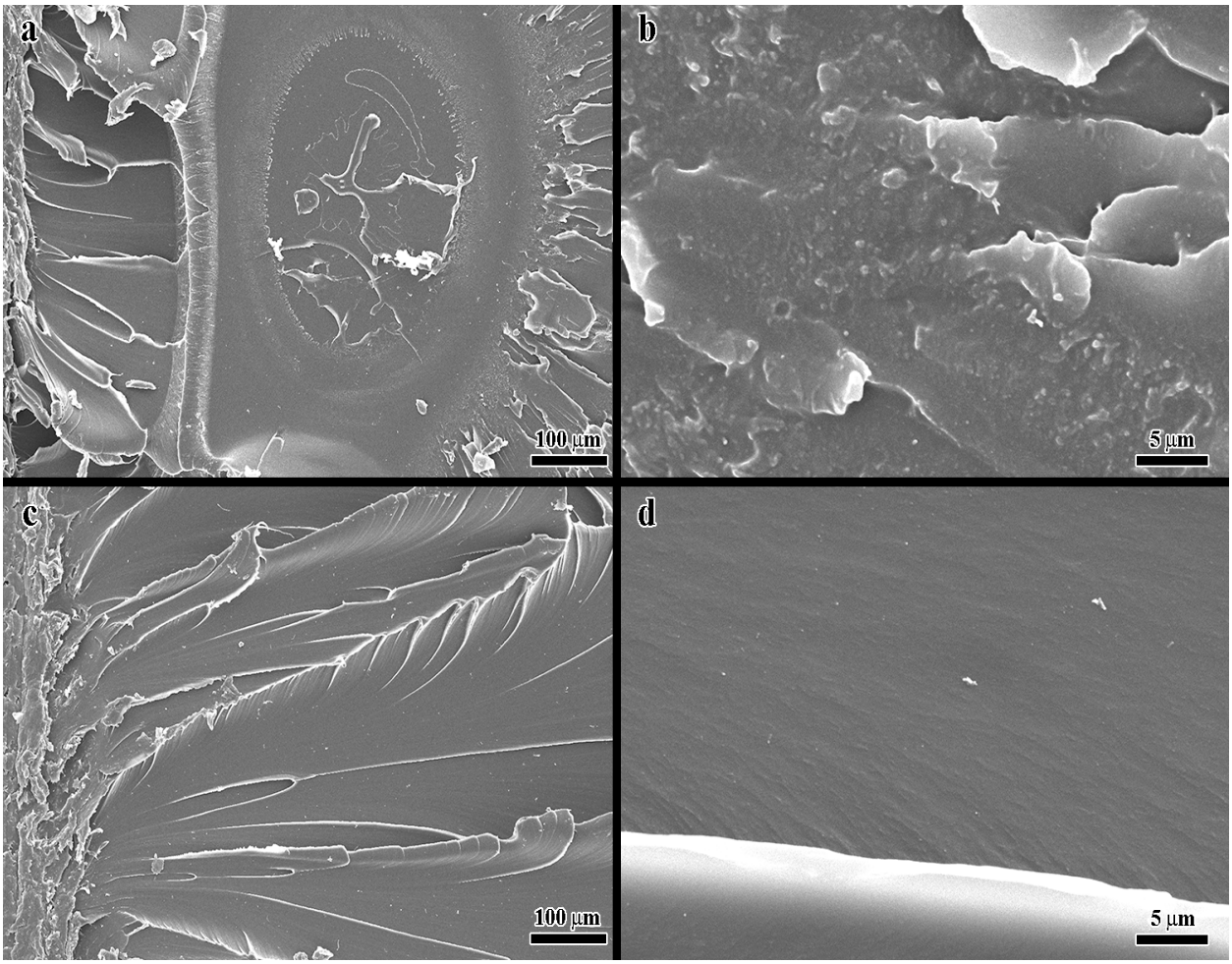

Figure 34. SEM figures of Dow PC (pure PC), a) Dow PC at 10 °C and X150; b) Dow PC at 10 °C and X3000; c) Dow PC at room temperature and X150; and d) Dow PC at room temperature and X3000.

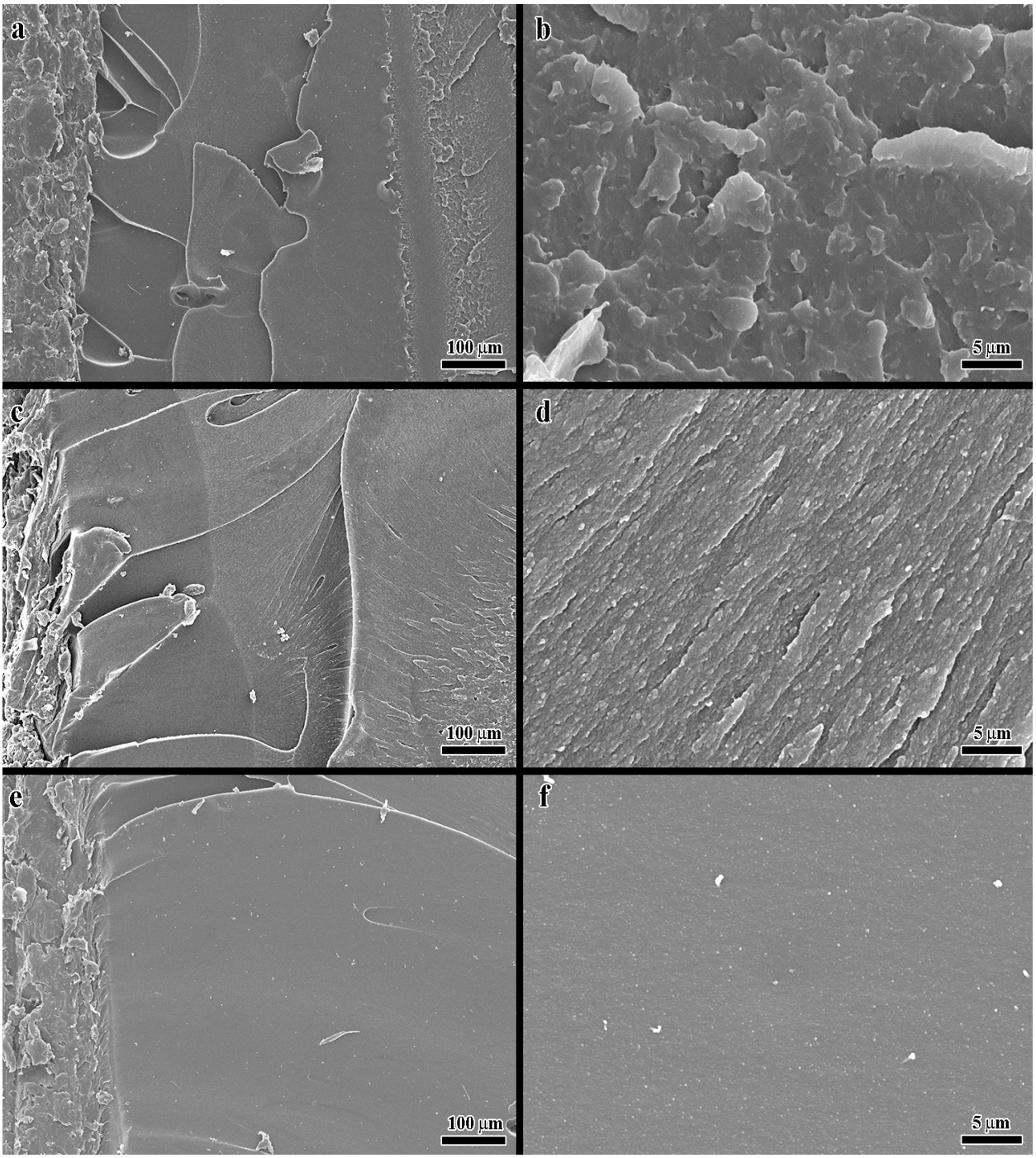

Figure 35. SEM figures of SABIC PC/PDMS, a) SABIC PC/PDMS at -40 °C and X150; b) SABIC PC/PDMS at -40 °C and X3000; c) SABIC PC/PDMS at -30 °C and X150; d) SABIC PC/PDMS at -30 °C and X3000; e) SABIC PC/PDMS at -20 °C and X150; and f) SABIC PC/PDMS at -20 °C and X3000.

In the fracture surfaces of these five materials below DBTT, it is easily found that there are protuberant ridges in the middle, which are shown in Figure 36-40s. Take T1 (PC3k-

PDMS12k_72%) in Figure 36 for an example. The ridge in Figure 36 a) suggests the generation of a fast stick-slip like crack propagation and the crack is temporarily slowed down in the ridge. Figure 36 b) shows a stress whitening in the stick-slip line, which implies large plastic deformation during the fracture and results in a slow crack propagation in the ridge. High magnifications of surface morphology before and in the protuberant ridge are shown in Figure 36 c) and d), respectively. It is noted that d) shows a more jagged and cratered appearance that suggests a rapid crack propagation, while c) contains shear-deformed cavitation that indicates plastic deformation.

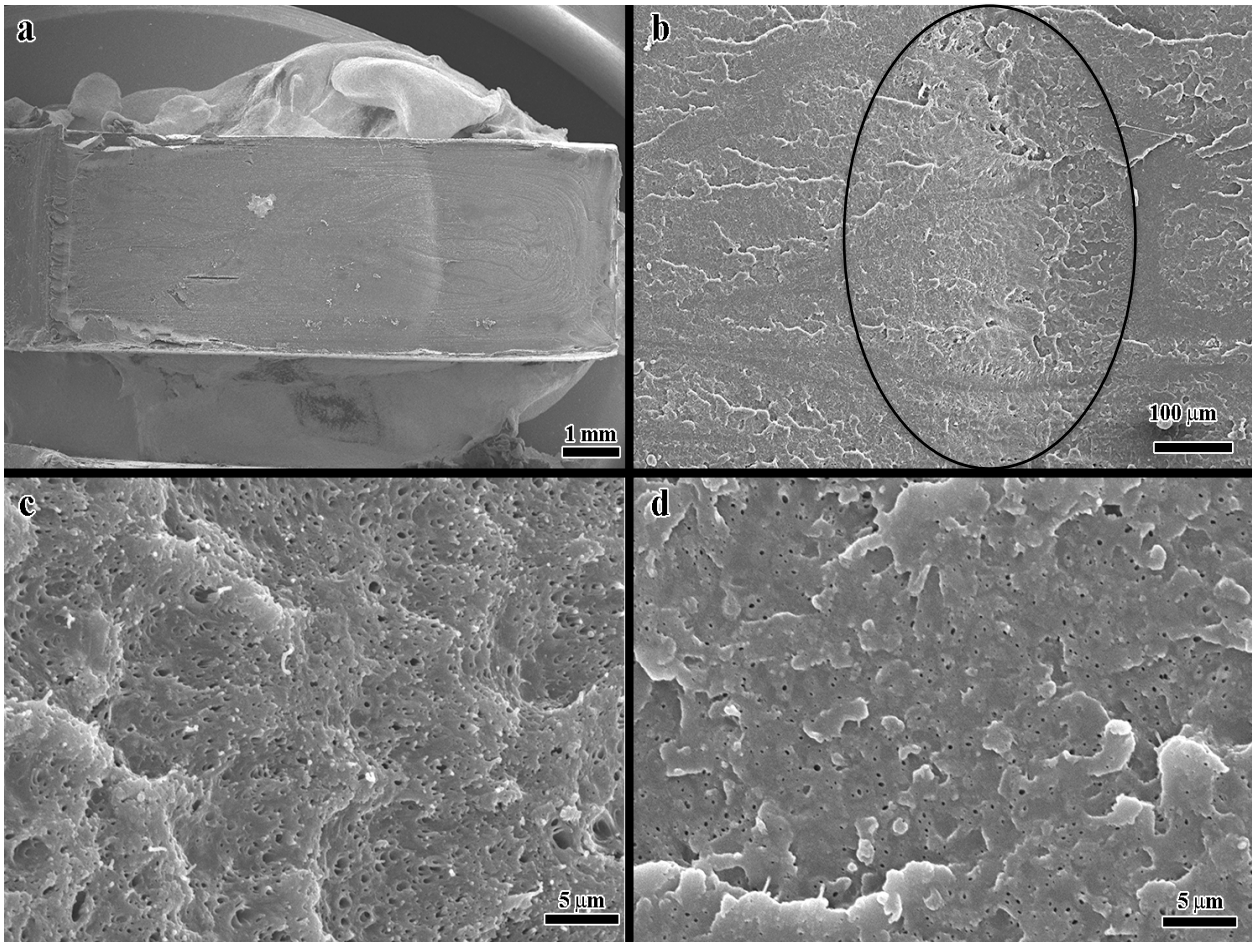

Figure 36. a) Stick-slip lines (ridge) in the middle of the fracture surface in T1 (PC3k-PDMS12k_72%) under DBTT at 10 °C and X11; b) ridge in T1 at 10 °C and X150; c) SEM figure for surface before the ridge at 10 °C and X3000; and d) SEM figure for surface after the ridge at 10 °C and X3000.

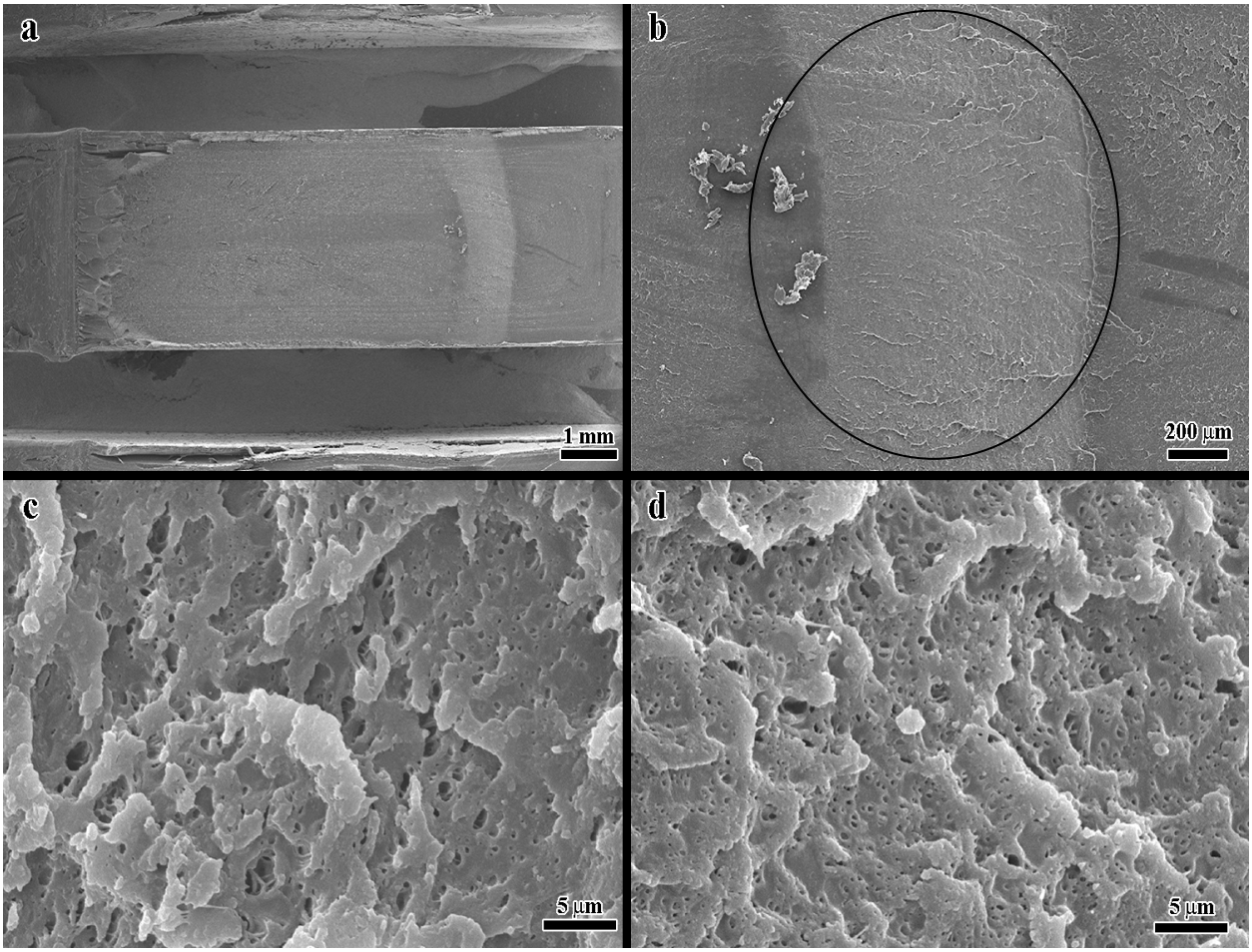

Figure 37. a) Stick-slip lies (ridge) in the middle of the fracture surface in T2 (PC5k-PDMS12k_57%) under the DBTT at -10 °C and X11; b) ridge in T2 at -10 °C and X60; c) SEM figure for surface in the ridge at -10 °C and X3000; and d) SEM figure for surface after the ridge at -10 °C and X3000.

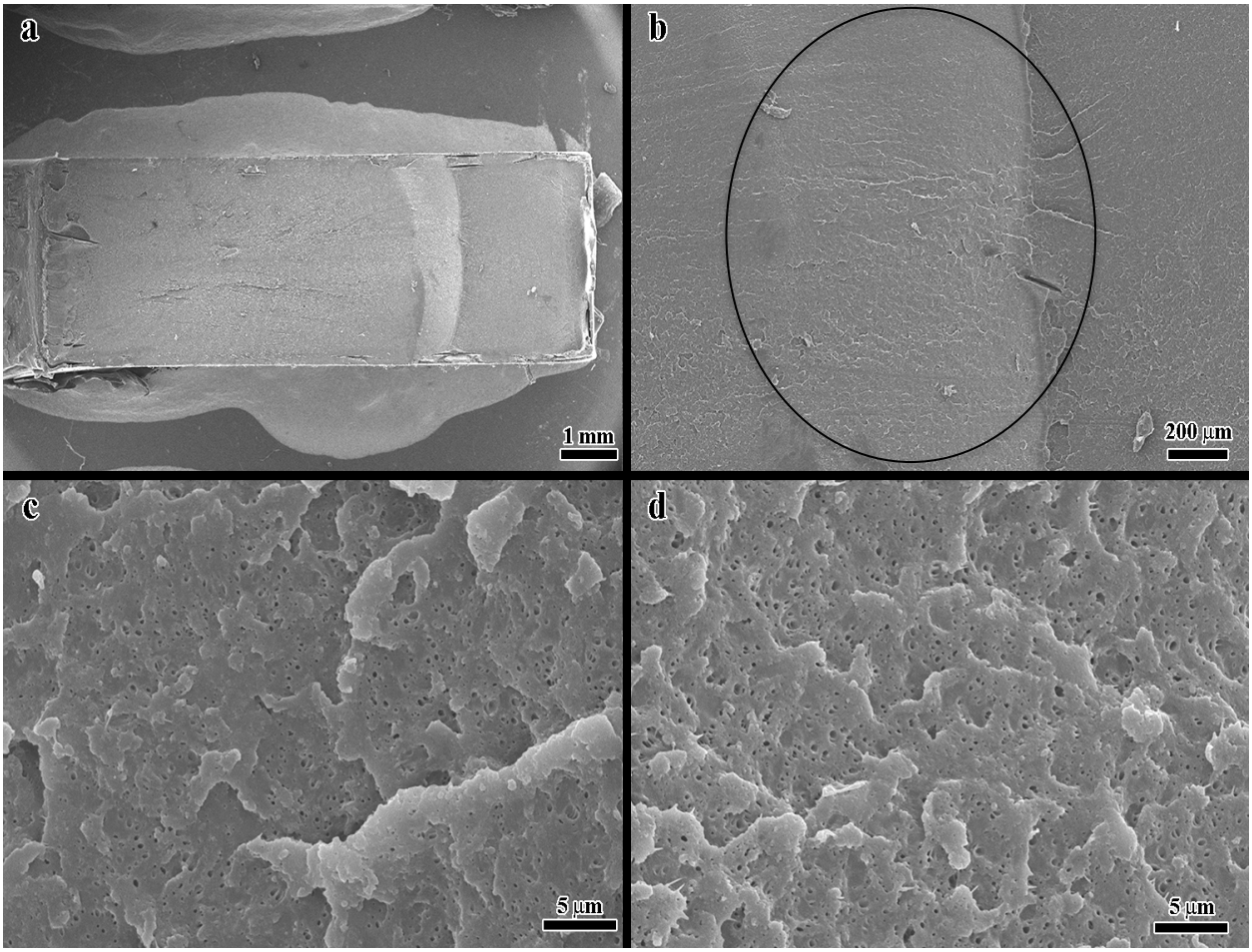

Figure 38. a) Stick-slip lies (ridge) in the middle of the fracture surface in T3 (PC5k-PDMS23k_72%) under DBTT at -30 °C and X11; b) ridge in T3 at -30 °C and X60; c) SEM figure for surface in the ridge at -30 °C and X3000; and d) SEM figure for surface after the ridge at -30 °C and X3000.

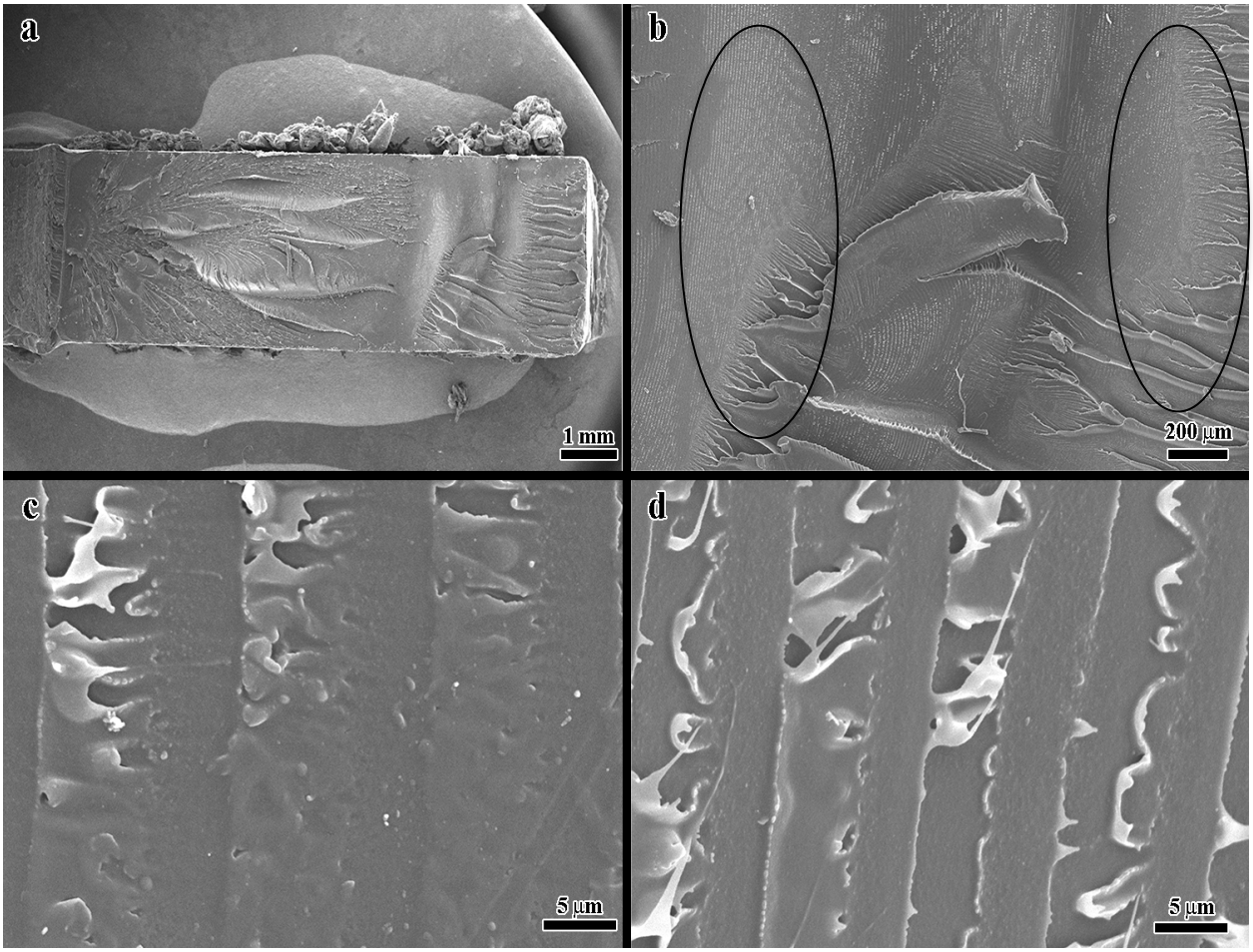

Figure 39. a) Stick-slip lies (ridge) in the middle of the fracture surface in Dow PC under DBTT at 10 °C and X11; b) ridge in Dow PC at 10 °C and X60; c) SEM figure for surface in the ridge at 10 °C and X3000; and d) SEM figure for surface after the ridge at 10 °C and X3000.

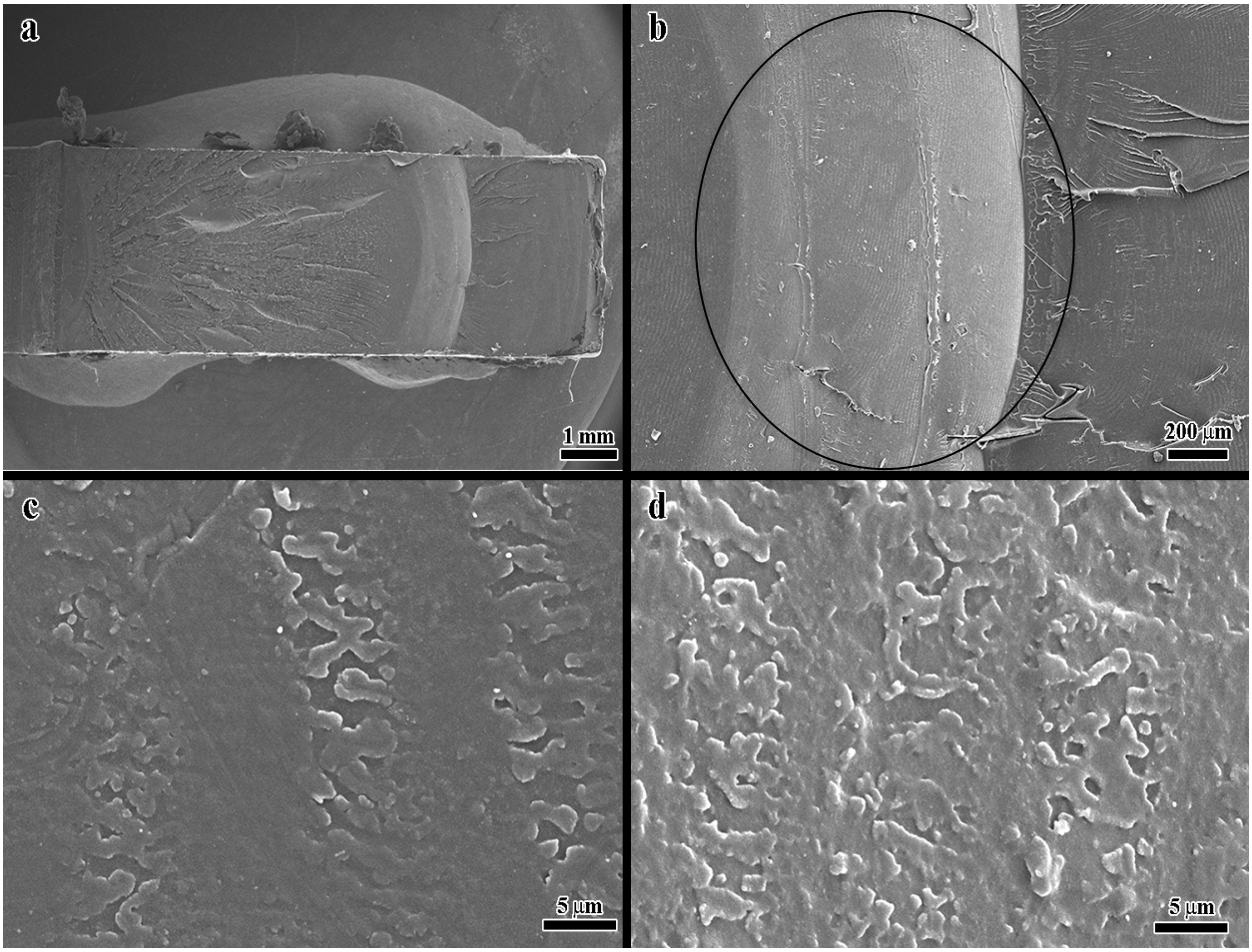

Figure 40. a) Stick-slip lies (ridge) in the middle of the fracture surface in SABIC PC/PDMS under DBTT at -40 °C and X11; b) ridge in SABIC PC/PDMS at -40 °C and X60; c) SEM figure for surface in the ridge at -40 °C and X3000; and d) SEM figure for surface after the ridge at -40 °C and X3000.

5.2.4. DMA

Similar to the DMA results of compressed specimens, T_g can be obtained from the curves of storage modulus and tan delta by TA Universal Analysis software. A typical DMA figure of triblock blends is shown in Figure 41. Similar to the experimental PC-PDMS block copolymers, α transition also occurs at a relatively high temperature in those triblock blends. On the other hand, a small peak is present in loss modulus (at -115 °C) and tan delta curves (at -114.46 °C) of

triblock blends at low temperature. Since this temperature is between the T_g of PDMS (-125 °C) and that of PC (150 °C), it is assumed to be the T_g of a mixture of PC and PDMS.

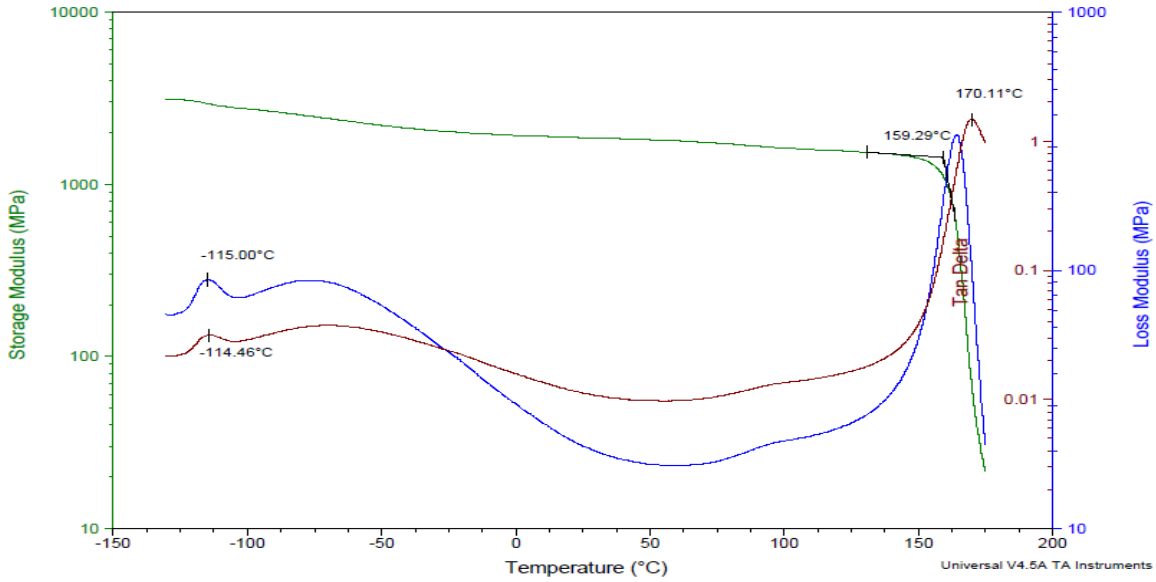

Figure 41 Typical DMA curves of PC/PC-PDMS-PC blends.

Figure 42 shows the storage modulus, loss modulus, and tan delta performances obtained by DMA of the three triblock blend specimens as well as Dow PC and SABIC PC/PDMS. The curves are obtained from the average data of three specimens for each sample. The left images are the DMA curves in the whole range of temperature and the right images are the ones that show the T_g of a mixture of PC and PDMS (-130 °C, -100 °C).

Different from the experimental PC-PDMS block copolymers, the values of storage modulus of these triblock blends are higher than those of Dow PC and SABIC PC/PDMS. This may be caused by the generation of interaction in the interface between C-H hydrogen of PDMS in triblock copolymer phase and the carbonate group of PC in PC matrix [92]. As is known, the interface is quite important for blends and the interaction formed in the interface plays a more important role in blends' properties. T1 (PC3k-PDMS12k_72%) is almost the same as T2 (PC5k-PDMS12k_57%), and both of them are lower than T3 (PC5k-PDMS23k_72%) in storage

modulus. This may be attributed to the higher block molecular weight of the triblock copolymer in T3 (PC5k-PDMS23k_72%) that indicates longer polymer chains. With longer polymer chains, more C-H hydrogen of PDMS in the triblock copolymer phase can interact with the carbonate group of PC in the PC matrix, which leads to a larger interaction between two phases in the blend and, subsequently, the flexibility of polymer chains decreases and storage modulus increases.

According to the area under loss modulus curves, which can be obtained by differential calculus in the range of (-130 °C, 180 °C), triblock blends have the most significant influence on the restriction on polymer chain movement compared to Dow PC and SABIC PC/PDMS. As a result, those blends have higher T_g, which is in accordance in the T_g results obtained by storage modulus and tan delta.

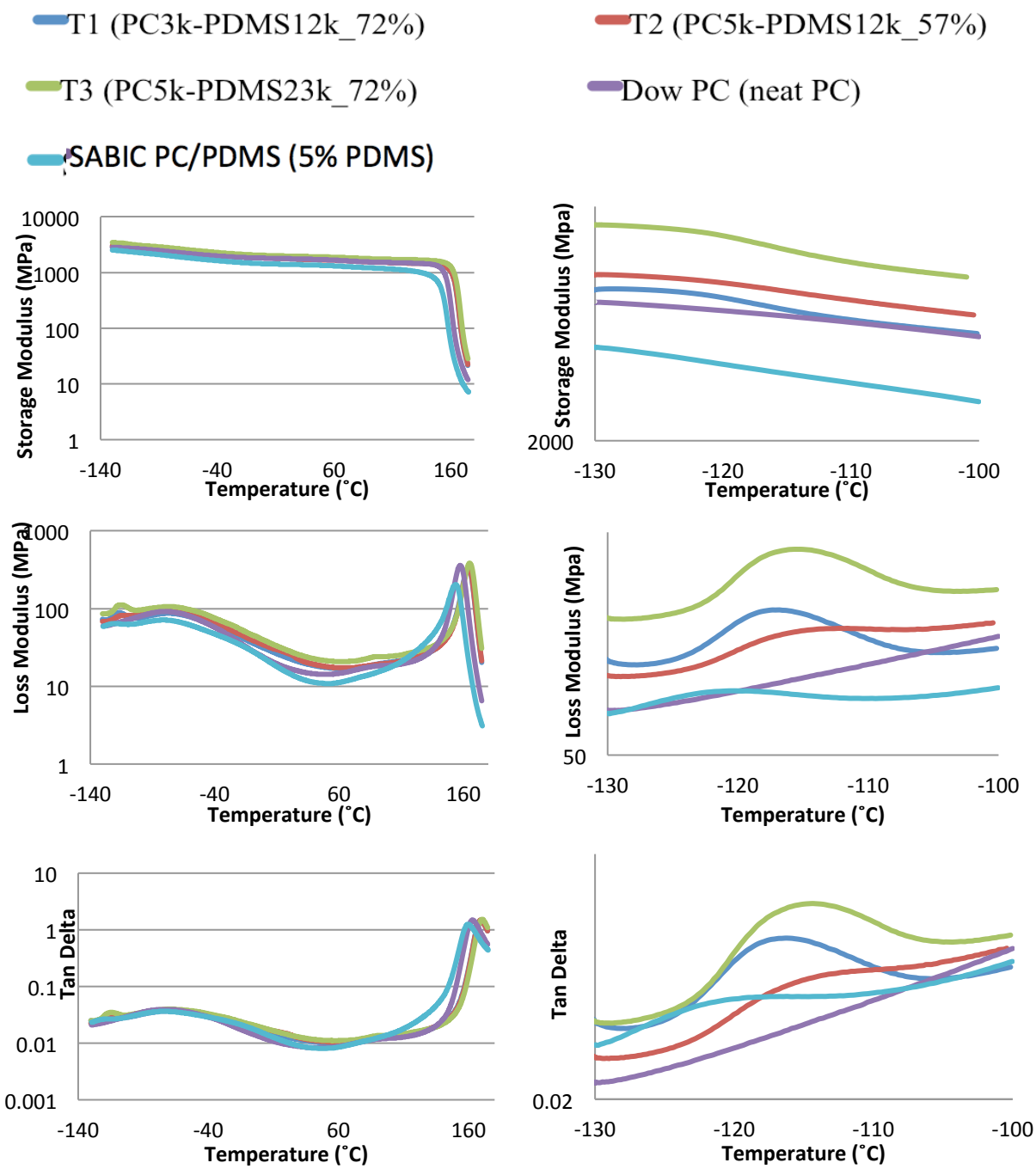

Figure 42. Comparison of DMA curves of triblock blends and Dow PC, SABIC PC/PDMS. The left figures are in the whole temperature scale, and the right ones are in the temperature range from -130℃ to -100℃.

The T_gs obtained from storage modulus and tan delta are shown in Figure 43. It can be observed that the T_g values of triblock blends are quite similar. This can be attributed to the small

amount of triblock copolymers in the blends. In addition, the T_gs of triblock blends are higher than those of Dow PC and SABIC PC/PDMS.

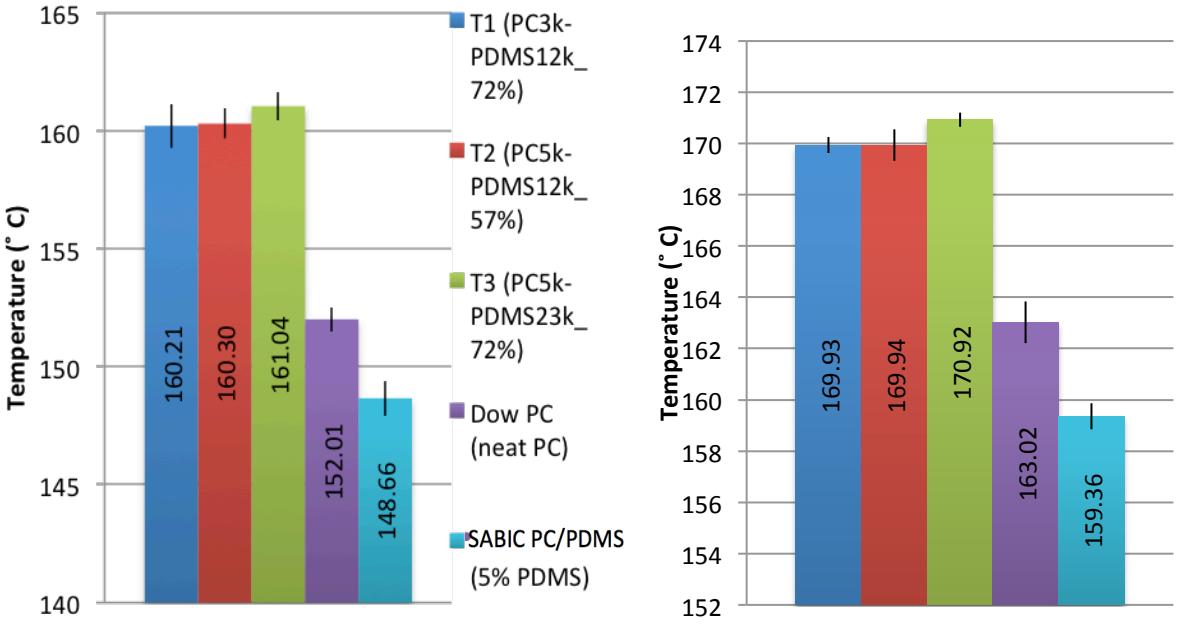

Figure 43. Comparison of T_g s obtained from storage modulus (left) and tan delta (right).

5.2.5. Rheologcial Results

Rheolocial results of triblock blends, Dow PC, and SABIC PC/PDMS are shown in Figure 44, which includes storage modulus (G') curves, loss modulus (G") curves, and complex viscosity curves.

It is observed that there is a slight difference between the three triblock blends because of the small amount of PDMS in the whole blend. Moreover, this small amount of PDMS leads the blends to perform rheological behavior more similarly with Dow PC compared to the experimental PC-PDMS block copolymers. In complex viscosity curves, T1 (PC3k-PDMS12k_72%) has lower complex viscosity compared to T2 (PC5k-PDMS12k_57%) and T3

(PC5k-PDMS23k_72%). This can be attributed to its lower molecular weights of both PC block and PDMS block in the triblock copolymer phase in T1 (PC3k-PDMS12k_72%).

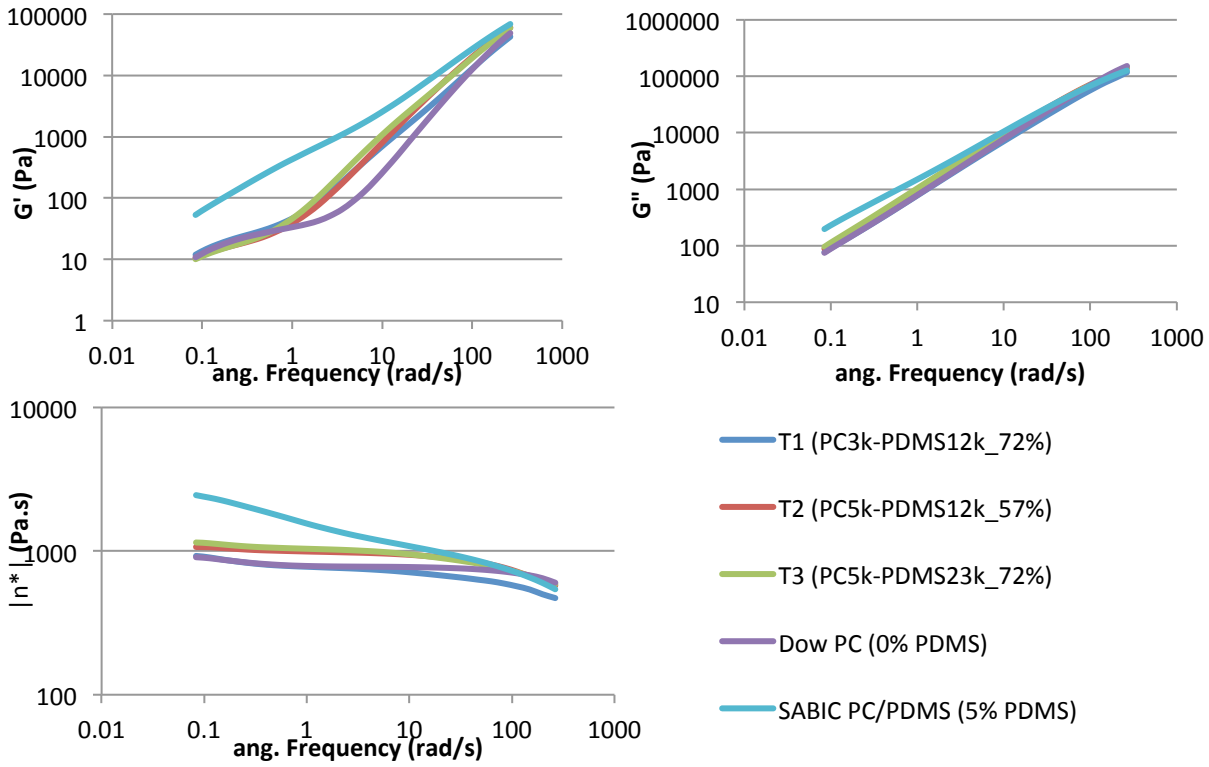

Figure 44. Rheological results of triblock blends and Dow PC, SABIC PC/PDMS at 270 ℃.

5.2.6. Tensile Results

The comparison of tensile modulus of triblock blends, Dow PC, and SABIC PC/PDMS is shown in Figure 45. As is known, the tensile modulus of blends is more affected by the component with lower tensile modulus, and it decreases with the increasing of low-tensile-modulus component content [93]. The tensile modulus of blends can be calculated by Kerner's equation [94]. The tensile modulus of PDMS is 360-870 KPa, while the one of PC is 1.79-3.24 GPa. This can explain the phenomenon that Dow PC (neat PC) has the highest tensile modulus, triblock blends (3 wt% PDMS) obtain the median tensile modulus, and SABIC PC/PDMS (5 wt% PDMS) is the lowest.

Comparing the triblock blends, there is little difference in tensile modulus among them. This may be because of the small portion of PC-PDMS copolymer in the blends. Although the PC-PDMS-PC copolymers are different in molecular weight and content in the blends, they still cannot affect the whole blends to make a significant change in tensile modulus.

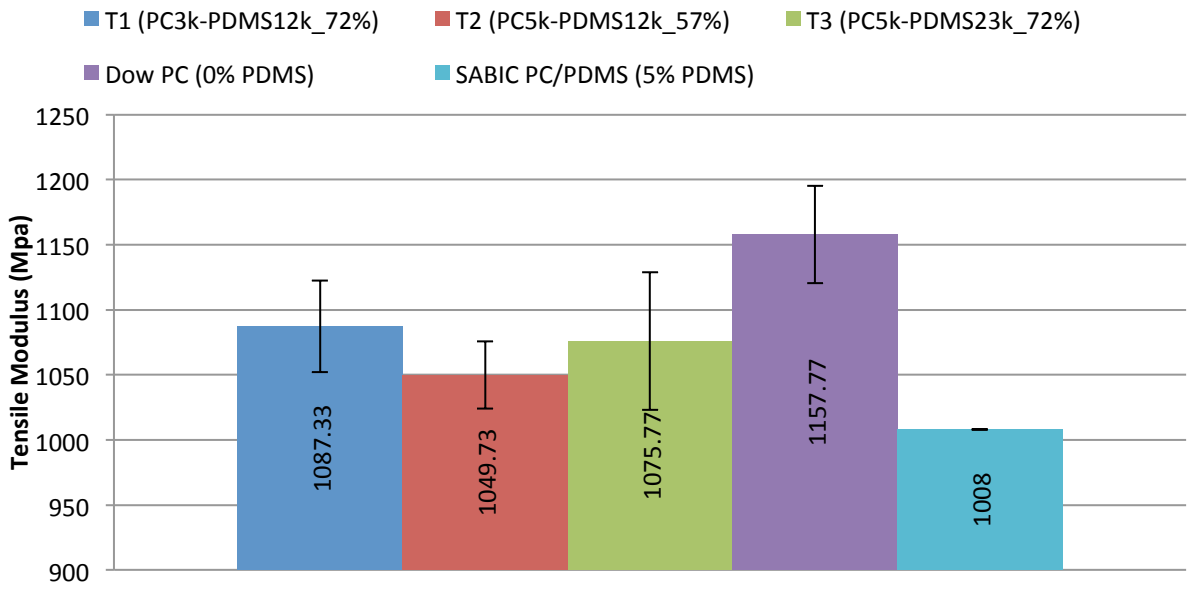

Figure 45. Tensile modulus of triblock blends, Dow PC, and SABIC PC/PDMS.

5.2.7. Three-Point Bending Flexural Results

Unlike the tensile test, the three-point bending flexural test induces both tensile and compressive stress on the same sample. Tensile stress is present at the convex face of the bend while compressive stress occurs at the concave face of the bend. The maximum tensile and compressive stress measurements can be obtained at the edge of the beam at the bending point.

The triblock blends, Dow PC, and SABIC PC/PDMS were used to run a three-point bending flexural test, which none failed before the 0.05 mm/mm strain. The results of flexural strength and flexural modulus are shown in Figure 46. It is noted that Dow PC has the highest flexural strength and flexural modulus, followed by SABIC PC/PDMS and the three triblock

blends. Again, the addition of PDMS lowers the flexural modulus of PC copolymers (SABIC PC/PDMS) and PC blends (triblock blends) because of its relatively low elasticity modulus.

When comparing the triblock blends, their flexural stress and flexural modulus are quite close to each other. This is also due to the small amount of triblock copolymer in the whole blends, which is similar to the tensile results.

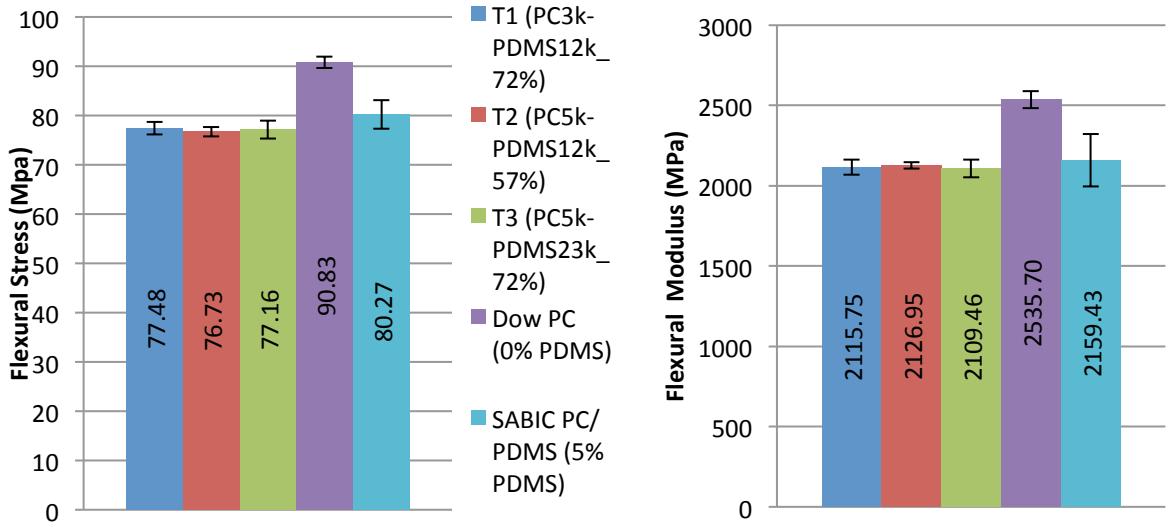

Figure 46. Flexural strength and flexural modulus of triblock blends, Dow PC, and SABIC PC/PDMS.

5.2.8. Optical Clarity

Although triblock copolymer is in a small portion of the whole blend, it significantly affects the optical clarity of the PC blend. Figure 47 compares the clarity of the Dow PC to the T1 (PC3k-PDMS12k_72%) blend. It is clear that the Dow PC is quite transparent and the T1 (PC3k-PDMS12k_72%) is completely opaque. The opaque quality in the T1 (PC3k-PDMS12k_72%) may be caused by the phase separation of the PC matrix and the copolymer phase.

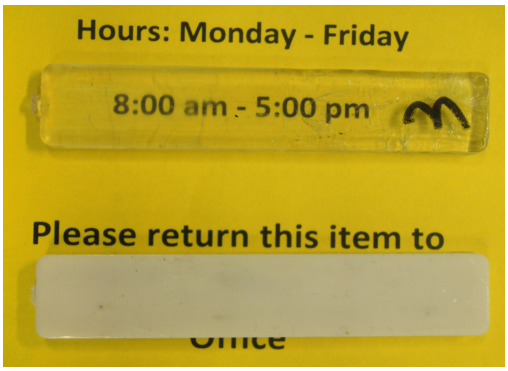

Figure 47. Comparison of clarity of Dow PC (top) and T1 (PC3k-PDMS12k_72%) (bottom) processed by injection molding.

5.3. Comparison of Compression Molding and Injection Molding

In order to compare the influence of processing methodology on the properties of materials, Dow PC and SABIC PC/PDMS were both compressed and injected to run the notched Izod impact, DMA, and rheological tests. The material information details are listed in the Table 11.

Table 11. Details of Dow PC, and SABIC PC/PDMS.

Sample	PC (wt%)	PDMS (wt%)	Mn (g/mol)
Dow PC	100	0	21900
SABIC PC/PDMS	95	5	27600

In compression molding, the polymers are placed in the cavity of a pre-heated mold in open status. Then the top plug is put on the polymers to close the mold and heated continually in an oven. After half an hour of heating, pressure is added to the mold so that the polymers uniformly fill the mold cavity to get shaped. Then, the polymers stay in the mold until they are cooled enough to be solid. During the whole compression process, the polymers sit in the mold with limited space to mix with each other. In addition, the pressure provides compression force

without any shear, so that the polymer chains cannot be oriented along one direction; instead, they disperse randomly.

For injection molding, the injection machine uses a ram injection with a plunger. The polymers are fed from a hopper into the barrel and heated by the heater through the barrel. The polymers melt and collect in the injection chamber and then are pushed forward by the plunging action that is driven by the hydraulic system of the machine. When the materials run through the nozzle, the flow speed changes due to the decrease of nozzle area, which generates shear stress at the nozzle part. Because of the shear stress, the polymer chains are oriented along the flow direction, which increase the chain confinement and then improve the mechanical properties of the materials. Therefore injection molding provides a better specimen quality than compression molding for the same material.

5.3.1. Comparison of Impact Strength

Only Dow PC and SABIC PC/PDMS were processed to run notched Izod impact tests. The comparison of the impact strength of compression and injection molded specimens are shown in Figure 48.

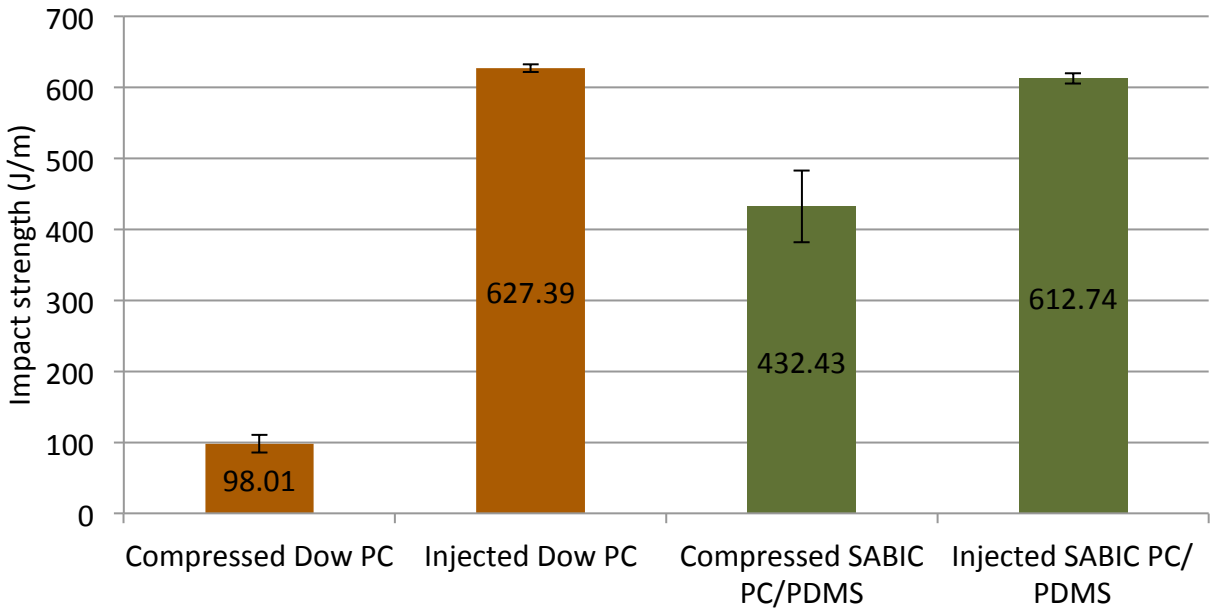

Figure 48. Comparison of the impact strength for compressed specimens and injected specimens.

The impact strength of injected specimens is much higher than that of compressed specimens. This can be attributed to the orientation of polymer chains due to the formation of shear stress at the nozzle of injection machine. Molding materials are sheared and then oriented because the area decreases at the nozzle of the injection machine. In contrast, they stay under compression pressure in the compression mold. The orientation of polymer chains provides higher impact strength and consistent properties in the sample.

It is worth noting that injection molding has more influence on Dow PC than SABIC PC/PDMS. The impact strengths of Dow PC are more dependent on processing method because its impact strength values of injection specimens are about six times of that of compression specimens, while SABIC PC/PDMS is about one and a half times. This may be attributed to the size of the molded material particles. Dow PC was in pellet form, and SABIC PC/PDMS was well dispersed as a powder. The powder is easier to process than pellet form due to its smaller size and, subsequently, it is easier to be well-mixed and thus is less influenced by processing.

Fracture surface after impact can support the impact results that a high impact strength is obtained by injection molding and a low value by compression molding. The fracture surfaces under stereoscopy of compressed and injected SABIC PC/PDMS specimens are shown in Figure 49. The compressed specimen (a) exhibits a fracture that is indicative of a brittle failure, whereas the injected specimen (b) shows a more ductile failure. In fracture surface (a), a typical brittle failure can be observed, especially the hackle area; while surface (b) is more blurred. This is because under stereoscopy the image gets blurred when the sample surface is not on the same height level. These two images are in good agreement with the SEM results of brittle facture (hackle area) and ductile fracture (fibrils morphology).

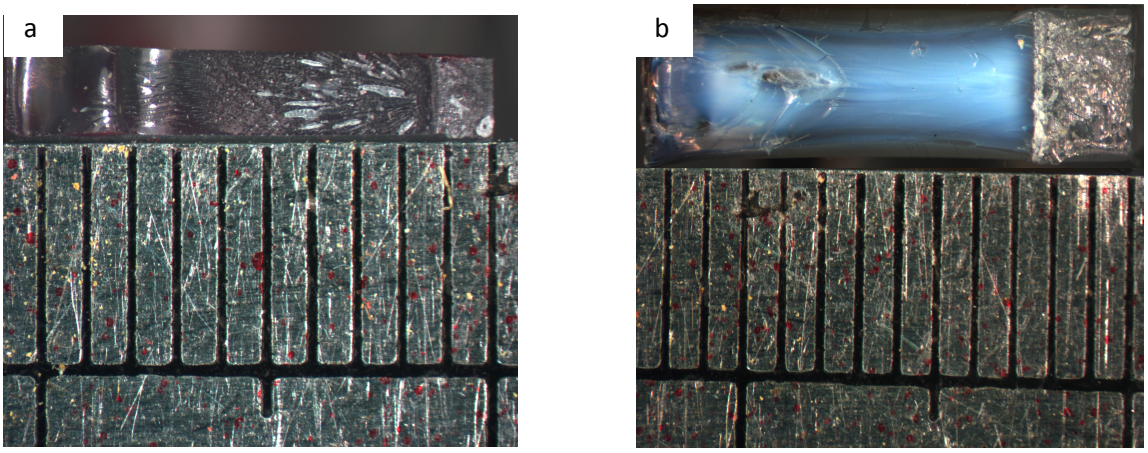

Figure 49. Fracture surface of compressed (a) and injected (b) SABIC PC/PDMS.

5.3.2. Comparison of DMA

Figure 50 and Figure 51 below show the processing influence on DMA performance of commercial PCs and their relative T_g values. For SABIC PC/PDMS, injection molding provides higher values of storage modulus and loss modulus due to the shear stress that orient the polymer chains along one direction. Meanwhile, injection molding slightly increases the T_g value that can be obtained from storage modulus and tan delta curves. On the other hand, Dow PC shows

different DMA behavior from SABIC PC/PDMS; the T_g obtained from injection molding is a little lower than that obtained from compression molding. This may be because SABIC PC/PDMS is a copolymer while Dow PC is a neat polymer. As a copolymer, SABIC PC/PDMS has two phases, PC and PDMS. Since these two phases are immiscible, the interaction between them should be considered. As discussed above, the injection molding introduces shear stress and provides a better mixture, which leads to a better compatibility between PC and PDMS; as a result, T_g increases in injection molding. While Dow PC is a pure PC, it only has one phase and thus does not need to consider the compatibility.

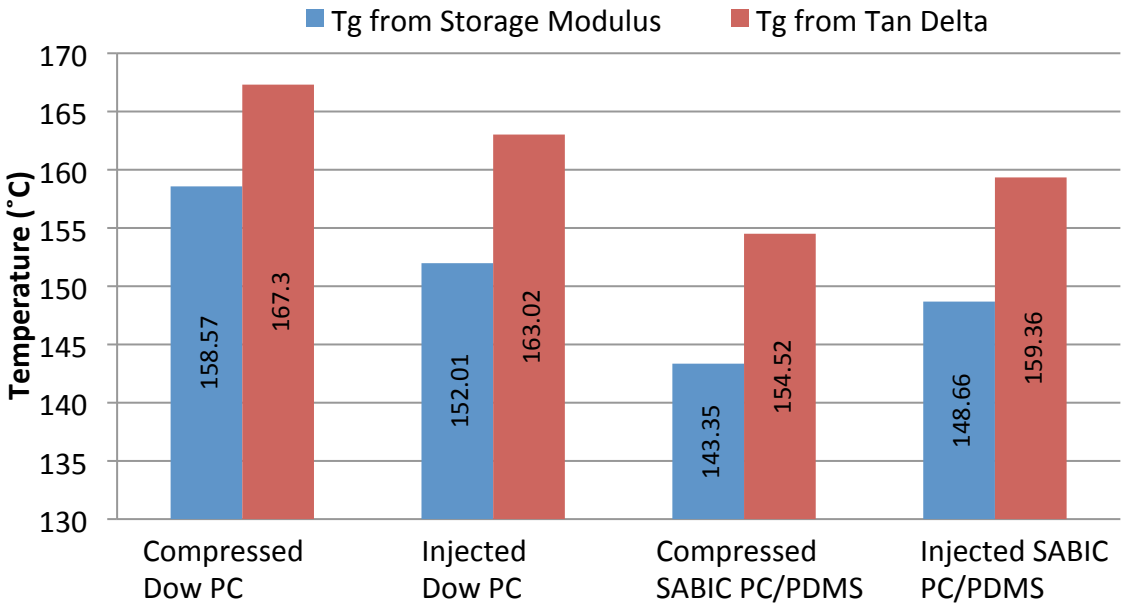

Figure 50. Comparison of T_g from storage modulus and tan delta of compressed and injected specimens.

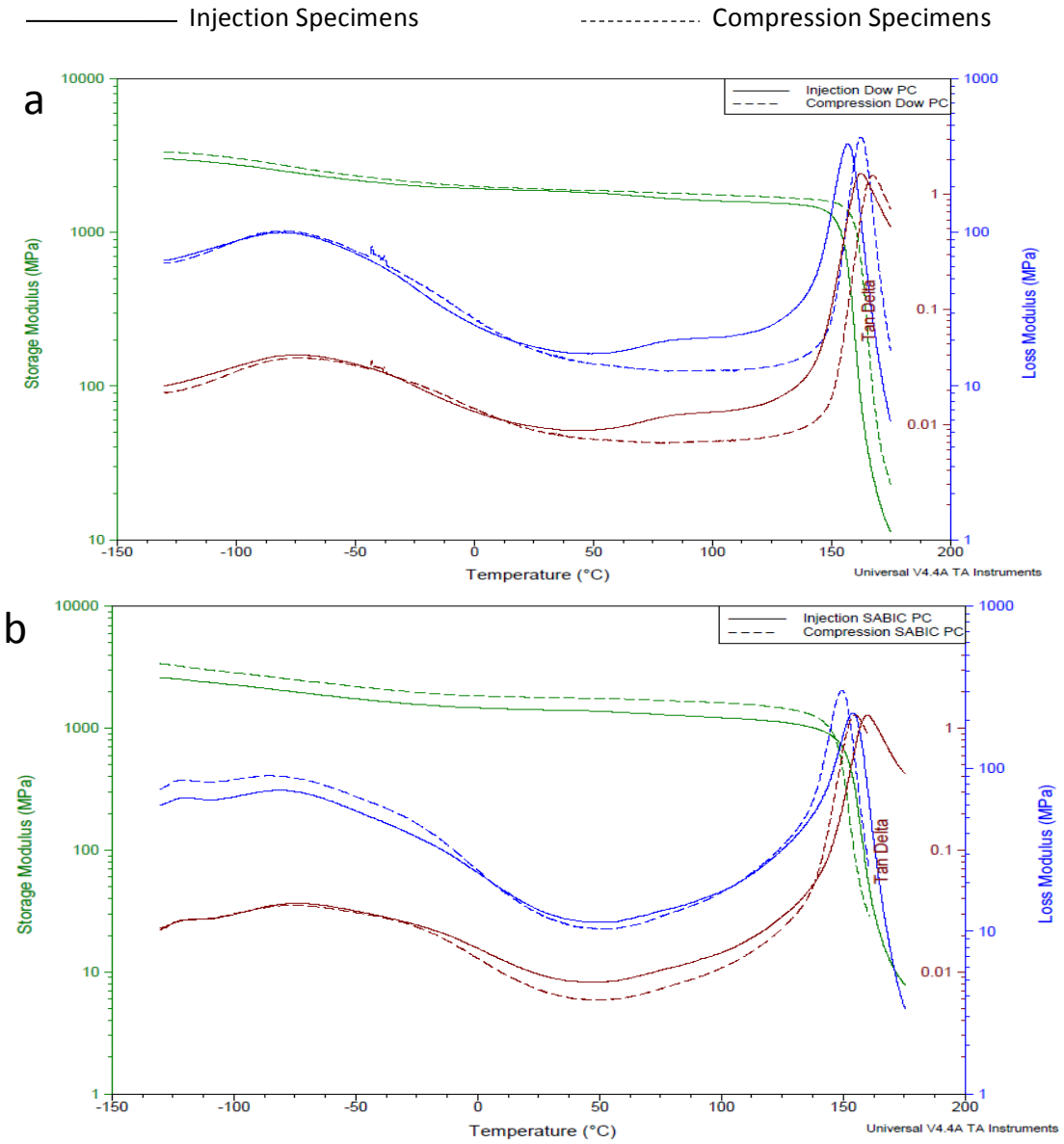

Figure 51. Comparison of DMA results of compression and injection samples: a) Dow PC; b) SABIC PC/PDMS

5.3.3. Comparison of Rheogical Behave Between Compressed and Injected Specimens

Dow PC and SABIC PC/PDMS were also used to run rheological tests to compare their flow states after processing by compression molding and injection molding. The results are shown in Figure 52. It is worth noting that processing methods have little influence on materials viscosity properties. This is because materials are measured for their rheological properties under melted state. Once melted, all previous thermal history caused by processing is removed, and the measured rheological properties are only determined by the intrinsic properties of the material. As a result, although processed in different ways, Dow PC and SABIC PC/PDMS show the same trend of storage modulus and loss modulus curves with increasing the angular frequency in compression-molding and injection-molding specimens.

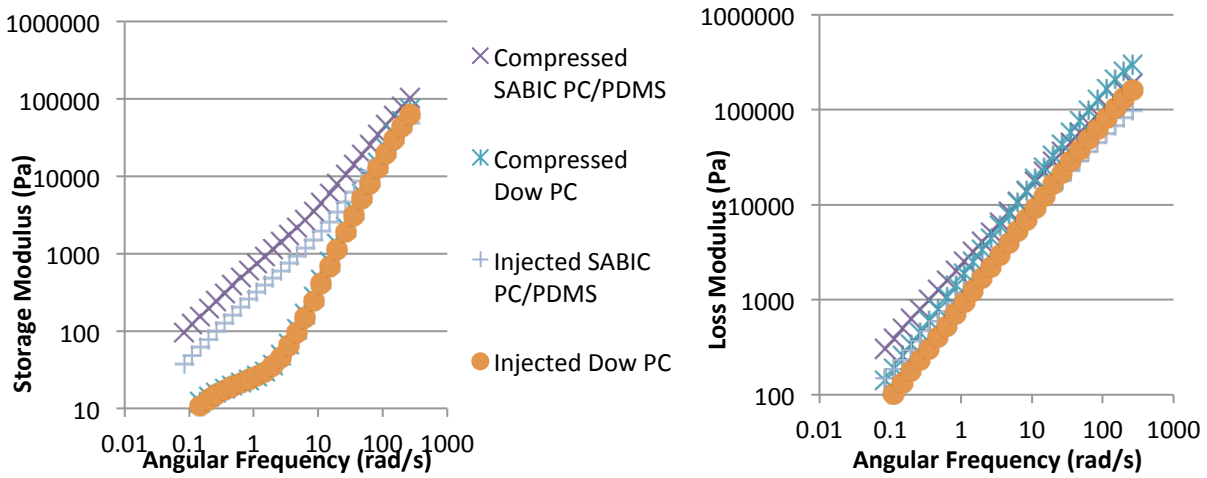

Figure 52. Comparison of storage modulus (left) and loss modulus (right) performance obtained by rheological test for compressed and injected specimens.

CHAPTER 6. CONCLUSION AND FUTURE RECOMMENDATION

As one of the most widely used engineering plastics, polycarbonate (PC) shows relatively high impact strength and transparency at the same time. These excellent properties contribute to its success in industry. However, PC undergoes notch sensitivity in notched impact tests. This notch sensitivity drastically decreases the impact strength of PC when compared to the impact strength under the non-notched condition. Plenty of research has been done to overcome the notch sensitivity of PC while maintaining its clarity. Rubber toughening is used in this study and polydimethylsiloxane (PDMS) is chosen to be the preferred toughening rubber due to its low glass transition temperature (T_g).

Two ways of rubber toughening were applied in this study: copolymerization and blending. In order to control the geometry of PDMS and PC to balance the enhancement in impact strength and transparency, a novel synthesis method of PC-PDMS multiblock copolymer was developed to control the PC and PDMS block length and block architecture. The second part of this thesis concerns the blends of PC and PC-PDMS-PC triblock. Compared to copolymerization, blending is a physical process that costs less and is preferred in industry. Different tests were applied to measure properties of PC-PDMS multiblock copolymers and PC/PC-PDMS-PC triblock blends. Furthermore, two processing methodologies (i.e. compression molding and injection molding) were applied to show the different effect on materials' properties.

This chapter concludes the results and discussion in Chapter 5 for PC-PDMS multiblock copolymers, PC/PC-PDMS-PC triblock blends, and the comparison of injection molding and compression molding. Based on the conclusions, some recommendations are made for future work in this project.

6.1. Conclusions

It can be concluded that the addition of PDMS and higher block molecular weight increase impact toughness of specimens but damage their transparency. In addition, injection molding shows advantage in polymer chain orientation and provides higher specimen quality than compression molding.

6.1.1. Influence of the Addition of PDMS

PDMS plays a role in copolymers' impact strength, chain entanglements, and optical clarity. The addition of PDMS can improve PC's impact strength by promoting multiple crazing to absorb impact energy. Also, it lowers copolymer's T_g due to the relatively low T_g of PDMS. In terms of transparency, PC-PDMS multiblock copolymers can be transparent at relatively low PDMS content; while the PC/PC-PDMS-PC triblock blends are totally opaque due to the phase separation between the PC matrix and the copolymer phase.

6.1.2. Influence of Higher Block Molecular Weight

Molecular weight of PC block and PDMS block also has influence on copolymers' impact toughness, chain movement, viscosity, and transparency. The impact strength of PC increases with higher block molecular weight due to the longer polymer chains that dissipate more impact energy. In addition, the higher block molecular weight can lower the ductile-brittle transition temperature of PC to increase its toughness at low temperatures. Moreover, the higher block molecular weight makes the polymer more difficult to transfer from glass state to rubber state and thus increases the T_g of specimens. However, higher block molecular weight has a negative effect on the transparency because of the microphase separation and mismatch of refractive index in PC and PDMS.

6.1.3. Influence of Processing Methodology

As is well known, specimen quality plays an important role in the test results, and it is correlated with processing methodology. In injection molding, decreasing the area at the nozzle of the injection machine introduces shear stress and better mixing, which leads to orientation of polymer chains, and increases the chain confinement that improves the mechanical properties of materials. On the other hand, in compression molding, materials are restricted in the mold and have limited space to flow. This difference in material flow shows the advantage of injection molding in polymer chain orientation and specimen properties. In addition, injection molding shows many advantages in manufacturing when comparing to compression molding, such as low mold preheating temperature and short molding cycle time.

6.2. Future Recommendations

In order to compare the degree of improvement PDMS makes on the impact strength of PC by copolymerization and blending, PC-PDMS multiblock copolymers and PC/PC-PDMS-PC triblock blends should be processed in the same way. In addition, the same mechanical tests and morphology characterization should be applied in both copolymers and blends to show the structure-property relationship. Regarding the rheology results, more work should be done to verify the friction model to explain the presence of the plateau at high frequency of the storage modulus and loss modulus curves. Moreover, in order to prove the advantage of injection molding in providing polymer chain orientation, different parts in injected specimens can be selected to characterize the polymer chain orientation by X-ray diffraction and infrared spectroscopy.

REFERENCE

1. W. F. Christopher, D. W. Fox, Polycarbonate, *Reinhold, New York*, 1962, Chap. 1, pp. 2-4
2. H. Schnell, Chemistry and Physics of Polycarbonates, *Interscience, New York*, 1964, pp. 3
3. G. A. V. Timoteo, G. J. M. Fechine, M. S. Rabello, Stress Cracking and Photodegradation Behavior of Polycarbonate. The Combination of Two Major Causes of Polymer Failure, *Polymer Engineering and Science*, 2008, Vol. 48, pp. 2003-2010
4. C. K. Kjellander, T. B. Nielsen, A. G. Siahkali, P. Kingshott, C. M. Hansen, K. Almdal, ESC Resistance of Commercial Grade Polycarbonate During Exposure to Butter and Related Chemicals, *Polymer Degradation and Stability*, 2008, Vol. 93, pp. 1468-1495
5. J. Mark, K. Ngai, W. Graessley, L. Mandelkern, E. Samnlshi, J. Koenig, G. Wignall, Physical Properties of Polymers, *Cambridge University Press*, 2004, Chap. 7, pp. 244
6. D. Wang, M. Kang, X. Wang, Research Advances and Market Analysis for Polycarbonate, *Materials Review*, 2002, Vol. 5, pp. 65-67
7. J. Mark, K. Ngai, W. Graessley, L. Mandelkern, E. Samnlshi, J. Koenig, G. Wignall, Physical Properties of Polymers, *Cambridge University Press*, 2004, Chap. 5, pp. 179-180
8. E. Turska, J. Hurek, L. Zmudzinski, X-Ray Studies of Structural Ordering Changes on Annealing A Non-crystalline Polycarbonate, *Polymer*, 1979, Vol. 20, pp. 321-323
9. R. Farmer, A Study of Crystallization in Bisphenol A Polycarbonate, *Master Thesis of Master of Science in Material Science and Engineering*, Virginia Polytechnic Institute and State University, 2001

10. http://www.matweb.com/search/DataSheet.aspx?MaTgUID=501acbb63cbc4f748faa7490884cdbca&ckck=1, accessed on Feb. 3rd, 2012

11. W. F. Chrisopher, D. W. Fox, Polycarbonates, *Reinhold Publishing Corporation, New York*, 1962, Chap. 4, pp. 46

12. G. A. V. Timoteo, G. J. M. Fechine, M. S. Rabello, Stress Cracking and Photodegradation Behavior of Polycarbonate. The Combination of Two Major Causes of Polymer Failure, *Polymer Engineering and Science*, 2008, Vol. 10, pp. 2003-2010

13. Zs. Geretovszky, B. Hopp, I. Bertoti, I. W. Boyd, Photodegradation of Polycarbonate Under Narrow Band Irradiation at 172 nm, *Applied Surface Science*, 2002, Vol. 186, pp. 85-90

14. M. Diepens, P. Gijsman, Influence of Light Intensity on the Photodegradation of Bisphenol A Polycarbonate, *Polymer Degradation and Stability*, 2009, Vol. 94, pp. 34-38

15. L. F. Al-Saidi, K. Mortensen, K. Almdal, Environmental Stress Cracking Resistance. Behavior of Polycarbonate in Different Chemicals by Determination of the Time-Dependence of Stress at Constant Strains, *Polymer Degradation and Stability*, 2003, Vol. 82, pp. 451-461

16. A. Raman, R. J. Farris, A. J. Lesser, Effect of Stress State and Polymer Morphology on Environmental Stress Cracking in Polycarbonate, *Journal of Applied Polymer Science*, 2003, Vol. 88, pp. 550-564

17. D. G. LeGrand, J. T. Bendler, Handbook of Polycarbonate Science and Technology, *Marcel Dekker, Inc.*, 2000, Chap. 6, pp. 116

18. J. H. Goldren, B. L. Hammant, E. A. Hazell, The Effect of Thermal Pretreatment on the Strength of Polycarbonate, *Journal of Applied Polymer Science*, 1967, Vol. 11, pp. 1571-1579

19. J. H. Goldren, B. L. Hammant, E. A. Hazell, Effects of Molecular Weight and Strain Rate on the Flexural Properties of Polycarbonate, *Journal of Applied Polymer Science*, 1968, Vol. 12, pp. 557-569

20. D. G. LeGrand, Crazing, Yielding, and Fracture of Polymers 1. Ductile-Brittle Transition in Polycarbonate, *Journal of Applied Polymer Science*, 1969, Vol. 13, pp. 2129-2147

21. G. Locati, A. V. Tobolosky, Studies of the Toughness of Polycarbonate of Bisphenolo A in Light of Its Secondary Transition, *Advances in Molecular Relaxation Processes*, 1970, Vol. 1, pp. 375-408

22. M. Parvin, J. G. Williams, Ductile-Brittle Fracture Transitions in Polycarbonate, *International Journal of Fracture*, Vol. 11, pp. 963-972

23. J. T. Ryan, Impact and Yield Properties of Polycarbonate as a Functionof Strain Rate, Molecular weight, Thermal Histoty, and Temperature, *Polymer Engineering and Science*, 1978, Vol. 18, pp. 264-267

24. G. Gubbels, Diamond Turning of Glassy Polymer, *Eindhoven: Technische Universiteit Eindhoven*, 2006, Chap. 1, pp. 2-5

25. R. M. Waxler, D. Horowitz, A. Feldman, Optical and Physical Parameters of Plexiglas 55 and Lexan, *Applied Optics*, 1979, Vol. 18, pp. 101-104

26. Lexan Resin Optical Properties, *General Electric Company*, Lexan Products Division, Pittsfield, MA, 1986

27. W. F. Chrisopher, D. W. Fox, Polycarbonates, *Reinhold Publishing Corporation, New York*, 1962, Chap. 9, pp. 179-224

28. A. G. Franklin, R. J. Krizek, Complex Viscosity of A Kaolin Clay, *Clays and Clay Minerals*, 1969, Vol. 17, pp. 101-110

29. A. Einhorn, Ueber Die Carbonate Der Dioxybenzole, *Liebigs Annalen der Chemie*, 1898, Vol. 300, pp. 135-155

30. C. A. Bischoff, A. V. Hedenstrom, Ueber Aromatische Ester Der Kohlensaure Und Oxalsaure, *Chemische Berichte*, 1902, Vol. 35, pp. 3431-3437

31. A. Baeyer, der Deutschen Chemischen Gesellschaft, *Berichte*, 1872, Vol. 5, pp. 25-26

32. J. E. Jansen, Preparation of Bis-Phenols, *U.S.Patent 2468982*

33. http://www.cxpa.com/Article/ShowArticle.asp?ArticleID=10402, accessed on Jan.30th, 2012

34. J. S. Wu, Y. W. Mai, A. F. Yee, Fracture-Toughness and Fracture Mechanism of Polybutylene-Terephthalate Polycarbonate Impact-Modifier Blends. 3. Fracture-Toughness and Mechanisms of PBT PC Blends Without Impact Modifiers, *Journal of Materials Science*, 1994, Vol. 29, pp. 4510-4522

35. G. Wildes, H. Keskkula, D. R. Paul, Fracture Characterization of PC/ABS Blends: Effect of Reactive Compatibilization, ABS Type and Rubber Concentration, *Polymer*, 1999, Vol. 40, pp. 7089-7107

36. H. V. Aert, L. Nelissen, P. J. Lemstra, D. J. Brunelle, Poly(bisphenol A carbonate)-Poly(dimethylsiloxane) Multiblock Copolymers, *Polymer*, 2001, Vol. 42, pp. 1782-1788

37. K. Cho, J. Yang, S. Yoon, M. H. Sobha, V. Nair, Toughening of Polycarbonate: Effect of Particle Size and Rubber Phase Contents of the Core-Shell Impact Modifier, *Journal of Applied Polymer Science*, 2005, Vol. 95, pp. 748-755

38. C. Cheng, N. Peduto, A. Hiltner, E. Baer, P. R. Soskey, S. G. Mylonakis, Comparison of Some Butadiene-Based Impact Modifiers for Polycarbonates, *Journal of Applied Polymer Science*, 1994, Vol. 53, pp. 513-525

39. W. G. Perking, Polymer Toughness and Impact Resistance, *Polymer Engineering and Science*, 1999, Vol39, pp. 2445-2460

40. J. Mark, K. Ngai, W. Graessley, L. Mandelkern, E. Samnlshi, J. Koenig, G. Wignall, Physical Properties of Polymers, *Cambridge University Press*, 2004, Chap. 1, pp. 9-10

41. X. H. Wang, Z. G. Wang, J. Wei, C. H. Liu, H. D. Yang, H. X. Zhang, B. Z. Jiang, Toughened Blend of Polycarbonate and Epoxidized Ethylene Propylene Diene Rubber, *Polymer*, 1997, Vol. 38, pp. 6251-6253

42. S. Y. Sun, Y. D. He, X. D. Wang, D. Z. Wu, Modification of Recycled Polycarbonate with Core-Shell Structured Latexes for Enhancement of Impact Resistance and Flame Retardancy, *Journal of Applied Polymer Science*, 2010, Vol. 116, pp. 2451-2464

43. H. A. Stretz, P. E. Cassidy, D. R. Paul, Blends of Bisphenol A Polycarbonate and Rubber-Toughened Styrene-Maleic Anhydride Copolymers, *Journal of Applied Polymer Science*, 1999, Vol. 74, pp. 1508-1515

44. B. Jiang, W. L. Dai, S. B. Chen, T. Hu, P. S. Liu, Mechanical Behavior and Fracture Toughness evaluation of K Resin Grafted with Maleic Anhydride Compatibilized Polycarbonate/K Resin Blends, *Material of Science and Engineering A,* 2007, Vol. 444, pp. 84-91

45. D. S. Parker, H. J. Sue, J. Huang, A. F. Yee, Toughening Mechanisms in Core-Shell Rubber Modified Polycarbonate, *Polymer*, 1990, Vol. 31, pp. 2267-2277

46. H. J. Xu, S. C. Tang, L. Yang, W. T. Hou, Toughening of Polycarbonate by Core-Shell Latex Particles: Influence of Particle Size and Spatial Distribution on Brittle-Ductile Transition, *Journal of Polymer Science: Part B: Polymer Physics*, 2010, Vol. 48, pp. 1970-1977

47. Y. Kayano, H. Keskkula, D. R. Paul, Effect of Polycarbonate Molecular Weight and Processing Conditions on Mechanical Behavior of Blends with a Core-Shell Impact Modifier, *Polymer*, 1996, Vol. 37, pp. 4506-4518

48. I. Goitisolo, J. I. Eguiazabal, J. Nazabal, Stiffening of Polycarbonate by Addition of a Highly Dispersed and Fibrillated Amorphous Polyamide-Based Nanocomposite, *Macromolucular Materials and Engeering*, 2010, Vol. 295, pp. 233-242

49. M. Tasdemir, Properties of Acrylonitrile-Butadiene-Styrene/Polycarbonate Blends with Styrene-Butdiene-Styrene Block Copolymer, *Journal of Applied Polymer Science*, 2004, Vol. 93, pp. 2521-2527

50. M. T. Pastorini, R. C. Nunes, Mica as a Filler for ABS/Polycarbonate Blends, *Journal of Applied Polymer Science*, 1999, Vol. 74, pp. 1361-1365

51. H. J. Sue, J. Huang, A. F. Yee, Interfacial Adhesion and Toughening Mechaninsms in an Alloy of Polycarboante/Polyethylene, *Polymer*, 1992, Vol. 33, pp. 4868-4871

52. D. Dhara, A. Purushotham, N. Rosenquist, W. D. Richards, K. Maruvada, G. Chatterjee, Physical Aging of Polycarbonate Block Copolymers: Ductility Rejuvenation below the Glass Transition Temperature, *Polymer Engineering and Science*, 2009, Vol. 49, pp. 1719-1726

53. Y. Abe, T. Gunji, Oligo- and Polysiloxanes, *Progress in Polymer Science*, 2004, Vol. 29, pp. 149-182

54. Y. Abe, K. Kagayama, N. Takamura, T. Gunji, T. Yoshihara, N. Takahashi, Preparation and Properties of Polysilsesquioxanes, Function and Characterization of Coating agents and Films, *Journal of Non-Crystalline Solids*, 2000, Vol. 261, pp. 39-51

55. Y. Abe, K. Kagayama, N. Takahashi, T. Gunji, Preparation and Properties of Polysilsesquioxanes, Polysilsesquioxanes as a Candidate to a Low Dielectrics for Electronic Devices, *Materials Research Society Symposium Proceedings*, 1999, Vol. 565, pp. 247

56. F. Abbasi, H. Mirzadeh, A. A. Katbab, Review: Modification of Polysiloxane Polymers for Biomedical Applications: A Review, *Polymer International*, 2001, Vol. 50, pp. 1279-1287

57. M. Lji, S. Serizawa, Silicone Derivatives as New Flame Retardants for Aromatic Thermoplastics Used in Electronic Devices, *Polymers for Advanced Technologies*, 1998, Vol. 9, pp.5 93-600

58. H. A. Vaughn, S. N. Y. Organopolysiloxane-Polycarbonate Block Copolymers, *U.S.Patent, 3189662*

59. C. C. M. Ma, J. T. Gu, L. H. Shauh, J. C. Yang, W. C. Fang, Bisphenol-Polycarbonate/Polydimethylsiloxane Multiblock Copolymers. I. Synthesis and Characterization, *Journal of Applied Polymer Science*, 1997, Vol. 66, pp. 57-66

60. W. Zhou, J. Osby, Siloxane Modification of Polycarbonate for Superior Flow and Impact Toughness, *Polymer*, 2010, Vol. 51, pp. 1990-1999

61. S. S. Pesetskii, B. Jurkowski, I. P. Storozcuk, V. N. Koval, Blends of Polycarbonate and Polysulphone-Polydimethylsiloxane Block Copolymers: Analysis of Compatibility and Impact Strength, *Journal of Applied Polymer Science*, 1999, Vol. 73, pp. 1823-1834

62. S. S. Pesetskii, B. Jurkowski, I. P. Storozcuk, V. N. Koval, Compatiblity, Adhesional Interaction of Components, Impact Strength, and Rheological Behavior of Plycarbonate/Polycarnate-Siloxane Block Copolymer, *Journal of Applied Polymer Science*, 2000, Vol. 78, pp. 858-869

63. H. A. Vaughn, The Synthesis and Properties of Alternating Block Polymers of Dimethylsiloxane and Bisphenol-A Carbonate, *Journal of Polymer Science Part B: Polymer Letters*, 1969, Vol. 7, pp. 569-572

64. S. H. Tang, E. A. Meinecke, J. S. Riffle, J. E. McGrath, Structure-Property Studies on a Series of Polycarbonate-Polydimethylsiloxane Block Copolymers, *Rubber Chemistry and Technology*, 1980, Vol. 53, pp. 1160-1169

65. S. H. Kim, H. G. Woo, S. H. Kim, H. G. Kang, W. G. Kim, Synthesis and Properties of Allyl-Terminated and Silicon-Containing Polycarbonates, *Macromolecules*, 1999, Vol. 32, pp. 6363-6366

66. Production Information Sheet, Dow Plastics, *The Dow Chemical Company*, Form No. 301-02927-898 SMG

67. http://www.theplasticshop.co.uk/plastic_technical_data_sheets/lexan_polycarbonate_9030_technical_properties_data_sheet.pdf, accessed on February 11th, 2012

68. http://www.ticona.com/home/tech/processing/compression_molding.htm, accessed on June 16th, 2012

69. J. Mark, K. Ngai, W. Graessley, L. Mandelkern, E. Samnlshi, J. Koenig, G. Wignall, Physical Properties of Polymers, *Cambridge University Press*, 2004, Chap. 3, pp. 103-104

70. W. H. Jo, H. G. Kim, S. H. Chae, Morphological, Rheological, and Mechanical Properties of Polyamide 6/Styrene-Acrylic Acid Copolymer Blends, *Journal of Polymer*, 1993, Vol. 25, pp. 1023-1031

71. X. H. Li, Y. Z. Meng, G. Q. Chen, R. K. Y. Li, Thermal Properties and Rheological Behavior of Biodegradable Aliphatic Polycarbonate Derived From Carbon Dioxide and Propylene Oxide, *Journal of Applied Polymer Science*, 2004, Vol. 94, pp. 711-716

72. H. T. Pham, C. L. Weckle, J. M. Ceraso, Rheology Enhancement in PC/ABS Blends, *Advanced Materials*, 2000, Vol. 12, pp. 1881-1885

73. Y. Matsumiya, M. Matsumoto, H. Watanabe, T. Kanaya, Y. Takahashi, Nonlinear Rheology and Structural Changes of (BS)n Multiblock Copolymers under Shear Flow, *Macromolecules*, 2007, Vol. 40, pp. 3724-3732

74. P. E. Rouse, A Theory of the Linear Viscoelastic Properties of Dilute Solutions of Coling Polymers, *Journal of Chemical Physics*, 1953, Vol. 21, pp. 1272-1280

75. P. G. D. Gennes, Entangled Polymer, *Physics Today*, 1983, Vol. 36, pp. 31-33

76. H. S. Jeon, A. I. Nakatani, C. C. Han, R. H. Colby, Melt Rheology of Lower Critical Solution Temperature Polybutadiene/Polyisoprene Blends, *Macromolecules*, 2000, Vol. 33, pp. 9732-9739

77. A. T. J. V. Helvoort, D. L. Dheeraj, H. Zhou, S. Gronsberg, G. Patriarchej, B. Fimland, H. Weman, Dark Field Transmission Electron Microscopy Techniques for Structural Characterization, *Journal of Physics: Conference Series*, 2004, Vol. 241, pp. 012084

78. S. Bals, C. Kisielowski, M. Croitoru, G. V. Tendeloo, Tomography Using Annular Dark Field Imaging In TEM, *Microsc Microanal*, 2005, Vol. 11, pp. 2118-2119

79. X. Chen, J. A. Gardella, Jr., Surface Modification of Polymers by Blending Siloxane Block Copolymers, *Macromolecules*, 1994, Vol. 27, pp. 3363-3369

80. J. M. G. Cowie, Polymers: Chemistry and Physics of Modern Materials, *CRC Press*, 1991, Chap. 8, pp. 159-160

81. L. Leibler, Theory of Microphase Separation in Block Copolymer, *Macromolecules*, 1980, Vol. 13, pp. 1602-1617

82. M. Zhang, P. Choi, U. Sundararaj, Molecular Dynamics and Thermal Analysis Study of Anomalous Thermodynamic Behavior of Poly(Ether Imide)/Polycarbonate Blends, *Polymer*, 2003, Vol. 44, pp. 1979-1986

83. E. A. Men'shikov, A. V. Bol'shakova, I. V. Yaminskii, Determination of the Flory-Huggins Parameter for a Pair of Polymer Unit from AFM Data for Thin Films of Block Copolymer, *Molecular and Supramolecular Structure at the Interfaces*, 2009, Vol. 45, pp. 295-299

84. R. J. Gaymans, M. J. J. Hamberg, J. P. E. Inberg, The Brittle-Ductile Transition Temperature of Polycarbonate as a Function of Test Speed, *Polymer Engineering and Science*, 2000, Vol. 40, pp. 256-262

85. R. J. Gaymans, M. J. Hanberg, J. P. F. Inberg, The Brittle-Ductile Transition Temperature of Polycarbonate as a Function of Test Speed, *Polymer Engineering and Science*, 2000, Vol. 40, pp. 256-262

86. M. A. Meyers, K. K. Chawla, Mechanical Behavior of Materials, *Cambridge University Press*, 2008, Chap. 8, pp. 507-512

87. L. H. Lee, Fracture Mechanisms in PVC and Other Thermoplastics, *Massachusetts Institute of Technology*, 1984

88. C. B. Bucknall, D. S. Ayre, D. J. Dijksta, Detection of Rubber Particle Cavitation in Toughened Plastics Using Thermal Contraction Tests, *Polymer*, 2000, Vol. 41, pp. 5937-5947

89. I. Riku, Y. Tomita, K. Mimura, Effect of Size-Dependent Cavitation on Micro- to Macroscopic Mechanical Behavior of Rubber-Blended Polymer, *Journal of Engineering Materials and Technology*, 2008, Vol. 30, pp. 021017. 1-021017. 9

90. E. M. Mount III, Control od Dispersed Polymer Domain Size Formation in Melt Processing, *Emmount Technologies*

91. C. B. Bucknall, Applications of Microscopy to the Deformation and Fracture of Rubber-Toughened Polymer, *Journal of Microscopy*, 2001, Vol. 201, pp. 221-229

92. S. Joseph, Compatibilisation of Polystyrene/Polybutadiene Blends, *Master Thesis of Mahatma Gandhi University*, 2010, Chap. 7, pp. 203-225

93. P. Sivaraman, N. R. Manoj, S. Barman, et al, Thermoplastic Copolyether Ester Elastomer Toughened Polycarbonate Blends, *Polymer Testing*, 2004, Vol. 23, pp. 527-532

94. E. D. Blizanakov, C. C. White, M. T. Shaw, Mechanical Properties of Blends of HDPE and Recycled Urea-Formaldehyde Resin, *Journal of Applied Polymer Science*, 2000, Vol.77, pp.3220-3227